DUDLEY KNOX LIBRARY
NAVAL POSTGRADUATE SCHOOL
MONTEREY, CALIFORNIA 93943

NAVA
MON

NPS-69-84-008

NAVAL POSTGRADUATE SCHOOL
Monterey, California

THESIS

FILMWISE CONDENSATION OF STEAM ON
LOW INTEGRAL-FINNED TUBES

by

Ioannis V. Georgiadis

September 1984

Thesis Advisor: P. J. Marto

Approved for public release; distribution unlimited

Prepared for:
National Science Foundation
Division of Engineering
Washington, DC 20550

T222082

NAVAL POSTGRADUATE SCHOOL
Monterey, California

Commodore Robert H. Shumaker
Superintendent

David A. Schrady
Provost

This thesis prepared in conjunction with research supported in part by National Science Foundation, Division of Engineering, Washington, DC under MEA82-03567.

Reproduction of all or part of this report is authorized.

Released as a
Technical Report by:

UNCLASSIFIED
SECURITY CLASSIFICATION OF THIS PAGE (*When Data Entered*)

REPORT DOCUMENTATION PAGE		READ INSTRUCTIONS BEFORE COMPLETING FORM
1. REPORT NUMBER NPS-69-84-008	2. GOVT ACCESSION NO.	3. RECIPIENT'S CATALOG NUMBER
4. TITLE (*and Subtitle*) Filmwise Condensation of Steam on Low Integral-Finned Tubes		5. TYPE OF REPORT & PERIOD COVERED Engineer's Thesis September 1984 6. PERFORMING ORG. REPORT NUMBER
7. AUTHOR(*s*) Ioannis V. Georgiadis		8. CONTRACT OR GRANT NUMBER(*s*) Agreement No. MEA82-03567
9. PERFORMING ORGANIZATION NAME AND ADDRESS Naval Postgraduate School Monterey, California 93943		10. PROGRAM ELEMENT, PROJECT, TASK AREA & WORK UNIT NUMBERS
11. CONTROLLING OFFICE NAME AND ADDRESS Naval Postgraduate School Monterey, California 93943		12. REPORT DATE September 1984 13. NUMBER OF PAGES 166
14. MONITORING AGENCY NAME & ADDRESS(*if different from Controlling Office*) National SCience Foundation Washington, dc 20550		15. SECURITY CLASS. (*of this report*) Unclassified 15a. DECLASSIFICATION/DOWNGRADING SCHEDULE

16. DISTRIBUTION STATEMENT (*of this Report*)

Approved for public release; distribution unlimited

17. DISTRIBUTION STATEMENT (*of the abstract entered in Block 20, if different from Report*)

18. SUPPLEMENTARY NOTES

19. KEY WORDS (*Continue on reverse side if necessary and identify by block number*)

Steam, Condensation, Filmwise, Tube, Low-Integral Fin, Heat-Transfer Coefficient, Enhancement

20. ABSTRACT (*Continue on reverse side if necessary and identify by block number*)

Filmwise condensation heat-transfer measurements of steam were made on horizontal tubes under vacuum and near-atmospheric pressures. Data were taken for a smooth tube and for 21 tubes which contained rectangularly-shaped, low integral fins. The fin geometry was systematically varied in order to investigate the dependence of the steam-side heat-transfer coefficient on fin spacing, thickness and height.

DD FORM 1 JAN 73 1473 EDITION OF 1 NOV 65 IS OBSOLETE
S/N 0102-LF-014-6601

UNCLASSIFIED
SECURITY CLASSIFICATION OF THIS PAGE (*When Data Entered*)

#20 - ABSTRACT - (CONTINUED)

The condensation process was found to be most sensitive to fin spacing and to be weakly dependent on fin thickness. When the fin height was increased from 1.0 to 2.0 mm, the increase in the heat-transfer coefficient was about 20 percent, while the increase in condensing area was 51 percent.

The best performing finned tube had a fin spacing of 1.5 mm, a fin thickness of 1.0 mm and a fin height of 2.0 mm. It showed an enhancement over the smooth tube of between 4 to 5 under vacuum conditions and around 6 at atmospheric conditions. Thus, the use of finned tubes may result in a significant reduction in the size and weight of present-day steam condensers.

Approved for public release; distribution unlimited.

Filmwise Condensation of Steam on Low Integral-Finned Tubes

by

Ioannis V. Georgiadis
Lieutenant, Hellenic Navy
B.S., Hellenic Naval Academy, 1975

Submitted in partial fulfillment of the
requirements for the degrees of

MASTER OF SCIENCE IN MECHANICAL ENGINEERING

and

MECHANICAL ENGINEER

from the

NAVAL POSTGRADUATE SCHOOL
September 1984

DUDLEY KNOX LIBRARY
NAVAL POSTGRADUATE SCHOOL
MONTEREY, CALIFORNIA 93943

Thesis
G2455
c.1

ABSTRACT

Filmwise condensation heat-transfer measurements of steam were made on horizontal tubes under vacuum and near-atmospheric pressures. Data were taken for a smooth tube and for 21 tubes which contained rectangularly-shaped, low integral fins. The fin geometry was systematically varied in order to investigate the dependence of the steam-side heat-transfer coefficient on fin spacing, thickness and height.

The condensation process was found to be most sensitive to fin spacing and to be weakly dependent on fin thickness. When the fin height was increased from 1.0 to 2.0 mm, the increase in the heat-transfer coefficient was about 20 percent, while the increase in condensing area was 51 percent.

The best performing finned tube had a fin spacing of 1.5 mm, a fin thickness of 1.0 mm and a fin height of 2.0 mm. It showed an enhancement over the smooth tube of between 4 to 5 under vacuum conditions and around 6 at atmospheric conditions. Thus, the use of finned tubes may result in a significant reduction in the size and weight of present-day steam condensers.

NA
MONTEREY, CALIFORNIA 93943

TABLE OF CONTENTS

I. INTRODUCTION ---------------------------------- 17
  A. FILMWISE CONDENSATION ON FINNED TUBES ------- 18
  B. SURVEY OF ANALYTICAL MODELS AND EXPERIMENTAL WORK ---------------------------- 22
  C. OBJECTIVES ---------------------------------- 28
II. DESCRIPTION OF APPARATUS ------------------------ 30
  A. SYSTEM OVERVIEW ----------------------------- 30
  B. SYSTEM INSTRUMENTATION ---------------------- 33
  C. DATA ACQUISITION SYSTEM --------------------- 34
  D. SYSTEM MODIFICATIONS ------------------------ 35
  E. VACUUM INTEGRITY ---------------------------- 38
  F. TUBES TESTED -------------------------------- 39
  G. INSERT -------------------------------------- 42
III. SYSTEM OPERATION AND PROBLEMS ------------------ 45
  A. THE DROPWISE CONDENSATION PROBLEM ----------- 47
  B. VAPOR VELOCITY LIMITATIONS ------------------ 49
IV. DATA REDUCTION ---------------------------------- 51
  A. PROGRAM SIEDER ------------------------------ 53
  B. MODIFIED WILSON PLOT PROGRAM ---------------- 55
  C. MAIN DATA REDUCTION PROGRAM (DRP4) ---------- 56
V. RESULTS AND DISCUSSION -------------------------- 57
  A. INSIDE HEAT-TRANSFER COEFFICIENT ------------ 57
    1. Instrumented Tube Results --------------- 57
    2. Uninstrumented Tube Results ------------- 64
    3. Summary of the Inside Heat-Transfer Coefficient ----------------------------- 66

B. PERFORMANCE OF FINNED TUBES ---------------- 69

1. Condensation on Fins in General --------- 69

2. Significance of Fin Spacing ------------- 75

3. Significance of Fin Thickness ----------- 99

4. Significance of Fin Height -------------- 107

5. Significance of Tube Diameter ----------- 116

VI. CONCLUSIONS AND RECOMMENDATIONS ---------------- 119

A. CONCLUSIONS -------------------------------- 119

B. RECOMMENDATIONS ---------------------------- 120

APPENDIX A: PREPARATION OF CONDENSER TUBES ----------- 122

APPENDIX B: SYSTEM START-UP AND SHUT-DOWN PROCEDURES - 123

APPENDIX C: RAW DATA OF UNINSTRUMENTED AND INSTRUMENTED TUBE ------------------------ 125

APPENDIX D: RAW DATA OF TUBES TESTED ----------------- 127

APPENDIX E: ERROR ANALYSIS --------------------------- 150

LIST OF REFERENCES ----------------------------------- 163

INITIAL DISTRIBUTION LIST ---------------------------- 165

LIST OF TABLES

I. Geometry of Finned Tubes --- 42

II. Instrumented Tube Results for the Vacuum Run --- 61

III. Instrumented Tube Results for the Atmospheric Run --- 61

IV. Constants of Equation (5.6) for All Tested Tubes --- 72

V. Raw Data of Uninstrumented Smooth Tube --- 125

VI. Raw Data of Instrumented Tube --- 126

VII. Raw Data of Tube with Fins of s = 0.5, t = 1.0 and e = 1.0 mm --- 128

VIII. Raw Data of Tube with Fins of s = 1.0, t = 1.0 and e = 1.0 mm --- 129

IX. Raw Data of Tube with Fins of s = 1.5, t = 1.0 and e = 1.0 mm --- 130

X. Raw Data of Tube with Fins of s = 2.0, t = 1.0 and e = 1.0 mm --- 131

XI. Raw Data of Tube with Fins of s = 4.0, t = 1.0 and e = 1.0 mm --- 132

XII. Raw Data of Tube with Fins of s = 0.5, t = 0.75 and e = 1.0 mm --- 133

XIII. Raw Data of Tube with Fins of s = 1.0, t = 0.75 and e = 1.0 mm --- 134

XIV. Raw Data of Tube with Fins of s = 1.5, t = 0.75 and e = 1.0 mm --- 135

XV. Raw Data of Tube with Fins of s = 2.0, t = 0.75 and e = 1.0 mm --- 136

XVI. Raw Data of Tube with Fins of s = 4.0, t = 0.75 and e = 1.0 mm --- 137

XVII. Raw Data of Tube with Fins of s = 0.5, 7 = 0.5 and e = 1.0 mm --- 138

XVIII. Raw Data of Tube with Fins of s = 1.0, t = 0.5 and e = 1.0 mm ---------------------------------- 139

XIX. Raw Data of Tube with Fins of s = 1.5, t = 0.5 and e = 1.0 mm ---------------------------------- 140

XX. Raw Data of Tube with Fins of s = 2.0, t = 0.5 and e = 1.0 mm ---------------------------------- 141

XXI. Raw Data of Tube with Fins of s = 4.0, t = 0.5 and e = 1.0 mm ---------------------------------- 142

XXII. Raw Data of Tube with Fins of s = 1.0, t = 1.0 and e = 2.0 mm ---------------------------------- 143

XXIII. Raw Data of Tube with Fins of s = 1.5, t = 1.0 and e = 2.0 mm ---------------------------------- 144

XXIV. Raw Data of Tube with Fins of s = 2.0, t = 1.0 and e = 2.0 mm ---------------------------------- 145

XXV. Raw Data of Tube with Fins of s = 4.0, t = 1.0 and e = 2.0 mm ---------------------------------- 146

XXVI. Raw Data of Tube with Fins of s = 1.0, t = 1.5 and e = 1.0 mm ---------------------------------- 147

XXVII. Raw Data of Tube with Fins of s = 1.25, t = 1.25 and e = 1.0 mm ------------------------ 148

XXVIII. Raw Data of Smooth Tube ------------------------ 149

LIST OF FIGURES

1.1 Condensate Profile at Top Part of Tube ---------- 19

1.2 Typical Schematic of Retention Angle ------------ 24

2.1 Schematic of Test Apparatus -------------------- 31

2.2 Schematic Details of Test Section (Insert not Shown) -- 32

2.3 Schematic Details of Purge System and Water Sump -- 37

2.4 Photograph of the Instrumented Tube ------------- 40

2.5 Photograph of a Set of Tested Tubes with Fins of t = 0.75 and e = 1.0 mm ---------------- 41

2.6 Photograph of the Insert Together with a Finned Tube Tested ---------------------------- 44

4.1 Mixing Chamber Calibration Curve --------------- 52

5.1 Temperature Distribution for Instrumented Tube (Vacuum Run) ----------------------------- 59

5.2 Temperature Distribution for Instrumented Tube (Atmospheric Run) ------------------------ 60

5.3 Correlation of the Water-Side Coefficient Obtained with Instrumented Smooth Tube --------- 63

5.4 Comparison of Smooth-Tube Data with Fujii Correlation ------------------------------------ 67

5.5 Variation of Heat Flux with Steam-Side Temperature Drop ------------------------------- 70

5.6 Variation of Condensing Coefficient with Heat Flux -- 73

5.7 Cross Plot Showing Best Fin Spacing Among Tubes with t = 1.0 and e = 1.0 mm --------------- 77

5.8 Miniscus Profile for Various Fin Sapcings (a) s = 1.0 mm, (b) s = 1.5 mm, (c) s = 2.0 mm -- 79

5.9 Normalized Enhancement Ratio Versus Fin Spacing for Tubes with Fins of t = 1.0 mm and e = 1.0 mm ---------------------------------- 80

5.10 Variation of Condensing Coefficient with Heat Flux for the Set of Tubes with t = 1.0 and e = 1.0 mm (Vac. Runs) ---------------------- 83

5.11 Variation of Heat Flux with Steam-Side Temperature Drop for Tubes with t = 1.0 and e = 1.0 mm (Vac. Runs) -------------------------- 84

5.12 Variation of Condensing Coefficient with Heat Flux for the Set of Tubes with t = 1.0 and e = 1.0 mm (Atm. Runs) ---------------------- 85

5.13 Variation of Heat Flux with Steam-Side Temperature Drop for the Set of Tubes with t = 1.0 and e = 1.0 mm (Atm. Runs) -------------- 86

5.14 Variation of Condensing Coefficient with Heat Flux for the Set of Tubes with t = 0.75 and e = 1.0 mm (Vac. Runs) ---------------------- 87

5.15 Variation of Heat Flux with Steam-Side Temperature Drop for the Set of Tubes with t = 0.75 and e = 1.0 mm (Vac. Runs) ------------- 88

5.16 Variation of Condensing Coefficient with Heat Flux for the Set of Tubes with t = 0.75 and e = 1.0 mm (Atm. Runs) ---------------------- 89

5.17 Variation of Heat Flux with Steam-Side Temperature Drop for the Set of Tubes with t = 0.75 and e = 1.0 mm (Atm. Runs) ------------- 90

5.18 Variation of Condensing Coefficient with Heat Flux for the Set of Tubes with t = 0.5 and e = 1.0 mm (Vac. Runs) ---------------------- 91

5.19 Variation of Heat Flux with Steam-Side Temperature Drop for the Set of Tubes with t = 0.5 and e = 1.0 mm (Vac. Runs) -------------- 92

5.20 Variation of Condensing Coefficient with Heat Flux for the Set of Tubes with t = 0.5 and e = 1.0 mm (Atm. Runs) ---------------------- 93

5.21 Variation of Heat Flux with Steam-Side Temperature Drop for the Set of Tubes with t = 0.5 and e = 1.0 mm (Atm. Runs) -------------- 94

5.22 Variation of Condensing Coefficient with Heat Flux for the Set of Tubes with t = 1.0 and e = 2.0 mm (Vac. Runs) ---------------------- 95

5.23 Variation of Heat Flux with Steam-Side Temperature Drop for the Set of Tubes with t = 1.0 and e = 2.0 mm (Vac. Runs) -------------- 96

5.24 Variation of Condensing Coefficient with Heat Flux for the Set of Tubes with t = 1.0 and e = 2.0 mm (Atm. Runs) ---------------------- 97

5.25 Variation of Condensing Coefficient with Heat Flux for the Set of Tubes with t = 1.0 and e = 2.0 mm (Atm. Runs) ---------------------- 98

5.26 Cross Plots Showing Best Fin Spacing Among Sets of Tubes with Fins of t = 0.5, 0.75 and 1.0 mm -- 100

5.27 Influence of Fin Thickness on Enhancement Ratio for Tubes with s = 1.0 mm, for both Pressure Conditions ----------------------------- 102

5.28 Variation of Condensing Coefficient with Heat Flux for Tubes with Fin Geometry Shown in the Figure (Vac. Runs) ----------------------- 108

5.29 Variation of Condensing Coefficient with Heat Flux for Tubes with Fin Geometry Shown in the Figure (Atm. Runs) ----------------------- 109

5.30 Cross Plot Showing Best Fin Spacing for Tubes with e = 2.0 mm and t = 1.0 mm, for both Pressure Conditions ------------------------ 110

5.31 Comparison of Enhancement Ratio Obtained on Sets of Tubes with e = 1.0 and e = 2.0 mm (Vac. Runs) ------------------------------------- 111

5.32 Condensate Profiles for Tubes with Fins of Different Height ---------------------------------- 113

5.33 Normalized Enhancement Ratio of Sets of Tubes with Fins of 1.0 and 2.0 mm Height -------- 115

5.34 Cross Plots Showing Best Fin Spacing for Tubes of Different Diameter --------------------- 117

E.1 Error Bands for a Tube Tested Under Vacuum Conditions ------------------------------------- 153

E.2 Error Bands for a Tube Tested Under Atmospheric Conditions --------------------------- 154

LIST OF SYMBOLS

A_{eff}	Effective Area of Finned Tube (See Eqn. 1.10)
A_f	Outside Area of Finned Tube
A_r	Outside Area of Smooth Tube
B	Constant Used with Sieder-Tate-type Equation
C	Constant Used with Sieder-Tate-type Equation
C_f	Correction Factor for Cooling Water Viscosity Changes
C_{pc}	Constant Pressure Specific Heat of Cooling Water
D_e	Equivalent Diameter Used with Beatty and Katz Equation
D_f	Diameter to Outside of Fins
D_i	Inside Diameter of Condenser Tube
D_o	Outside Diameter of Smooth Tube, Equal to Root Diameter of Finned Tube
e	Fin Height
F	$gD_o\mu_f h_{fg}/V_v^2 k_f \Delta T$
g	Local Gravitational Acceleration
h_{BK}	Average Heat-transfer Coefficient Given by Beatty and Katz Model
h_c	Heat-transfer Coefficient Based on Smooth Tube Diameter
h_{eff}	Heat-transfer Coefficient on the Flooded Part of the Tube
h_{fg}	Specific Enthalpy of Vaporization
h_i,hi	Water-side Heat-transfer Coefficient
h_L	Effective Heat-transfer Coefficient on the Flooded Part of the Tube

h_o,ho	Steam-side Heat-transfer Coefficient
h_{ow}	Average Heat-transfer Coefficient Given by Owen et al. Model
h_{RW}	Average Heat-transfer Coefficient Given by Rudy and Webb Model
h_u	Heat-transfer Coefficient on the Upper Tube Portion
k_c	Thermal Conductivity of Cooling Water
k_{eff}	Effective Thermal Conductivity
k_f	Thermal Conductivity of Condensate
k_{fin}	Thermal Conductivity of Fin Material
$\dot{m}_{act}$	Actual Cooling Water Mass Flow Rate
$\dot{m}_{calc}$	Calculated Cooling Water Mass Flow Rate
L	Condensing Tube Length
LMTD	Logarithmic-mean-temperature Difference
N	Fin Density
Nu	Water-side Nusselt Number, $h_i D_i / k_c$
Nu_g	Steam-side Nusselt Number, $h_o D_o / k_f$
ΔP_{AB},ΔP_{CB}	Pressure Difference Between Points C and B or Points A and B (Fig. 1.1)
P_A,P_B,P_C	Pressure in Condensate (Fig. 1.1)
Pr	Prandtl Number of Cooling Water, $C_{pc} \mu_c / k_c$
P_v	Pressure of Steam
q	Heat Flux Based on Outside Area of Smooth Tube
Re	Coolant-side Reynolds Number, $\rho_c V_c D_i / \mu_c$
$\tilde{Re}$	Steam-side Reynolds Number, $\rho_f V_v D_o / \mu_f$
s	Fin Spacing
t	Fin Thickness

Tin	Cooling Water Inlet Temperature
T_s or Ts	Temperature of Steam
Tout	Cooling Water Outlet Temperature
T_{wo}	Average Outer all Temperature, Temperature at Root of Fins
ΔT	Local Temperature Drop Across Condensate Film
$\overline{\Delta T}$	Average Temperature Drop Across Condensate Film $(T_s - \overline{T}_{wo})$
ΔT_c	Cooling Water Temperature Drop
r_A, r_B, r_C	Radius of Curvature of the Miniscus Profile in the Interfin Space at the Top Part of the Tube (Fig. 1.1)
U_o	Overall Heat-transfer Coefficient
V_c,Vw	Cooling Water Velocity
V_v	Steam Velocity
X	Average Fin Height (Defined by Equation (1.11))
x	Coordinate Axis (Fig. 1.1)
y	Coordinate Axis (Fig. 1.1)

Greek symbols

θ	Angle Measured from Top of Tube
μ_c	Viscosity of Cooling Water at Bulk Temperature
μ_f	Viscosity of Condensate at Film Temperature
μ_w	Viscosity of Cooling Water at Inner Wall Temperature
ρ_c	Density of Cooling Water
ρ_f	Density of Condensate
ρ_v	Density of Steam
σ	Surface Tension of Condensate

ϕ	Fin Efficiency
ψ	Condensate Retention Angle Measured from the Bottom of the Tube to the Position at Which the Condensate Just Fills the Interfin Space

ACKNOWLEDGEMENTS

This thesis was completed because of the careful and good-willing help of the following persons:

1. Dr. P. J. Marto, my advisor.
2. Dr. J. W. Rose, co-advisor in the project.
3. Dr. A. S. Wanniarachchi, my second advisor.
3. Mr. Tom Christian and the workers in the machine shop of the Mechanical Engineering Department, and
4. Artemis, my wife.

I would like to express to them my deep feelings by just saying "Thank you very much."

I. INTRODUCTION

Modern marine propulsion plants must be designed to provide maximum power with small size, low weight and reasonable cost. A heavy power plant may have an impact on ship dimensions and displacement since the power required to achieve a given speed increases with the displacement. A sizeable propulsion plant will occupy space that is valuable, while the machinery room will have poor accessibility.

A significant decrease in size and weight of a steam power plant can be achieved by reducing the size of the condenser. Present condensers are large because of the use of smooth tubes and generous design margins. The heat-transfer performance of any condenser tube is limited by the thermal resistances on the water-side, in the wall and on the steam-side of the tube. Reduction of any of these resistances will contribute to a lighter and smaller condenser.

In recent years, various efforts have been made in order to increase the outside (i.e., steam-side) heat-transfer coefficient, and these methods have been thoroughly reviewed by Marto [Ref. 1]. Outside enhancement techniques include the use of low integral fins, roped tubes, fluted tubes, drainage strips attached on the tubes and applied coatings to promote dropwise condensation.

A. FILMWISE CONDENSATION ON FINNED TUBES

Filmwise condensation heat transfer on a smooth tube is limited by the thickness of the condensate layer. This layer forms a relatively high conduction resistance between the vapor and the tube surface. To enhance filmwise condensation heat transfer, it is then important to thin this condensate film. One common way to decrease this condensate film is to use radial fins attached to the external surface of the tube in order to promote surface-tension effects.

The theoretical treatment of this problem is very difficult owing to the large number of controlling parameters such as the three-dimensional condensate flow pattern, vapor shear, surface-tension forces, wall conduction effects and condensate retention. Studies following Gregorig [Ref. 2] have demonstrated the important role of surface tension in modifying the condensate film over the fin surface. The presence of fins causes three main effects:

1. the condensing area increases,
2. the surface-tension forces thin the condensate film over the tip of the fins causing improved heat transfer, and
3. the fins may cause condensate retention especially on the lower part of the tube.

The first two effects are beneficial, while the third undermines the heat-transfer performance. The second effect is most important in the upper portion of the tube, where there is little condensate retention. For steam condensation data on finned tubes, Yau et al. [Ref. 3] measured enhancement ratios (i.e., the ratio of vapor-side coefficient of a finned tube to the value of smooth tube) in excess of the increase in condensing area. This additional enhancement is most probably due to the thinning effect of the surface-tension forces acting on the condensate film. This phenomenon can be explained by referring to Figure 1.1.

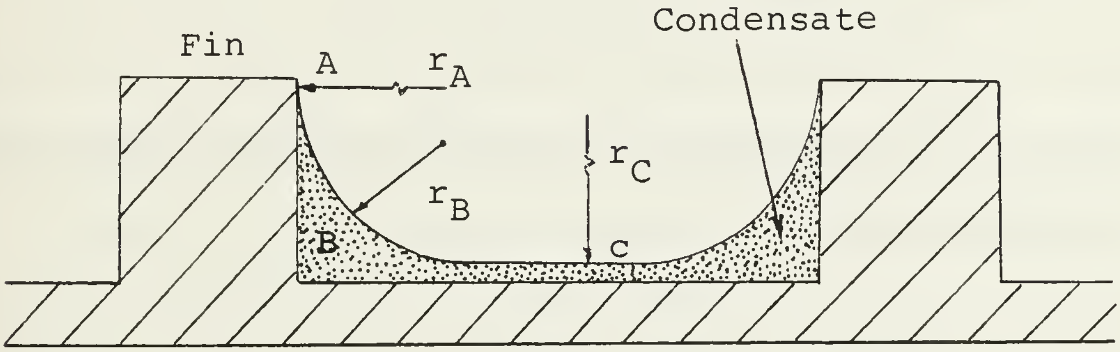

Figure 1.1. Condensate Profile at Top Part of Tube

Since the condensate film has a concave shape at point A, the pressure within the condensate at this point is smaller than the local vapor pressure, and is given by:

$$P_A = P_v - \frac{\sigma}{r_A} \tag{1.1}$$

A similar expression may be written at point C.

$$P_C = P_v - \frac{\sigma}{r_C} \tag{1.2}$$

Note that the local radii of curvature at points A and C are very large; therefore, the liquid pressure at these points nearly equals the vapor pressure. On the other hand, at point B the condensate profile has a more concave shape, thus resulting in a lower pressure than at either points A or C:

$$P_B = P_V - \frac{\sigma}{r_B} \qquad (1.3)$$

As a result, there exists a pressure difference from point A to point B as given by:

$$\Delta P_{AB} = \sigma\left(\frac{1}{r_B} - \frac{1}{r_A}\right) \qquad (1.4)$$

and in a similar way from point C to point B as given by:

$$\Delta P_{CB} = \sigma\left(\frac{1}{r_B} - \frac{1}{r_C}\right) \qquad (1.5)$$

In general, these pressure differences are positive, causing the condensate to be pulled toward point B (which acts as a condensate run-off channel), thus thinning the condensate film on the fins as well as in the interfin area. This thinning effect, therefore, increases the heat-transfer performance in excess of the surface area gain.

On the other hand, as mentioned above, the third effect of the fins which is to retain the condensate, especially on the lower part of the tube, creates a relatively thick condensate film, causing lower heat transfer. When the fin spacing is reduced, a high surface-tension condensate will bridge the fins; therefore, the heat-transfer performance may decrease despite that the condensing area has increased. Thus, owing to the competing nature of these effects, the selection of a best fin geometry needs considerable attention.

The effect of fin spacing and fluid properties (such as surface tension) on condensate retention has been well studied by various investigators [Refs. 4,5,6]. A detailed discussion of these studies is presented in the next section.

One more important effect that is common for both smooth and finned tubes is the oscillation of the condensate layer resulting from the intermittent departure of condensate droplets from the lower part of the tube surface. When a droplet departs, the nearby film stretches (becomes thinner) and higher heat transfer takes place locally. After the droplet has departed, the film grows again and becomes thicker. The frequency and amplitude of this oscillation are functions of the heat flux, fin geometry and the properties of the fluid. To the best of this author's knowledge, this transient phenomenon has not yet been investigated.

B. SURVEY OF ANALYTICAL MODELS AND EXPERIMENTAL WORK

In 1948, Beatty and Katz [Ref. 7] developed a simple analytical model to predict the condensing heat-transfer coefficient on a horizontal finned tube. Their model was supported by various other researchers, as stated in [Ref. 8]. The final form of the Beatty and Katz prediction has the following equations:

$$h_{Bk} = 0.689 \left\{ \frac{k_f^3 \rho_f (\rho_f - \rho_v) g h_{fg}}{\mu_f \overline{\Delta T}} \right\}^{1/4} [\frac{1}{D_e}]^{1/4} \tag{1.6}$$

where

$$[\frac{1}{D_e}]^{1/4} = \frac{A_r}{A_{eff}} \frac{1}{D_o^{1/4}} + 1.3 \frac{\phi A_f}{A_{eff}} \frac{1}{X^{1/4}} , \tag{1.7}$$

$$A_r = \pi D_o L \tag{1.8}$$

$$A_f = \frac{\pi}{2}(D_f^2 - D_o^2) NL , \tag{1.9}$$

$$A_{eff} = A_r + \phi A_f , \text{ and} \tag{1.10}$$

$$X = \frac{\pi (D_f^2 - D_o^2)}{4 D_f} . \tag{1.11}$$

The major fault with their model was the neglect of any surface-tension effects. They therefore assumed that the

Nusselt equation can be applied to all the external surfaces of the tube (i.e., tip, sides of fins and interfin space). According to [Ref. 8 and 9], this model overpredicts the condensing coefficient especially for those fluids that have high surface tensions (for example, water).

Rudy et al. [Ref. 5] attempted to include the surface-tension effect by modifying the original Beatty and Katz equation. To obtain this modification, they first investigated the retention angle problem. They performed static (i.e., with no condensation) and dynamic (i.e., with condensation) measurements of the retention angle on tubes with fin densities from 0.75 to 1.38 fins/mm. They found that the retention angle (see Figure 1.2) can be very well predicted (within ±10 percent) by the following equation:

$$\psi = \cos^{-1}\left[1 - \frac{4\sigma}{\rho_f g s D_f}\right] \qquad (1.12)$$

The above equation was tested against many fluids such as refrigerant-11, pentane and water. It is worth mentioning that Honda et al. [Ref. 6] and Owen et al. [Ref. 8], obtained essentially the same equation by using different models. Next, Rudy et al. modelled the condensation process assuming no heat transfer in the flooded portion of the tube. They developed the following prediction:

$$h_{RW} = \left(1 - \frac{\psi}{\pi}\right) h_{BK} \qquad (1.13)$$

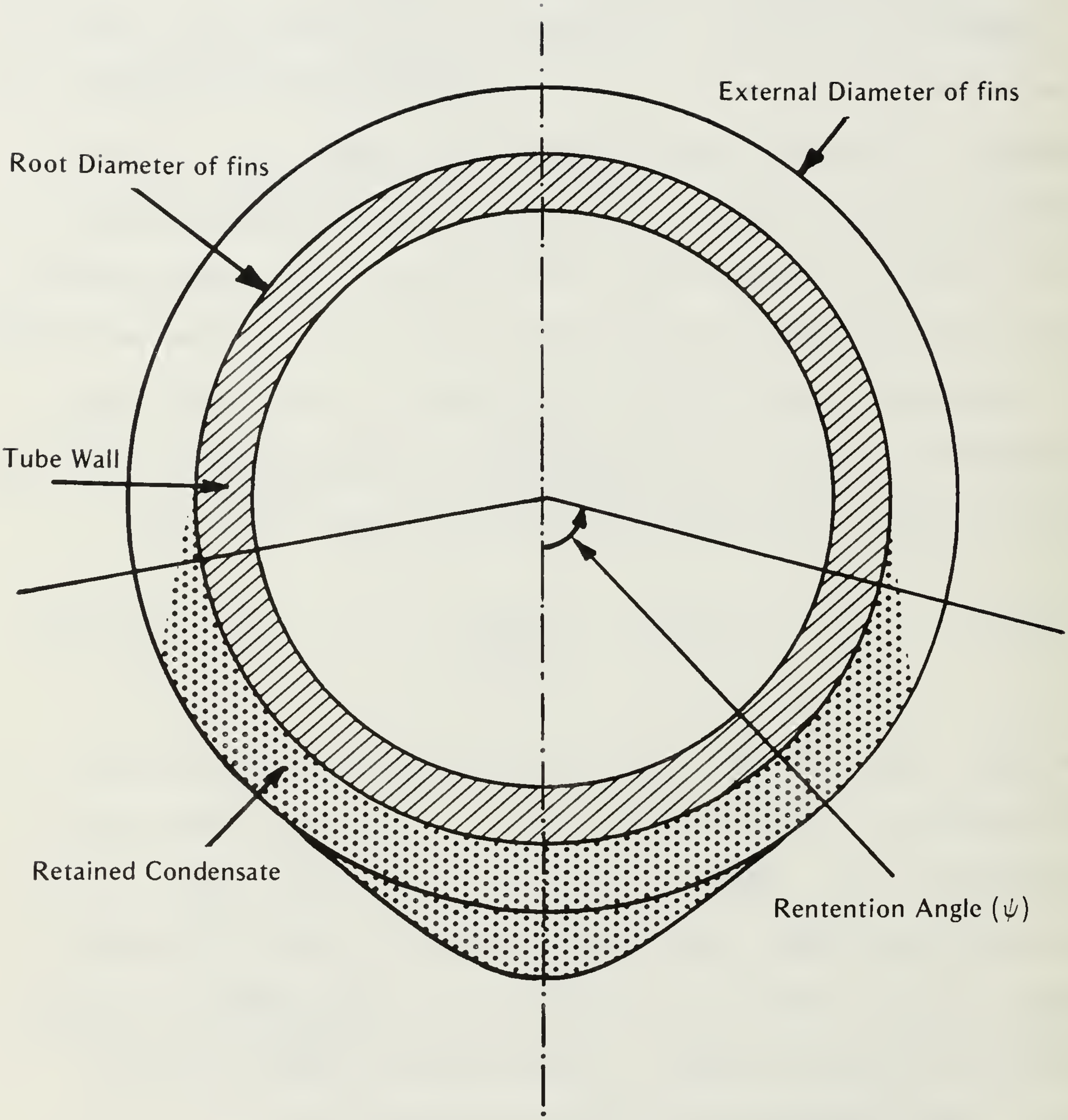
External Diameter of fins
Root Diameter of fins
Tube Wall
Retained Condensate
Rentention Angle (ψ)

Figure 1.2. Typical Schematic of Retention Angle

where h_{BK} is given by equation (1.6). Unfortunately, this model tends to underpredict most of the available experimental data by as much as about 60 percent [Ref. 9].

Owen et al. [Ref. 8] modified the Rudy et al. model by including heat transfer from the flooded part of the tube. For the fluids that they tested, their model predicted the condensing coefficient within ±30 percent. The prediction that they developed is based on the following equations:

$$h_{ow} = (1 - \frac{\psi}{\pi}) h_u + \frac{\psi}{\pi} h_L \tag{1.14}$$

$$h_u = 0.725 \left\{ \frac{k_f^3 \rho_f (\rho_f - \rho_v) g h_{fg}}{\mu_f \overline{\Delta T}} \right\}^{1/4} [\frac{1}{D_e}]^{1/4} \quad ; \tag{1.15}$$

$$h_L = (\frac{1}{h_{eff}} - \frac{1}{h_c})^{-1} \tag{1.16}$$

where

$$h_c = 0.725 \left\{ \frac{k_f^3 \rho_f (\rho_f - \rho_v) g h_{fg}}{\mu_f \overline{\Delta T}} \right\}^{1/4} [\frac{1}{D_f}]^{1/4} \quad , \text{ and} \tag{1.17}$$

$$h_{eff} = \frac{k_{eff}}{e} \quad , \tag{1.18}$$

where

$$k_{eff} = (1 - sN) k_{fin} + sN k_f \tag{1.19}$$

The above analysis uses Beatty and Katz prediction (equation (1.6)) for the unflooded part of the tube. As mentioned earlier, the surface-tension effect is not included in equation (1.6). However, as discussed in the previous section (Section A), the surface-tension forces play an important role in filmwise condensation by thinning the condensate film. Therefore, the Owen model needs further improvements to account for the surface-tension effect at the unflooded part of the tube.

Recently, Honda et al. [Ref. 9], developed a model to predict the condensing coefficient by accounting for surface-tension effects and for the non-isothermal behavior of the fins. Their model can predict most of the available experimental data including 11 fluids and 22 tubes within ±20 percent. Honda et al. provide a comparison of these four models with experimental data. It is worth mentioning that the worst disagreement (within ±30 percent) between the data and their model occurs for the steam data of Rose [Ref. 3]. This is probably owing to the high surface tension of water, as the surface-tension effects are still inadequately accounted for even in this model. Further, it is shown that all the models except that of Honda overpredict these steam data. In comparison with the other models, the Honda model shows considerable promise. However, it must be noted that this model is rather laborious as it requires considerable computer time for iterative finite difference techniques.

The Honda model may require further improvements to predict steam data more accurately. Also, most importantly, a more practical model must be developed so that the designers may use it with confidence. Such a model may consist of a combination of a few correlations. Thus, it is extremely important to generate a sufficient amount of experimental data covering all important geometric variables (such as fin spacing, fin thickness, fin height, fin shape, tube diameter, etc.) for condensation of steam on finned tubes.

In 1961, Staub [Ref. 10] conducted steam condensation experiments with horizontal fluted tubes under vacuum and atmospheric conditions. He used a bell-shaped (rather than rectangular) fin profile on a root diameter of 14.9 mm. These fins had a pitch of 1.0 mm, a thickness of 0.4 mm at the root of the fin and a height of 0.5 mm. He reported a vapor-side heat-transfer-coefficient enhancement (i.e., the ratio of vapor-side coefficient of finned tube to the value of smooth tube) of around 3 for both vacuum and atmospheric pressure conditions.

At Queen Mary College of London, Yau et al. [Ref. 3] obtained steam condensation data at atmospheric pressure on various rectangularly-shaped finned tubes having a root diameter of 12.7 mm. They found an optimum spacing of 1.5 mm for a fin thickness of 0.5 mm and a fin height of 1 mm. Their optimum tube resulted in a vapor-side heat-transfer coefficient enhancement of 3 to 4.

On-going research is underway at the Naval Postgraduate School to study the feasibility of using low integral-finned tubes with steam. A test apparatus has been constructed by Krohn [Ref. 11] to systematically study steam condensation on a single horizontal tube. The test apparatus was instrumented and tested by Graber [Ref. 12], and further system improvements for leak tightness were made by Poole [Ref. 13]. Poole conducted experiments both under vacuum and at pressures near-atmospheric. He used machined, rectangular fins with a fin thickness and a fin height of 1 mm on a root diameter of 19 mm. He tested a total of six finned tubes with fin spacings of 0.5, 1.0, 1.5, 2.0 , 4.0 and 9.0 mm as well as a smooth tube. His results showed that the best enhancement of 3 to 4 occurred for the tube with a fin spacing of 1.5 mm. However, Poole had problems with partial dropwise condensation since the total filmwise mode lasted only for about 20 minutes during his experimental runs. Thus, it became necessary to repeat his test runs in order to verify his preliminary results.

C. OBJECTIVES

The main objectives of this research effort were, therefore, to:

1) establish a preparation procedure that will ensure filmwise condensation on copper finned tubes.

2) take data on an instrumented smooth tube to determine the water-side heat-transfer coefficient with internal enhancement.

3) take data on a smooth tube to check the data-reduction program and to establish a basis for comparison with the finned tubes.

4) take data on tubes with rectangularly shaped fins of various fin spacings, fin thicknesses and fin heights to obtain a possible optimum fin geometry.

II. DESCRIPTION OF APPARATUS

A. SYSTEM OVERVIEW

The apparatus used for this research was essentially the same used in [Ref. 13], with several small modifications. A schematic of the system is shown in Figure 2.1. Steam was generated in a 304.8 mm (12 in) diameter Pyrex glass boiler using ten 4000 Watt, 480 Volt Watlow immersion heaters. Passing through a 304.8 mm (12 in) to 152.4 mm (6 in) reducing section, the steam travelled upward through a Pyrex glass section 2.44 m (8 ft) in length, around a 180-degree bend and back down a straightening section 1.52 m (5 ft) in length before entering the stainless-steel test section. The condenser tube to be tested was mounted horizontally in the test section behind a viewport to permit visual observation of the condensing process. Figure 2.2 shows the details of the test tube mounted in the test section.

Steam that did not condense on the test tube passed into a stainless steel auxiliary condenser, and all condensate was returned via gravity to the boiler. The auxiliary condenser was constructed of two 9.5 mm (3/8 in) diameter, water-cooled copper lines helically coiled to a height of 457 mm (18 in).

Cooling water for the test tube was provided, on a once-through basis, by two centrifugal pumps connected in series.

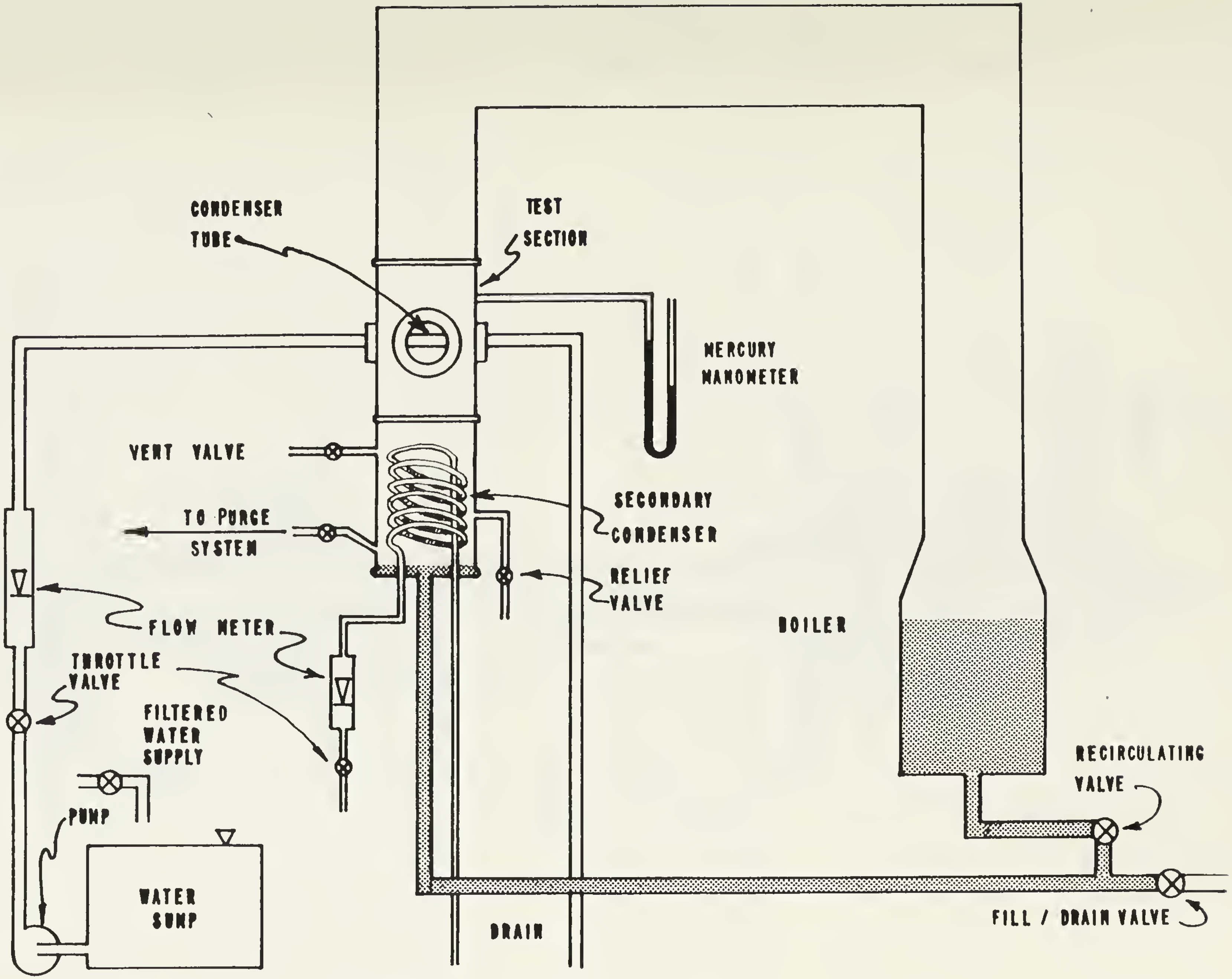
CONDENSER TUBE
TEST SECTION
MERCURY MANOMETER
VENT VALVE
TO PURGE SYSTEM
SECONDARY CONDENSER
RELIEF VALVE
BOILER
FLOW METER
THROTTLE VALVE
FILTERED WATER SUPPLY
PUMP
WATER SUMP
DRAIN
RECIRCULATING VALVE
FILL / DRAIN VALVE

Figure 2.1. Schematic of Test Apparatus

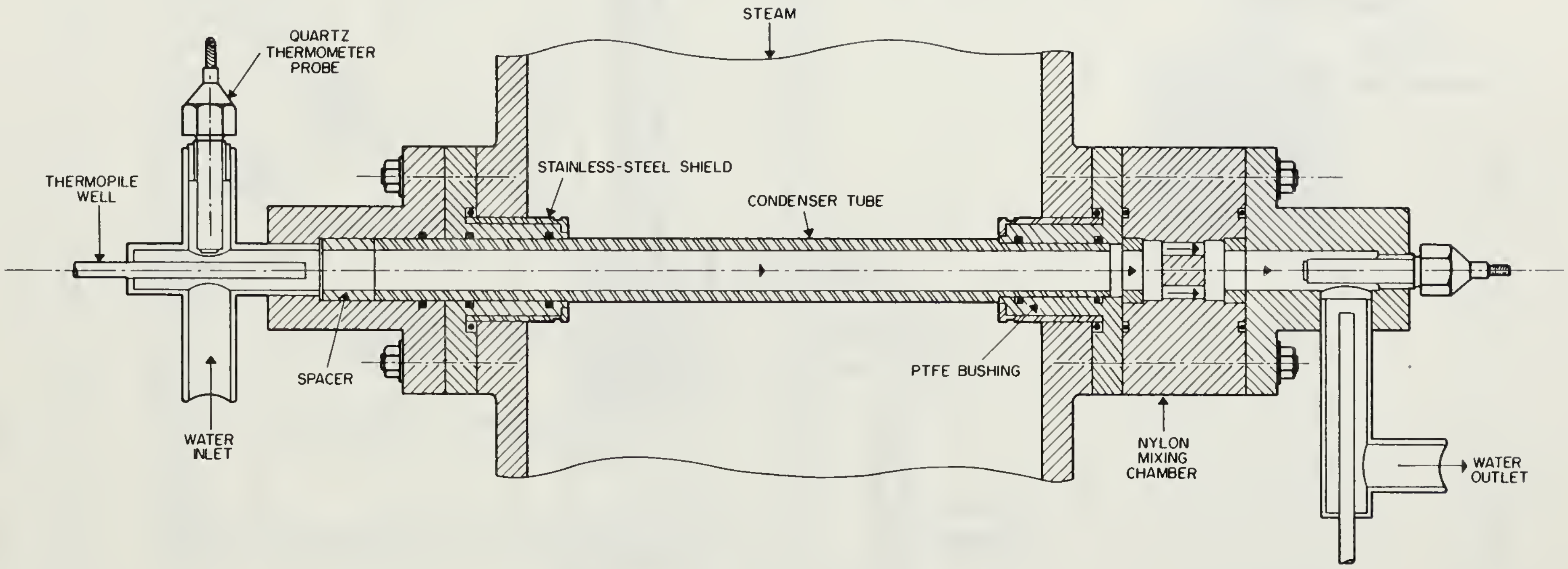
STEAM
QUARTZ THERMOMETER PROBE
THERMOPILE WELL
STAINLESS-STEEL SHIELD
CONDENSER TUBE
SPACER
PTFE BUSHING
WATER INLET
NYLON MIXING CHAMBER
WATER OUTLET

Figure 2.2. Schematic Details of Test Section (Insert not Shown)

Water to these pumps was provided through a large sump (capacity about 0.4 m^3), which was filled with a continuous supply of filtered tap water. The water could be throttled from zero to 0.55 l/s (8.8 gpm), giving a maximum water velocity of 4.4 m/s (14.4 ft/sec) through the tube.

A continuous supply of tap water was used for cooling the auxiliary condenser. Throttling the flow of tap water through the auxiliary condenser was the means used to vary the internal pressure of the test apparatus.

A vacuum pump was used to create vacuum and for removal of noncondensing gases from the test section. The vacuum pump was in operation throughout the data collection time interval.

B. SYSTEM INSTRUMENTATION

The input power to the heaters was changed through a panel-mounted potentiometer. A converter with an input voltage of 440 VAC generated a signal, which was fed to the data acquisition system in order to calculate the power input to the heaters. A complete explanation of the converter function is given by Poole [Ref. 13].

The internal pressure of the system was measured manually by a U-tube, mercury-in-glass manometer graduated in millimeters. Unavoidably, steam would condense in the manometer. Therefore, the varying height of the water column in the manometer needed to be accounted for when measuring the system pressure.

All temperatures were measured using 0.25 mm diameter, copper-constantan thermocouples. Two thermocouples were used for the steam, one for the condensate return and one for the ambient. The calibration procedure for these thermocouples is described in [Ref. 13]. The temperature rise of the cooling water through the test section was measured by two Hewlett-Packard (HP) 2804A quartz thermometers as well as by a 10-junction, series-connected, copper-constantan thermopile. The temperatures were fed directly into the data-acquisition system as described below. During this entire investigation, these two independent means of cooling-water-temperature rise measurements agreed to within ±0.02 K. Note that the coolant temperature rise was as low as 0.7 K for the smooth tube (under vacuum conditions), while it was in excess of 1.2 K for the finned tubes. Thus, the coolant temperature rise was measured with an uncertainty better than ±3 percent for finned tubes.

C. DATA ACQUISITION SYSTEM

An HP 3497A Data Acquisition System, as controlled by an HP 9826A computer, was used to monitor the system temperatures and the converter's signal representing the power input to the heaters. The data were immediately processed and also were stored on computer disks for later reduction and evaluation.

D. SYSTEM MODIFICATIONS

For some of the early data taken near atmospheric pressure, the measured steam-side heat-transfer coefficient, when operating with a closed system, disagreed by as much as ±30 percent between different data runs. This was later found to be due to the malfunctioning of the relief valve provided on the apparatus for safety reasons (see Figure 2.1). This valve had a designed relief gauge pressure of 52 mmHg. However, occasionally it was found to open with a system gauge pressure of only about 7 mmHg. Once opened, the valve remained open even if the system operating pressure was 10 mmHg below atmospheric, thus allowing air to enter the apparatus. To avoid this problem, subsequent runs were made without the relief valve and a new, more reliable, valve was ordered. In the meantime, extreme care had to be exercised to avoid system pressurization.

Originally, the apparatus was provided with a 10.6 kW (3 ton) air-conditioning system to cool the cooling water sump. However, as also mentioned by Poole [Ref. 13], this system was inadequate to keep the sump temperature from rising. For this reason, this air-conditioning system was removed. By removing this unit, the cooling water friction losses were reduced and the maximum water velocity was increased from 4.2 to 4.4 m/s. In the previous stage of the investigation, fresh tap water was continuously fed to a sump while an equal amount of water was being drained, maintaining

TABLE I

Geometry of Finned Tubes

Fin Spacing (mm)	Fin Thickness (mm)	Fin Height (mm)
0.5, 1.0, 1.5, 2.0, 4.0	1.0	1.0
0.5, 1.0, 1.5, 2.0, 4.0	0.75	1.0
0.5, 1.0, 1.5, 2.0, 4.0	0.5	1.0
1.0, 1.5, 2.0, 4.0	1.0	2.0
1.0	1.5	1.0
1.25	1.25	1.0

G. INSERT

Early investigations showed that with no internal enhancement, the water-side thermal resistance could be as much as 90 percent of the overall resistance. Under such conditions, even a small discrepancy on the water-side resistance will translate into a substantially greater discrepancy on the condensing heat-transfer coefficient. Therefore, in order to improve the accuracy of the condensing heat-transfer coefficient, a decision was made to enhance the inside heat-transfer coefficient.

For this purpose, a spiral insert was fabricated. The insert consisted of a 6.4 mm diameter stainless-steel rod together with a copper wire that was wrapped around the rod. The diameter and the pitch of the wrapped wire were 3.2 mm and 20 mm respectively. After wrapping, the wire was properly soldered on the rod and then it was machined down to give a clearance of 0.5 mm between the outer wire diameter and the tube inside wall. This clearance was considered important to avoid heat conduction from the tube wall to the insert. Figure 2.6 is a photograph of the insert with one of the finned tubes.

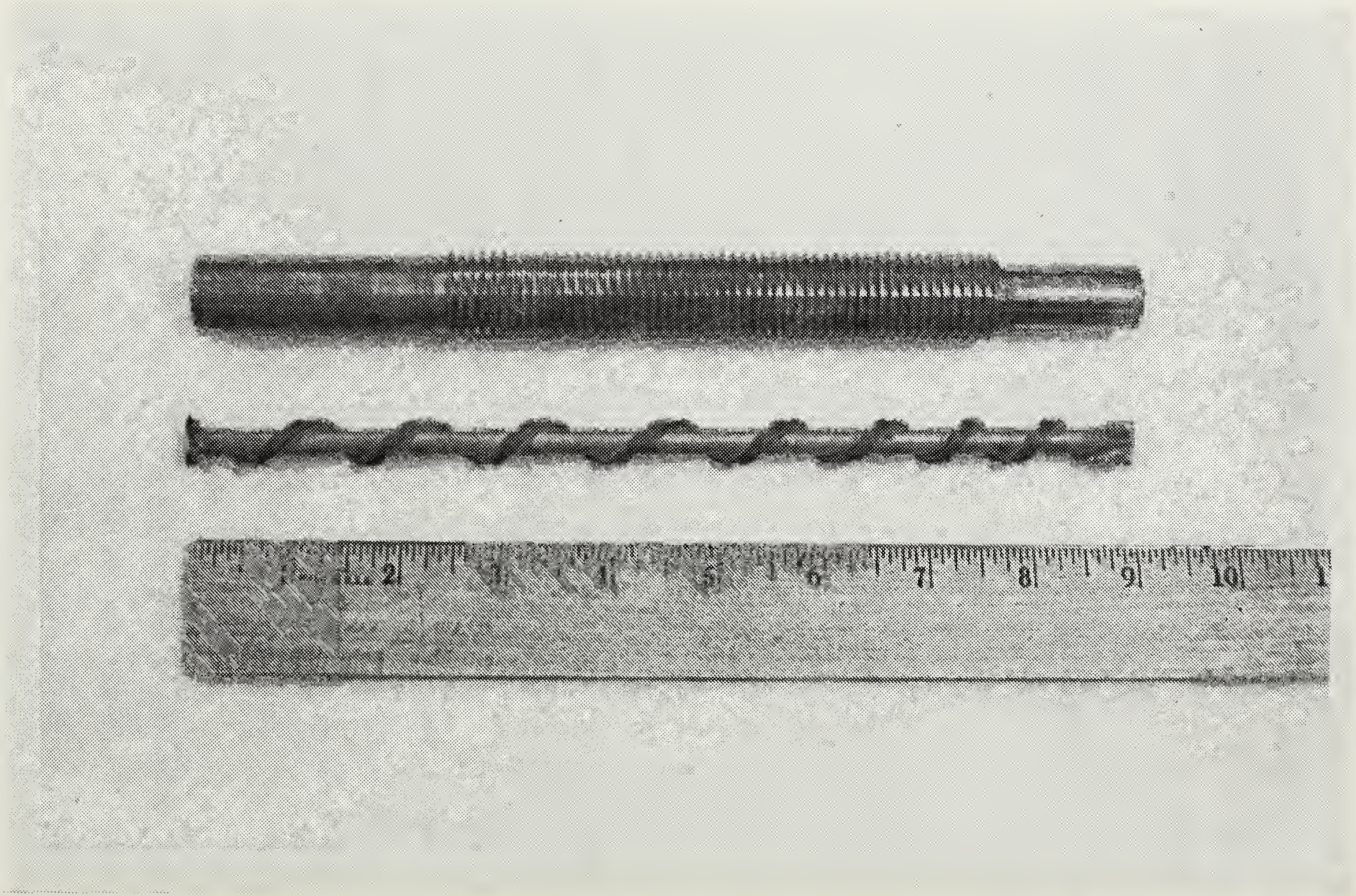
2
3
4
5
6
7
8
9
10

Figure 2.6. Photograph of the Insert Together with a Finned Tube Tested

III. SYSTEM OPERATION AND PROBLEMS

Each tube to be tested was cleaned following the procedures listed in Appendix A. After installing a tube, the system was brought to operating pressure by following the procedures listed in Appendix B. The data were collected when steady-state conditions were achieved which were assumed to occur when the temperature of the steam in the test section and the inlet-outlet water temperatures were stabilized. Double data sets were taken for each flow setting starting with a cooling water flow rate of 80% (4.4 m/s). The next water flowmeter settings were 70, 60, 45, 35, 26, and 20 percent followed by 55 and 80 percent. These settings were selected to provide nearly equal-spaced heat flux data points.

Since the tubes were fabricated from copper, a highly conductive material, the time interval required to achieve steady-state conditions was not more than two minutes. A whole run (18 data sets) was completed in a time interval of less than one hour. After each change in the cooling water flow rate, the system pressure changed slightly. In order to keep this system pressure nearly constant, it was necessary to adjust the flow rate through the auxiliary condenser.

During the early stages of this experiment, it was observed that the thermocouple readings were disturbed by an external radio-frequency (RF) signal. This RF signal was generated by the special device used to control the power input to the boiler heaters. This device consisted of a silicon-controlled rectifier that chopped the input signal to obtain the necessary electrical power, while the chopped portion was emitted as an RF signal. This RF signal caused, for example, the steam temperature to fluctuate within ±4 K, while the thermopile readings fluctuated within ±0.5 K (note that the thermopile readings measuring temperature rise of cooling water can be as low as 0.5 K). To alleviate these problems, all thermocouples were shielded against the RF signal using braided copper cables. This substantially reduced the temperature fluctuations. For example, after the shielding was installed, the thermopile readings fluctuated less than ±0.04 K. Further efforts revealed that the small fluctuations which persisted were due to the presence of a cable that carried an indication of the voltage to the boiler heaters. This voltage is of "DC" type and it was fed to the data acquisition system. Unfortunately, this voltage was not truly DC; instead it consisted of the RF disturbances described earlier. When this cable was disconnected, absolutely no fluctuations were observed. Thus, a switch was added on this cable to disconnect the source of the RF signal while thermocouple readings were being recorded. Software was modified to gather all thermocouple readings while this switch was turned off. When the computer was ready to 'read' the voltage to the boiler heaters, the program was coded to 'pause' and then remind the operator to turn on the switch. Immediately after taking this reading, the computer reminds the operator to turn off this switch again.

The appearance of the condensate film was regularly observed through the viewport. In the event the condensate film appeared to be patchy, the data run was discontinued and the data already collected were discarded. During some runs, the film appeared to be totally filmwise, but the final data set indicated a condensing coefficient up to 10 percent greater than the value for the initial data point. Recall that the initial and final data sets were for the same cooling water flow rate. It is worth noticing that it was easier to obtain filmwise condensation under vacuum conditions than at near-atmospheric pressures. This is probably due to lower vapor velocities associated with atmospheric runs (2 m/s for vacuum and 1 m/s for atmospheric conditions). All the data presented in this thesis showed less than ±5 percent disagreement in condensing coefficient between initial and final data sets.

A. THE DROPWISE CONDENSATION PROBLEM

The main objective of this thesis effort was to take data under strict filmwise condensation conditions using copper tubes. Pure copper has low wettability with water in the presence of a minute contamination; thus, it has the tendency to condense steam under the dropwise mode. Such a minute contamination is generally difficult to avoid. A slightly hydrophobic surface condition can lead to very false conclusions since the dropwise condensation mode of heat transfer is much more effective than the filmwise mode.

In the first stage of this thesis effort, the tubes were prepared following the procedure recommended by Poole [Ref. 13]. This procedure included the cleaning of tubes with a mixture of sodium hydroxide and ethyl alcohol (equal amounts by mass) at a temperature of about 80 °C. This procedure was soon proven inadequate as the copper tube showed partial dropwise condensation within 20 minutes. This was verified during a four-hour endurance test. The water flow rate was held constant and every 30 minutes the temperature rise of the cooling water was recorded. This rise continuously increased and gradually the condensation changed to the dropwise mode.

As a solution to this problem, it was decided to oxidize the tube surface more thoroughly using the above-mentioned mixture (50 percent) aqueous sodium hydroxide mixed with an equal part of ethyl alcohol). The tube was painted with this mixture and was then heated with steam for about an hour with no water flowing inside the tube. This process resulted in the formation of a dark oxide layer on the copper surface, which had high wetting characteristics and an insignificant thermal resistance. After the oxidation, new endurance tests were made. For a time period of three hours, the cooling water temperature rise was essentially unchanged, while the condensate film appearance was excellent. Steam-side coefficients obtained with and without oxidation agreed to within ±2 percent. This was probably due to the avoidance of even minute areas undergoing dropwise condensation.

The most significant achievement of this oxidation was the reduction of data scattering (less than ±1 percent), and the very good repeatability of similar runs (within ±3 percent).

B. VAPOR VELOCITY LIMITATIONS

The major assumption in the Nusselt theory is that the vapor velocity does not induce shear forces on the vapor-liquid interface. This assumption is not realistic in practice. In order to regulate the pressure in the test section, it is necessary to have some steam condensed in the auxiliary condenser. This means that there must be steam flow into the auxiliary condenser. The steam flow rate (i.e., the vapor velocity) is a function of the power input to the heaters. In order to achieve low vapor velocities, the power input should be decreased. At low pressures, however, it was evident that the fluctuation of system pressure increased with a decrease in boiler power. This fluctuation was due to the intermittent breakup of vapor bubbles on the water-vapor interface in the boiler. Surprisingly, this small fluctuation in system pressure, and hence vapor velocity, reflected in the cooling water outlet temperature. To minimize this fluctuation, a vapor velocity of approximately 2 m/s past the tube was selected for vacuum runs. For the atmospheric runs (maximum power input), the cooling water outlet temperature fluctuation was less than ±0.005 K, while for the vacuum runs (half of maximum power input), the fluctuation was less than ±0.05 K.

A low vapor velocity is also undesirable from the filmwise point of view. When the vapor flow is low, then the condensation rate decreases and the film can very easily break, resulting in a change of the condensation mode. Once the film has broken, there is no possibility for the tube to resume the filmwise mode. Also, when the vapor velocity is high, there is a very strong wash-off effect on the tube, resulting in the reduction in the tendency of the tube to change the condensation mode.

It was decided to use 2 m/s and 1 m/s vapor velocities for the vacuum and atmospheric runs respectively. These velocities are considered much smaller than the actual ones in condensers. However, due to the limited power input, the 1.0 m/s used for the atmospheric runs was indeed the maximum possible. For the vacuum runs, the 2.0 m/s vapor velocity was achieved by using half of the available power. Some attempts were made to increase the vapor velocity to 4.0 m/s, but it was considered unsafe due to the violent and rapid explosions of the vapor bubbles in the boiler.

IV. DATA REDUCTION

During this thesis effort, all the programs, including property functions and the calibration curves for the cooling water flowmeter and for all thermocouples, were carefully checked. Only a very few minor corrections had to be made. The programs have the following noteworthy features:

1. In order to obtain a meaningful mixing-cup temperature at the coolant outlet, a mixing chamber was provided at the outlet as shown in Figure 2.2. As also discussed by Poole [Ref. 13], the considerable pressure drop created by this mixing chamber introduced a temperature rise in the cooling water. With no steam condensation taking place, the coolant temperature rise was measured for various water velocities. The results were plotted as shown in Figure 4.1. When taking condensation data, the coolant temperature rise was corrected by subtracting the temperature rise due to this frictional heating at the mixing chamber. For this purpose, the least-squares line shown in Figure 4.1 was used.

2. The smooth end sections of the tube, which were necessary to hold the tube in place (see Figure 2.2), were acting as axial fins. Since copper has a very large thermal conductivity, axial heat conduction occurred. This heat conduction was incorporated into the data reduction process by computing the fin efficiency of the smooth end sections of the tube.

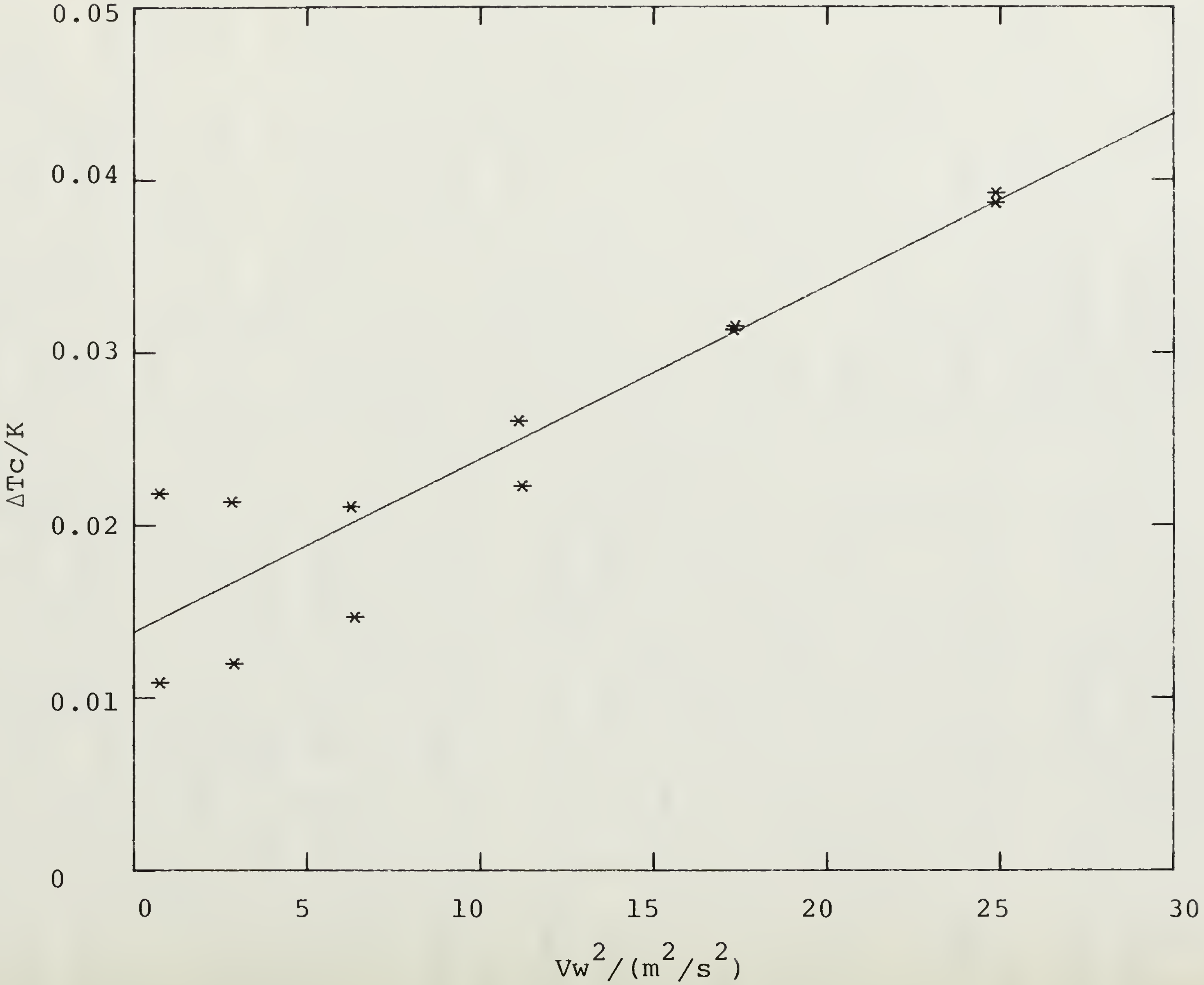

Figure 4.1. Mixing Chamber Calibration Curve

3. The tap water temperature changes considerably depend-on the season: it is about 15 °C in winter and about 22 °C in summer. Because of these changes, it was necessary to incorporate water property variations in calibrating the flowmeter. For this purpose, the following function was used, as done so in [Ref. 15], to calculate a correction factor for viscosity changes.

$$C_f = 1.0365 - 1.9644(10^{-3})Tin + 5.25(10^{-6})Tin^2 \qquad (4.1)$$

The value of the above function at the time of flowmeter calibration (i.e., at Tin = 22.0 °C) was 0.995. Thus, in order to obtain the actual mass flow rate for an inlet temperature of Tin, the following equation was used:

$$\dot{m}_{act} = \dot{m}_{calc} \frac{C_f}{0.995} \qquad (4.2)$$

The major steps for the data-reduction programs are listed below.

A. PROGRAM SIEDER

This program calculates the constants of the Sieder-Tate type equation from the instrumented-tube data.

1. Read the cooling water inlet and outlet temperatures and compute the average temperature.

2. Read the six wall thermocouples and compute the average wall temperature.

3. Convert the water volume flowmeter setting to mass flow rate by dividing the volumetric water flow rate with the water velocity.

4. From continuity, compute the cooling water velocity.

5. Correct the outlet water temperature for the mixing chamber effect and then re-compute the average temperature.

6. Compute the amount of heat transferred to the cooling water.

7. Compute the wall thermal resistance and then find the inner wall temperature (from step 2, the average temperature at the radial location of the thermocouples, is known).

8. Compute the log-mean-temperature difference.

9. Compute the efficiency of the left and right tube extensions.

10. Compute the inside heat-transfer coefficient.

11. Compute the Nusselt number.

12. Compute the leading constant of the Sieder-Tate coefficient for this data set.

13. Repeat steps 1 to 12 for all the data sets of the run.

14. Make a least-squares straight line fitting of the form:

$$Nu = C\ Re^{0.8}\ Pr^{1/3}\ \left(\frac{\mu_c}{\mu_w}\right)^{0.14} + B \qquad (4.3)$$

The C is the unknown leading constant, while B is an additional constant found to give an improved fitting.

B. MODIFIED WILSON PLOT PROGRAM

This program calculates the leading constant of the Sieder-Tate equation from the smooth-tube data.

1. Assume a value for the leading constant of the Sieder-Tate equation.

2. Make the steps 1, 3, 4 and 5 of previous program "SIEDER."

3. Compute the heat flux from the specific heat of water, the mass flow rate, the cooling water temperature difference and the outside tube surface.

4. Compute the log-mean-temperature difference between the steam temperature and the inlet and outlet cooling water temperatures.

5. Compute the overall heat-transfer coefficient.

6. Assume an outer tube surface temperature in order to determine the film temperature for the evaluation of condensate properties.

7. Calculate the outside heat-transfer coefficient by using the Nusselt equation.

8. Compute the outer tube surface temperature.

9. Iterate between steps 7 and 8 until two successive outer surface wall temperatures are within ±1 percent.

10. Assume a viscosity correction factor for the Sieder-Tate equation.

11. Compute the fin efficiency of the extending parts of the tube.

12. Compute the inside heat-transfer coefficient.

13. Compute the inner surface temperature in order to find the film temperature on the coolant side.

14. Compute the viscosity correction factor and iterate between steps 11 through 14 until two successive viscosity correction factors are within ±1 percent.

15. Compute the new Sieder-Tate coefficient and iterate between steps 2 through 15 until two successive Sieder-Tate coefficients are within ±0.5 percent.

16. Compute the Sieder-Tate coefficient for all the data sets of the run.

17. Make a least square straight line fitting to establish the final leading constant that satisfies all the data sets.

C. MAIN DATA REDUCTION PROGRAM (DRP4)

This program was used for computing the condensing heat-transfer coefficient for both finned and smooth tubes.

1. Make steps 1 through 5 of program "SIEDER."

2. Compute the log-mean temperature difference between the steam temperature, and the inlet and outlet cooling water temperatures.

3. Compute the heat flux.

4. Compute the overall heat-transfer coefficient.

5. Compute the wall conduction resistance.

6. Compute the inside heat-transfer coefficient.

7. Compute the condensing heat-transfer coefficient by subtracting the wall and the inside resistances from the overall resistance.

V. RESULTS AND DISCUSSION

Numerous data runs were made using the procedures described in Chapter III. Each tube was tested at least three times, on different days, in order to obtain repeatable results. Data were taken for all the tubes at both near-atmospheric and vacuum (85 mmHg, 1.7 psia) conditions. Complete filmwise condensation was maintained for the data runs and the mass concentration of non-condensing gases was held between 0.0 and -1.5 percent during all the testings. The negative value was indicative of either a slight superheat or an inaccurate manometer reading. It was estimated that an error of ±0.2 K in steam temperature or an error of 1.0 mmHg in system pressure translates into approximately ±1.2 percent error in the non-condensing gas concentration. Thus, the non-condensing gas concentration was essentially zero to within the accuracy of the measurements.

A. INSIDE HEAT-TRANSFER COEFFICIENT

1. Instrumented Tube Results

The instrumented tube was used to determine the inside heat-transfer coefficient mainly owning to the use of the insert to enhance the heat-transfer performance. By the use of the instrumented tube, the wall temperature was determined after averaging the six thermocouple readings. Therefore, the main assumption in the calculation of the inside heat-transfer coefficient is that the wall temperature profile is uniform. However, Figures 5.1 and 5.2 show the experimentally-measured temperature profiles around the tube, for the maximum and minimum cooling water flow rate settings, for the vacuum and near-atmospheric runs, respectively. It is obvious that the wall temperature profile is not uniform; therefore, this direct averaging procedure may introduce an uncertainty the magnitude of which is unknown. However, owing to the time constraint, further evaluation of this uncertainty was considered to be beyond the scope of this investigation. These figures also show least-squares-fit cosine curves of the form:

$$\frac{\Delta T}{\overline{\Delta T}} = 1 - a \cos \frac{\theta}{\pi} \qquad (5.1)$$

It is worth noticing that the temperature profile corresponding to the high heat flux is flatter than the profile corresponding to the low heat flux. Also, the temperature profile of the near-atmospheric run is flatter than the temperature profile of the vacuum run. It is concluded that as the heat flux increases, hi increases, hence ho/hi decreases and the temperature profile becomes more uniform; therefore, the assumption of an isothermal wall becomes more reasonable. This is one more reason why the internal enhancement (use of insert) improves the accuracy of the data.

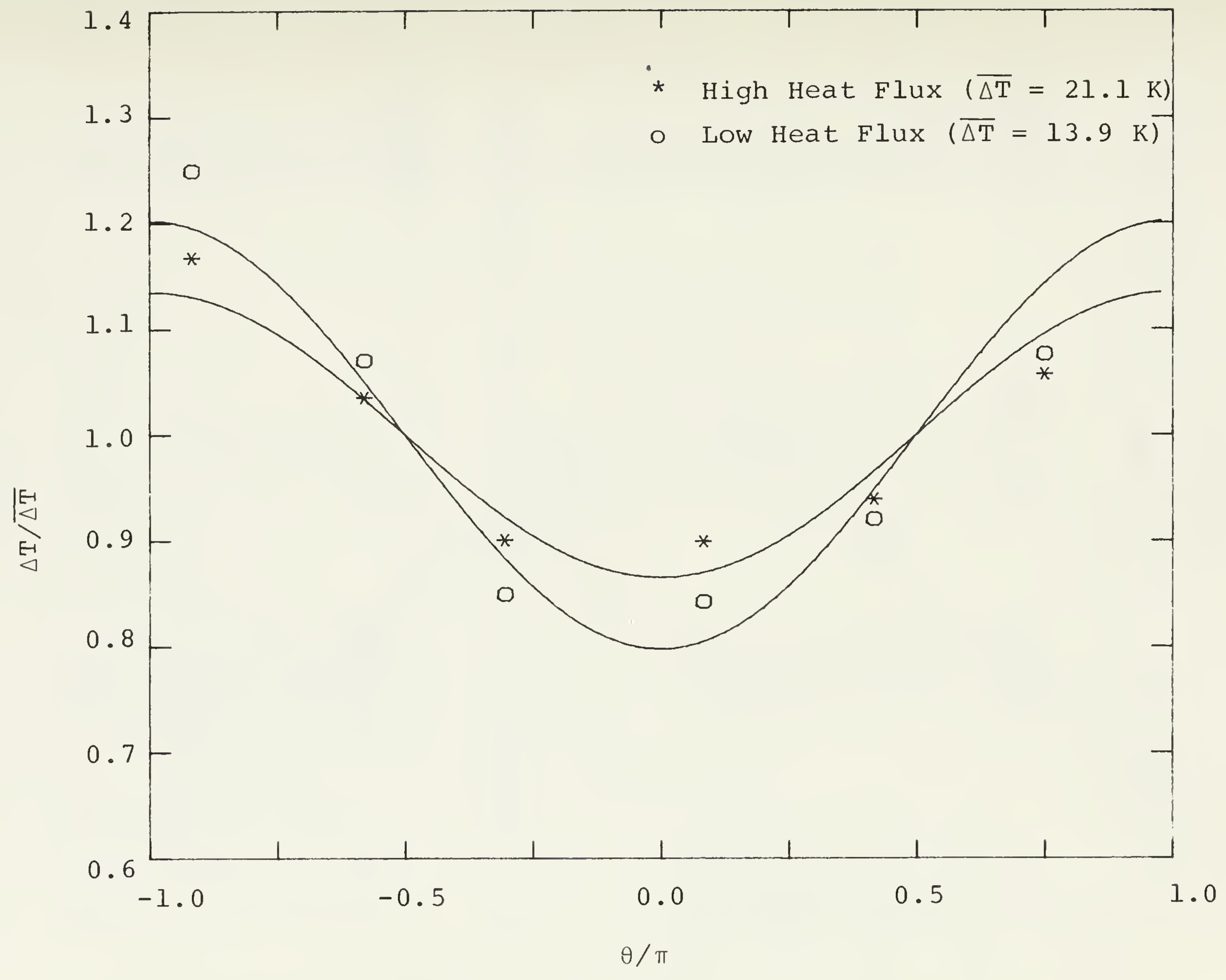

Figure 5.1. Temperature Distribution for Instrumented Tube (Vacuum Run)

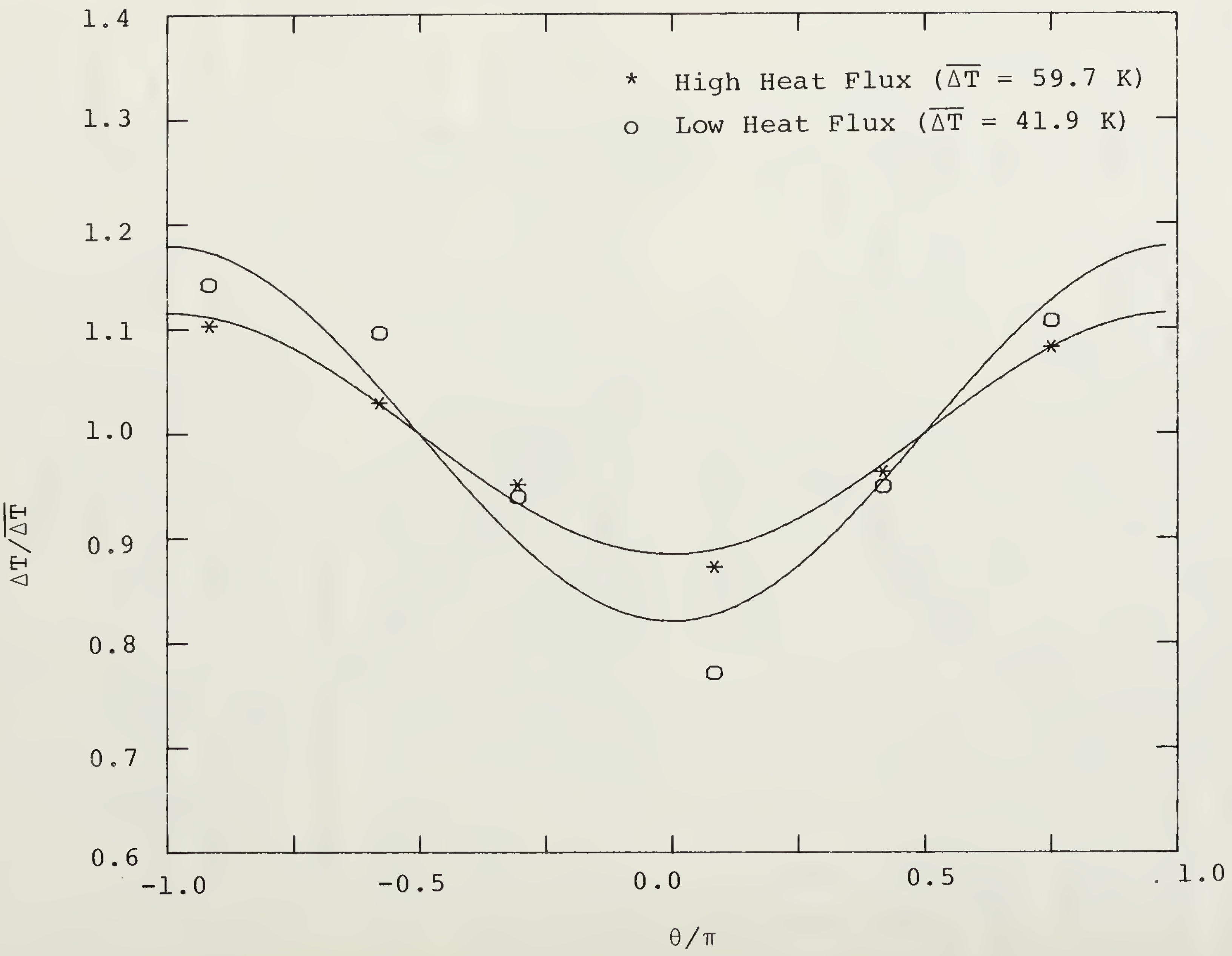

Figure 5.2. Temperature Distribution for Instrumented Tube (Atmospheric Run)

Tables II and III give the values of the amplitude of the cosine fit for all data points taken, under both pressure conditions.

TABLE II

Instrumented Tube Results for the Vaccum Run

Heat Flux (MW/m^2)	ho ($kW/m^2.K$)	ho/hi	a
0.209	10.89	0.301	0.135
0.207	11.28	0.348	0.142
0.199	11.45	0.430	0.158
0.191	11.61	0.507	0.168
0.184	11.76	0.567	0.178
0.173	12.05	0.692	0.185
0.160	12.09	0.832	0.202

TABLE III

Instrumented Tube Results for the Atmospheric Run

Heat Flux (MW/m^2)	ho ($kW/m^2.K$)	ho/hi	a
0.488	9.18	0.201	0.115
0.486	9.19	0.221	0.119
0.479	9.25	0.249	0.133
0.462	9.38	0.289	0.137
0.447	9.49	0.346	0.149
0.417	9.75	0.437	0.164
0.384	10.05	0.585	0.179

Also the same tables contain additional information about the heat flux, the outside heat-transfer coefficient and the ratio of outside to inside heat-transfer coefficients for all the cooling water flow rate settings.

By using the average reading of all thermocouples for the wall temperature, the complete form of the Sieder-Tate-type equation was determined to be:

$$Nu = 0.0635\ Re^{0.8}\ Pr^{1/3}\ \left(\frac{\mu_c}{\mu_w}\right)^{0.14} + 26.4 \qquad (5.2)$$

The constant B = 26.4 is an additional constant found to improve the fitting. Note that the leading coefficient is about 2.5 times greater than the well-known Sieder-Tate coefficient of 0.027 [Ref. 16] for plain tubes. This significant difference is mainly due to the coiled insert used to boost the inside heat-transfer coefficient. A discussion of the advantages and disadvantages of the coiled insert was given in Chapter II, Section G. Figure 5.3 shows the data points for both pressure conditions together with a fit of equation (5.2).

It is worth mentioning that the use of thermocouples to determine the wall temperature may introduce yet another uncertainty (in addition to the incorrect averaging mentioned earlier) in the measurement of each local wall temperature. This is due to the completely different thermal conductivity of the wall area in the immediate vicinity of the thermocouple

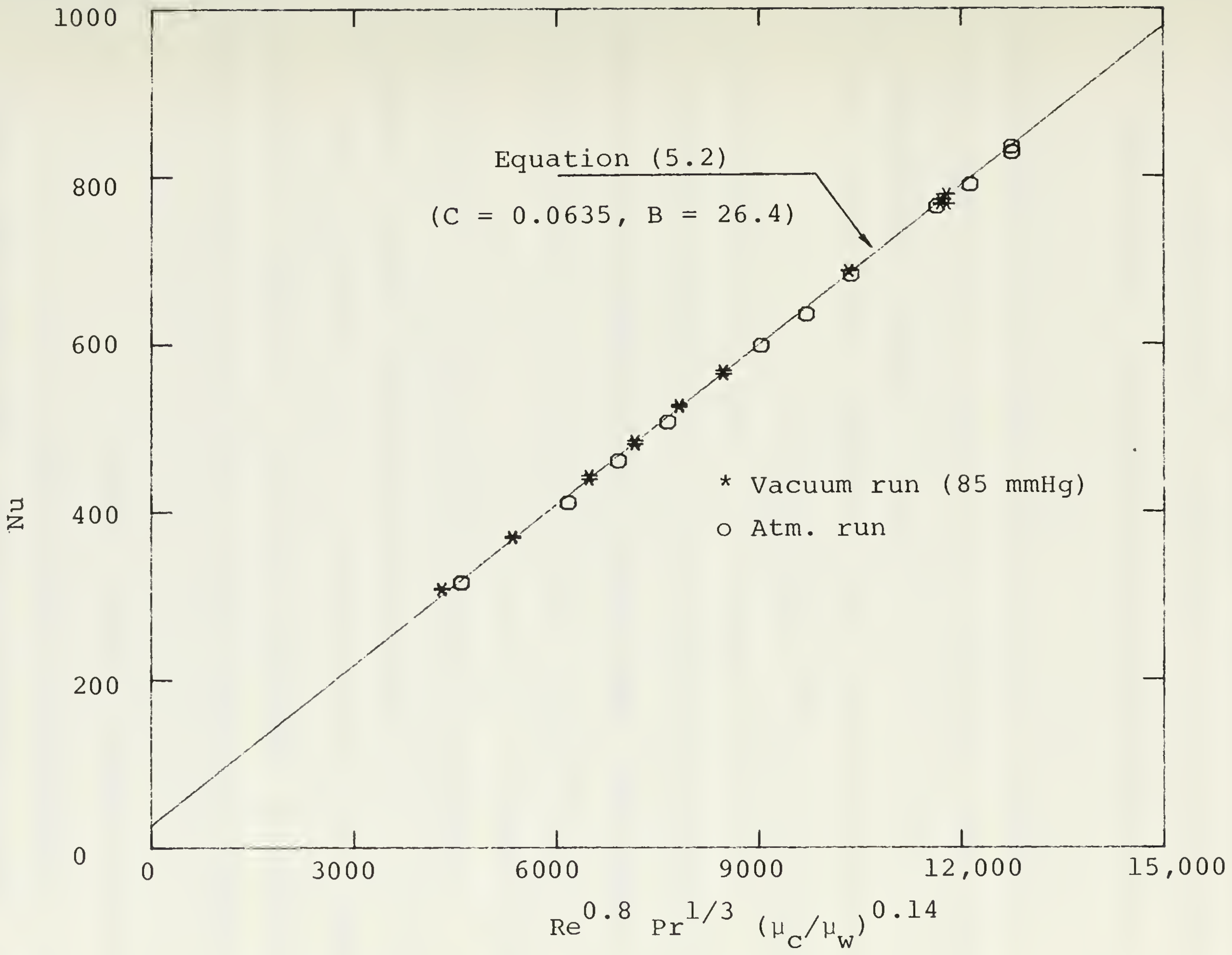

Figure 5.3. Correlation of the Water-Side Coefficient Obtained with Instrumented Smooth Tube

hot junction. For example, the thermocouple wires are covered with plastic; therefore, they present a low thermal conductivity. Also, in order to embed the thermocouple, there must be sufficient clearance, which certainly presents an additional thermal resistance to the heat flow.

The advantages of the use of the instrumented tube are:

1. It does not depend on other theoretical formulations that may have unavoidable errors owing to the assumptions made to formulate the problem (for example, the Modified Wilson Plot technique uses the Nusselt-type equation for the outside heat-transfer coefficient).

2. It is not too sensitive to vapor shear effects since these effects are lumped into the thermocouple readings (i.e., the vapor shear reduces the thickness of the condensate layer; therefore, the thermocouples would give higher temperatures).

A computer program, named "SIEDER," was written to reduce the data taken on the instrumented tube. For completeness, the raw data taken on the instrumented tube for both pressure conditions are given in Appendix C, Table VI. Hereinafter, the data reduction method that uses the instrumented tube water-side heat-transfer coefficient will be referred to as the "Direct" method.

2. Uninstrumented Tube Results

The uninstrumented smooth-tube data were used to determine the inside heat-transfer coefficient by the use of the modified Wilson plot technique. Hereinafter, this technique will be referred to as the "Wilson" method. Also the smooth tube results concerning the outside heat-transfer coefficient were used as a basis for comparison with the finned-tube results.

The analysis procedures used for the Wilson method is the same as that given in [Ref. 17]. While a Sieder-Tate-type equation was used to represent the inside heat-transfer coefficient, a Nusselt type expression was used for the outside coefficient as given by:

$$h_o = \alpha\left[\frac{k_f^3 \rho_f (\rho_f - \rho_v) h_{fg}}{\mu_f D_o q}\right]^{1/3} \tag{5.3}$$

where α is a disposable constant that must be found iteratively. Note that with zero vapor velocity, the Nusselt prediction results in a value of 0.655 for α. However, since it is impossible to obtain zero vapor velocity, a higher value is generally obtained. During this work, an approximate value of 0.72 was obtained for α.

A computer program, named "WILSON," was written to run the Wilson method on the smooth-tube data. A total of four runs (two each under vacuum and at near-atmospheric pressures) were made. These runs resulted in values of the Sieder-Tate coefficient of 0.0716, 0.0714, 0.0700 and 0.0708, with an average value of 0.071. This value is about 10 percent higher than the value found with the instrumented tube; i.e., the Wilson method results in a 10 percent smaller water-side resistance (less conservative) than the resistance predicted by the use of the instrumented tube. Again for completeness, the raw data taken on the uninstrumented tube under both pressure conditions are given in Appendix C, Table V.

3. Summary of the Inside Heat-Transfer Coefficient

In order to compare the two above-mentioned methods (Direct and Wilson), the data taken on a smooth tube under vacuum conditions were reduced to yield the outside heat-transfer coefficients using the water-side coefficients derived by each method. For this purpose, these data were plotted in Figure 5.4 together with the original Nusselt equation for a single horizontal tube, re-written in terms of the indicated non-dimensionalized terms:

$$\frac{Nu_s}{\tilde{Re}^{0.5}} = 0.725 \ F^{1/5} \qquad (5.4)$$

Also shown in this figure is the correlation of Fujii, et al [Ref. 18]:

$$\frac{Nu_s}{\tilde{Re}^{0.5}} = 0.96 \ F^{1/5} \qquad (5.5)$$

The Fujii et al. correlation is based on numerous data taken on tube bundles in both in-line and staggered arrangements. It can be seen that the coefficient on the right-hand

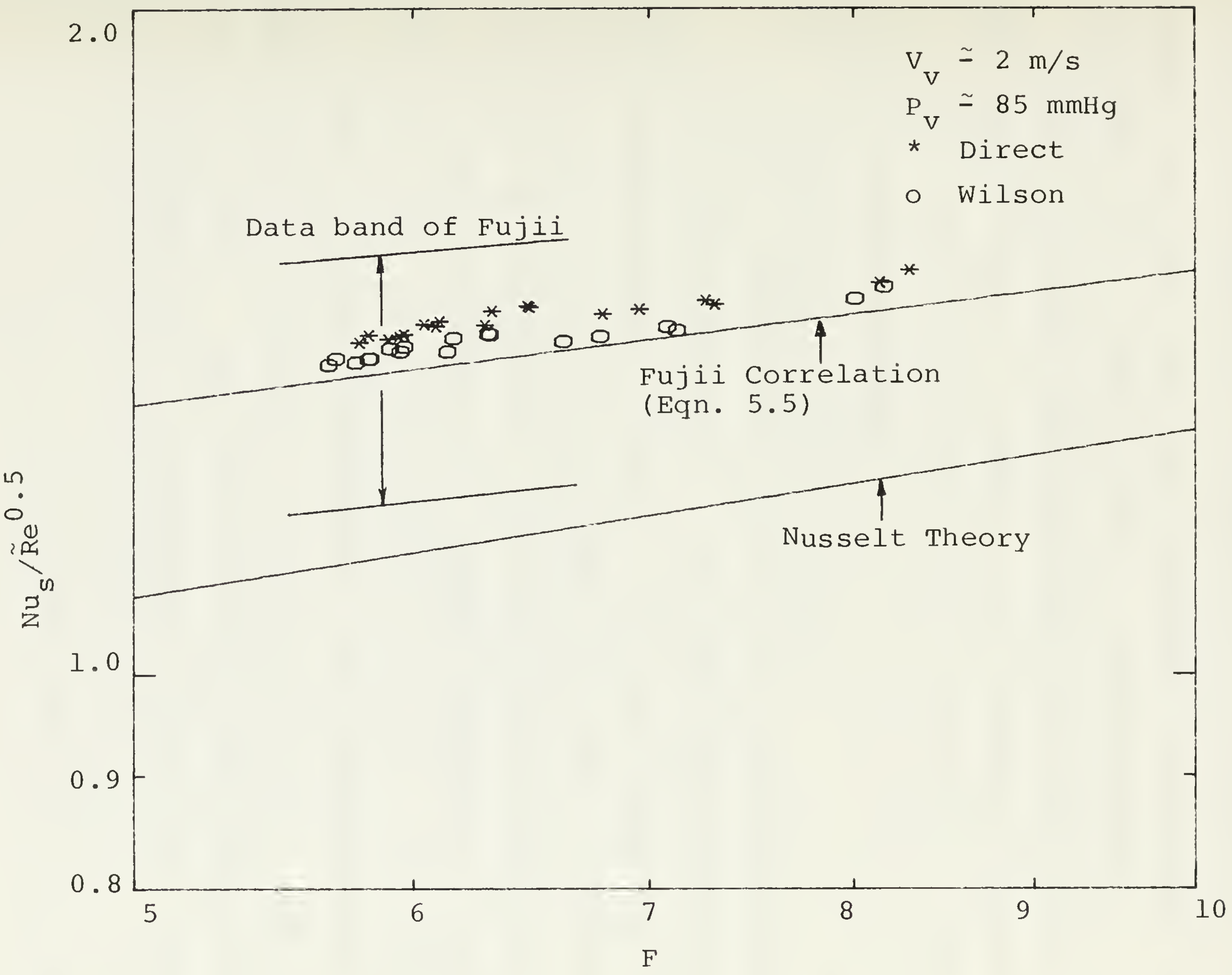

Figure 5.4. Comparison of Smooth-Tube Data with Fujii Correlation

side of equation (5.5) is larger than the value in equation (5.4) owing to the presence of vapor shear (recall that the Nusselt equation is derived for zero-vapor-shear conditions). For completeness, the error bands of the data used for this correlation are also shown.

Note in Figure 5.4 that the data of this investigation on the smooth tube are slightly higher than those predicted by equation (5.5). Also, it is worth noting that the use of the Wilson method results in data that are in better agreement with the Fujii correlation than the data given by the use of the Direct method. Thus, with an appropriate function for the outside heat-transfer coefficient and accurate smooth-tube data, the modified Wilson plot technique appears to offer a satisfactory and simple method for obtaining the inside heat-transfer correlation. However, since the error band of the Fujii correlation is much wider than the disagreement between this correlation and the present data, it may be unwise to draw any conclusions as to the accuracy of these two methods (Direct or Wilson). As a result, it is not possible to say which method of measuring the inside heat-transfer coefficient is more accurate. However, except where noted below, all the outside heat-transfer coefficients obtained in this thesis were calculated using the Direct method.

B. PERFORMANCE OF FINNED TUBES

Data were taken for the finned tubes given by Table I, under vacuum (85 mmHg) and at near-atmospheric pressures with vapor velocities of 2 m/s and 1 m/s respectively. The computed steam-side coefficient was based on the smooth tube outside area (i.e., the area if the fins were machined off).

The data reductions were performed using the program named "DRP4." This is a revised version of the program (DRP2) used by Poole [Ref. 13]. The raw data taken on finned tubes are presented in Appendix D.

1. Condensation on Fins in General

Figure 5.5 shows the variation of heat flux with the steam-side temperature drop for a set of five finned tubes under vacuum conditions. Both the thickness and height of the fins were 1.0 mm, while the spacings were 0.5, 1.0, 1.5, 2.0 and 4.0 mm. Notice that the slope of the curves increases with fin spacing up to the point where the optimum spacing (1.5 mm) is reached and then the slope decreases with further increase in fin spacing. This means that the enhancement of the condensation process is highly dependent on the fin spacing. The data were fitted with least-squares curves using the following relation:

$$q = a\,\overline{\Delta T}^{b} , \tag{5.6}$$

and $\overline{\Delta T}$ was computed by using the following relation:

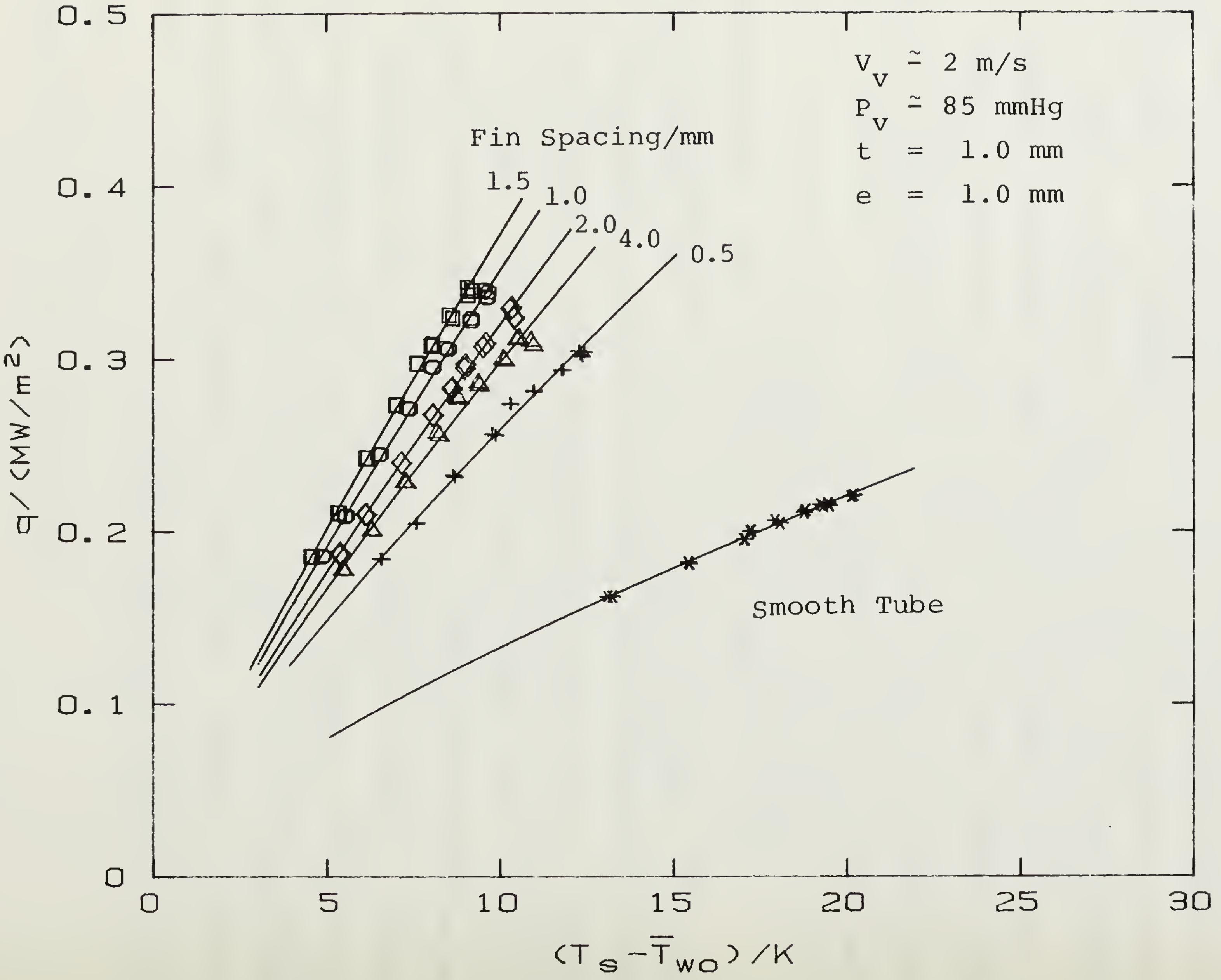

Figure 5.5. Variation of Heat Flux with Steam-Side Temperature Drop

$$q = h_o \overline{\Delta T} \tag{5.7}$$

where q was measured experimentally, while h_o was obtained by subtracting inside and wall resistances from the measured overall resistance. From equation (5.6), it is possible to calculate the heat flux for any temperature difference between the steam and the tube wall when the constants a and b are known.

Table IV gives the values of a and b for all the tubes tested for both pressure conditions. Notice that the value of the constant a has almost the same range for all the finned tested tubes for both pressure conditions. The values of both constants a and b increase as the fin spacing increases up to the spacing of 1.5 mm (it will be shown later that this is the optimum spacing) and then they decrease. The range of the exponent b is different between the vacuum and near-atmospheric runs; i.e., the range for the vacuum runs is 0.76 to 0.89, while for the near-atmospheric runs it is 0.87 to 0.94.

Figure 5.6 shows a relative plot of the outside condensing coefficient for the same set of tubes just described. For comparison purposes, the smooth-tube data and the Nusselt prediction are plotted on the same figure. All tubes tested show good enhancement over the smooth tube. It is worth noticing that even the smooth tube results are higher than the Nusselt prediction; this is mainly

TABLE IV

Constants of Equation (5.6) for All Tested Tubes

Tube			VACUUM RUNS		ATMOSPHERIC RUNS	
s (mm)	t (mm)	e (mm)	a	b	a	b
Plain			24476	0.7338	27837	0.7254
0.5	1.0	1.0	40536	0.8045	42178	0.9147
1.0	1.0	1.0	46364	0.8780	45716	0.9385
1.5	1.0	1.0	48280	0.8854	51164	0.9280
2.0	1.0	1.0	44157	0.8588	43294	0.9375
4.0	1.0	1.0	43123	0.8380	44345	0.8835
0.5	0.75	1.0	47556	0.7808	41621	0.9357
1.0	0.75	1.0	49167	0.8118	49313	0.9175
1.5	0.75	1.0	55912	0.7926	47902	0.9472
2.0	0.75	1.0	53905	0.7908	48853	0.9314
4.0	0.75	1.0	51081	0.7869	44132	0.8837
0.5	0.5	1.0	45461	0.7772	41221	0.9307
1.0	0.5	1.0	48863	0.7970	46422	0.9162
1.5	0.5	1.0	51298	0.8085	48595	0.9336
2.0	0.5	1.0	50841	0.7990	46221	0.9275
4.0	0.5	1.0	44050	0.7621	41954	0.8788
1.0	1.0	2.0	51989	0.8722	51391	0.9346
1.5	1.0	2.0	56091	0.8917	56529	0.9339
2.0	1.0	2.0	55823	0.8799	55598	0.9300
4.0	1.0	2.0	46376	0.8736	45563	0.9208
1.0	1.5	1.0	42655	0.8740	47814	0.8988
1.25	1.25	1.0	48005	0.8594	51914	0.8957

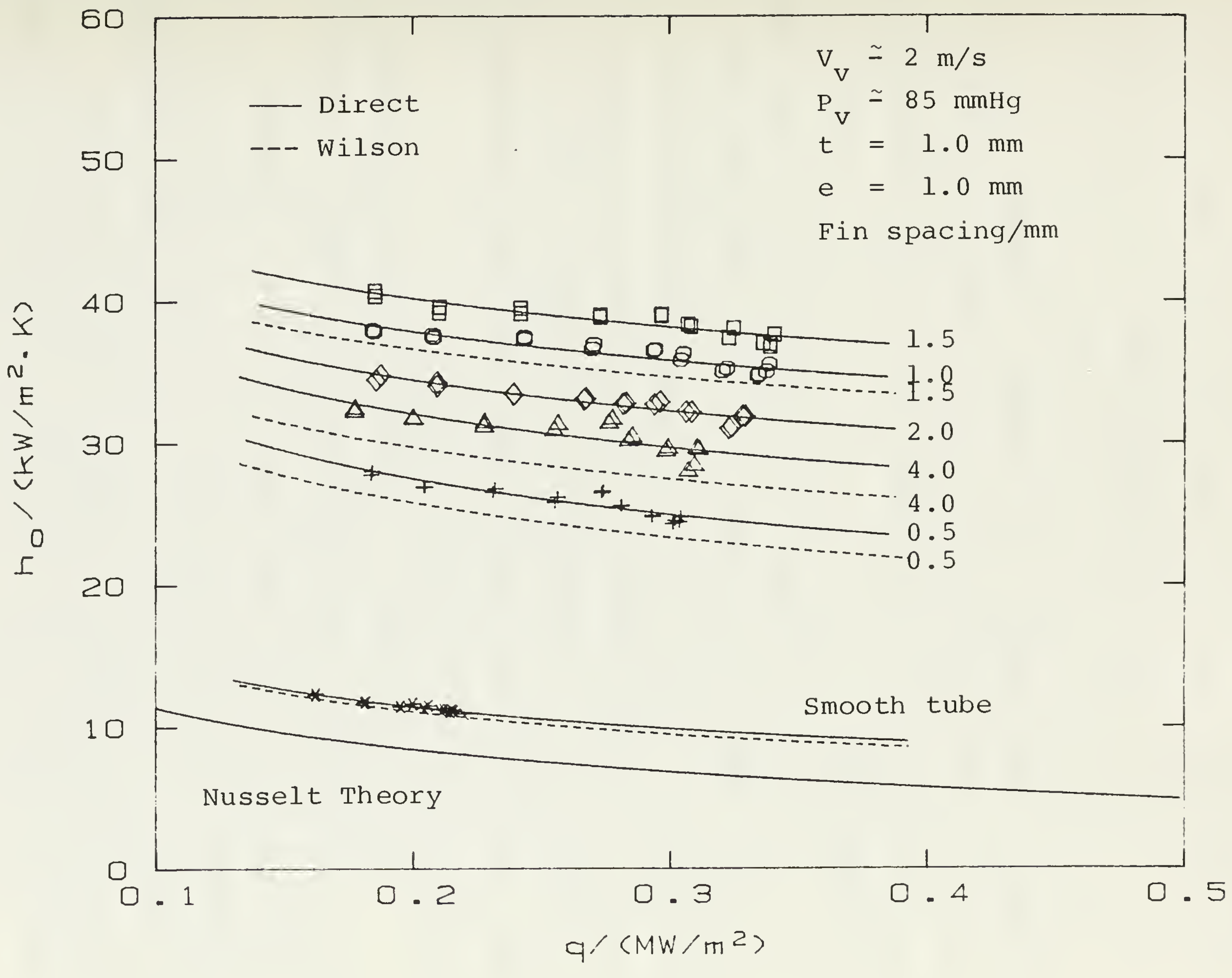

Figure 5.6. Variation of Condensing Heat-Transfer Coefficient with Heat Flux

attributable to Nusselt's conservative assumption which neglects vapor shear.

Combining equations (5.6) and (5.7), h_o can be written as:

$$h_o = a^{1/b} q^{(b-1)/b} \tag{5.8}$$

It appears that equation (5.8) results in curves almost parallel to the Nusselt prediction, indicating that the effect of heat flux is the same on the finned surface as on the smooth tube.

On the above figure, the dotted lines represent the fittings of the data when the data were processed by the Wilson method. Notice that the condensing coefficients given by the Wilson method are lower by about 10 percent than those given by the Direct method (recall that the water-side resistance given by the Direct method is higher than that given by the Wilson method).

It is also shown in the above figure that as the heat flux decreases, the vapor-side heat-transfer coefficient increases. Note that there is about a 10 percent difference between the high and the low heat flux results. The reason for this increase is that, as the flux decreases, the condensate thickness decreases, resulting in less conduction resistance and improved heat-transfer coefficient.

2. Significance of Fin Spacing

This section presents results showing the variation of the condensing coefficient with heat flux, as well as the variation of heat flux with steam-side temperature drop for both pressure conditions, for the four sets of finned tubes. Figures 5.10 to 5.25 show that for all the fin thicknesses (i.e., 1.0, 0.75 and 0.5 mm) and for each of the fin heights (i.e., 1.0 and 2.0 mm), the best performance was obtained with the tubes of 1.5 mm fin spacing. This was true for both pressure conditions. The second best performance was given by the tubes with spacings of either 1.0 mm or 2.0 mm. The third best performance was given by the tubes with fin spacing of 4.0 mm and the tubes with a fin spacing of 0.5 mm showed the poorest performance. The performances of the last two tubes however were interchanged as the pressure conditions were changed from vacuum to near-atmospheric. An effort to explain this behavior will be made in the next sections, where the influence of the fin thickness and height on the heat-transfer performance is discussed.

As shown in Appendix E (Error Analysis), the error in the calculation of the condensing coefficient increases as the heat flux decreases. For this reason, the comparison of finned tubes should be done in the regime where the error is the minimum possible. This means that the data points corresponding to the high-heat-flux settings should be chosen. The comparison of the finned tubes is made through the enhancement ratio, which is defined to be the ratio of the outside heat-transfer coefficient of a finned tube to the smooth-tube value (both evaluated on the same heat flux). However, the capability of the smooth tube to remove heat is limited (see Figure 5.6 showing that the maximum heat flux on the smooth tube is only about 30 percent of the maximum heat flux on the best finned tube). Thus, it was necessary to extrapolate the smooth-tube data to higher heat fluxes in order to make the comparison of the finned tubes on an equal heat flux basis.

Choosing 0.35 and 1.0 MW/m^2 as reference heat fluxes for the vacuum and near-atmospheric runs, respectively, cross plots of the enhancement ratio versus the fin spacing are given in Figure 5.7 for the set of tubes with 1.0 mm fin thickness and height. It is shown that the optimum fin spacing found is 1.5 mm. The 0.5-mm fin spacing which provides the most area increment has one of the worst performances. This poor performance can be easily explained by the fact that the entire interfin area was covered by the condensate. Visual observations showed that the condensate retention angle was 180 degrees, which is also very well predicted by equation (1.12). The thermal resistance induced by this thick condensate layer deteriorates any benefit from increased area; therefore, the heat-transfer performance is highly reduced.

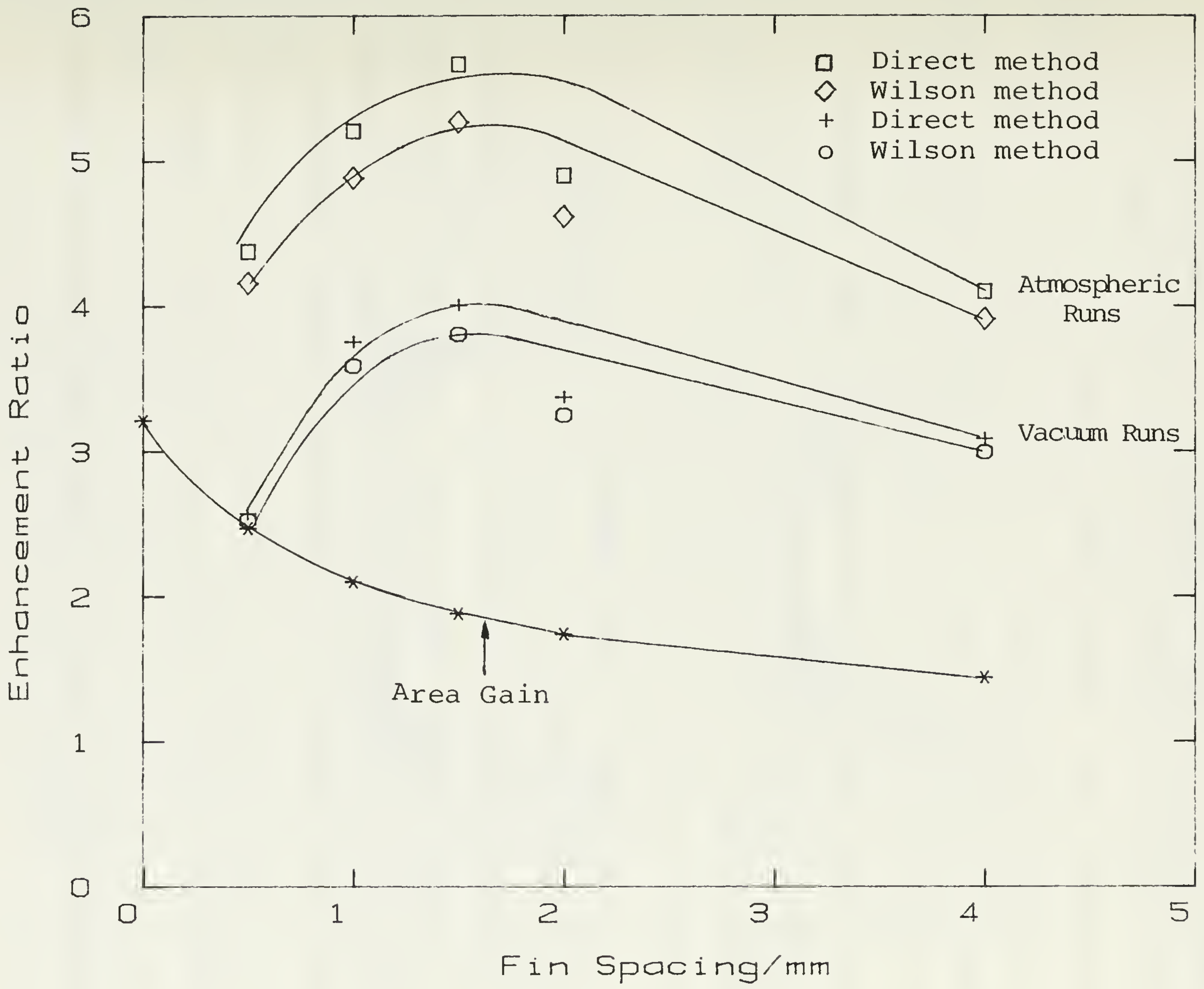

Figure 5.7. Cross Plot Showing Best Fin Spacing Among Tubes with t = 1 mm and e = 1 mm

As the fin spacing increased from 0.5 to 1.0 mm, the retention angle decreased and a miniscus in the interfin area at the top of the tube appeared (see Figure 5.8(a)). For the 1.0 mm fin spacing, the retention angle was about 110 degrees. The change of the flooding characteristics is the reason for the sudden increase of the enhancement ratio as the fin spacing changed from 0.5 to 1 mm. Visual observations showed that the optimum fin spacing (1.5 mm) resulted in a condensate film profile (in the interfin area at the top part of the tube) similar to that shown in Figure 5.8(b). Notice that the bottom of the miniscus is just touching the tube surface. When the fin spacing is further increased, the miniscus radius becomes larger and the retention angle reduces even more. At the 2.0 mm fin spacing, the miniscus is no longer an arc of a circle (see Figure 5.8(c)).

As mentioned in the beginning of this chapter, the condensing-coefficient calculation is based on the smooth tube external diameter; therefore, the effect of area addition is lumped together with all the other factors that may influence the heat-transfer process. In order to give some insight to the effect of all the other factors, the enhancement ratio was divided by the area gain (i.e., the ratio of the condensing area of finned tube to the area of smooth tube) of each finned tube in order to obtain the normalized enhancement ratio. Figure 5.9 shows this normalized enhancement ratio. It is clear that the enhancement is due to

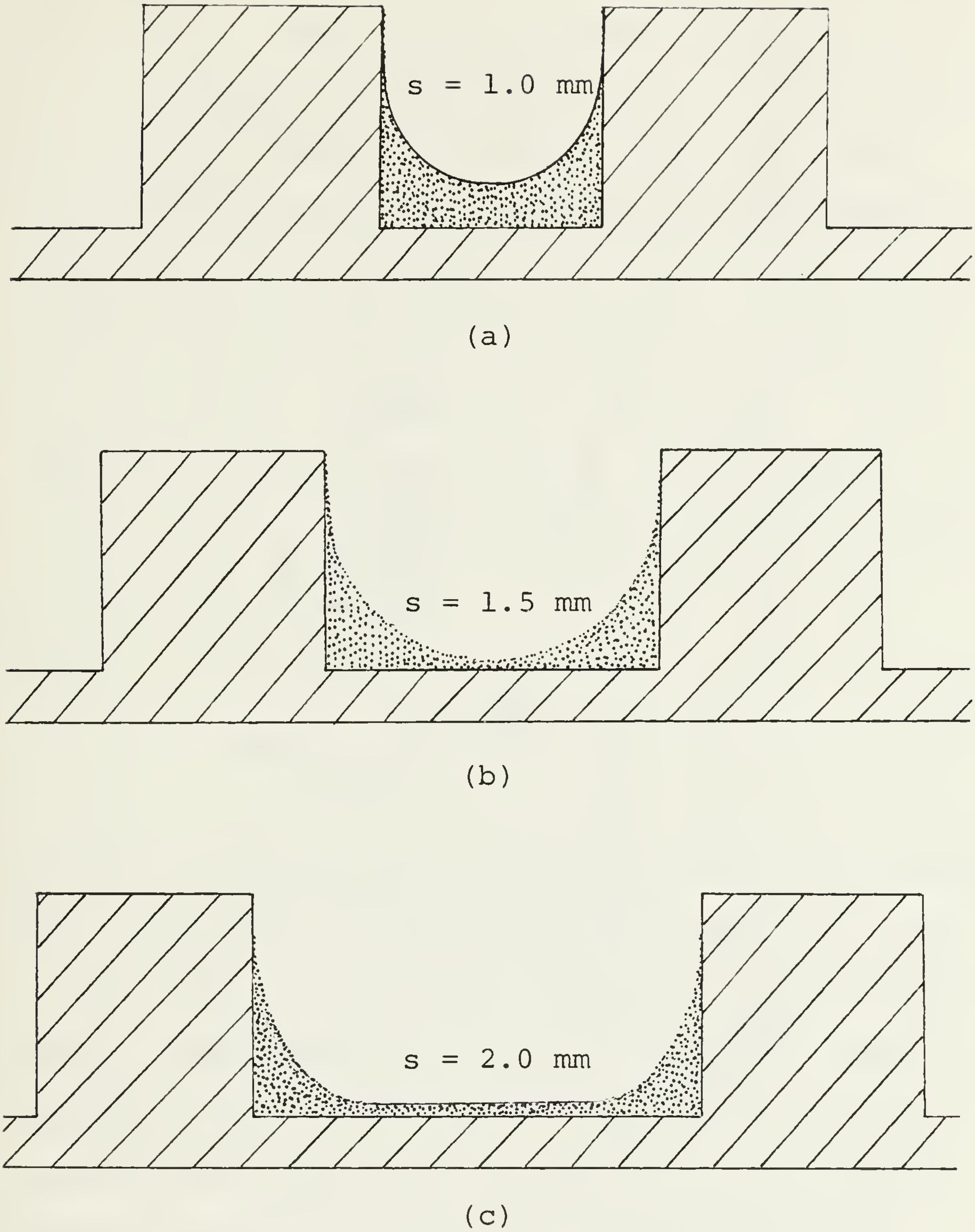
s = 1.0 mm
(a)
s = 1.5 mm
(b)
s = 2.0 mm
(c)

Figure 5.8. Miniscus Profile for Various Fin Spacings
(a) s = 1.0 mm, (b) s = 1.5 mm, (c) s = 2.0 mm

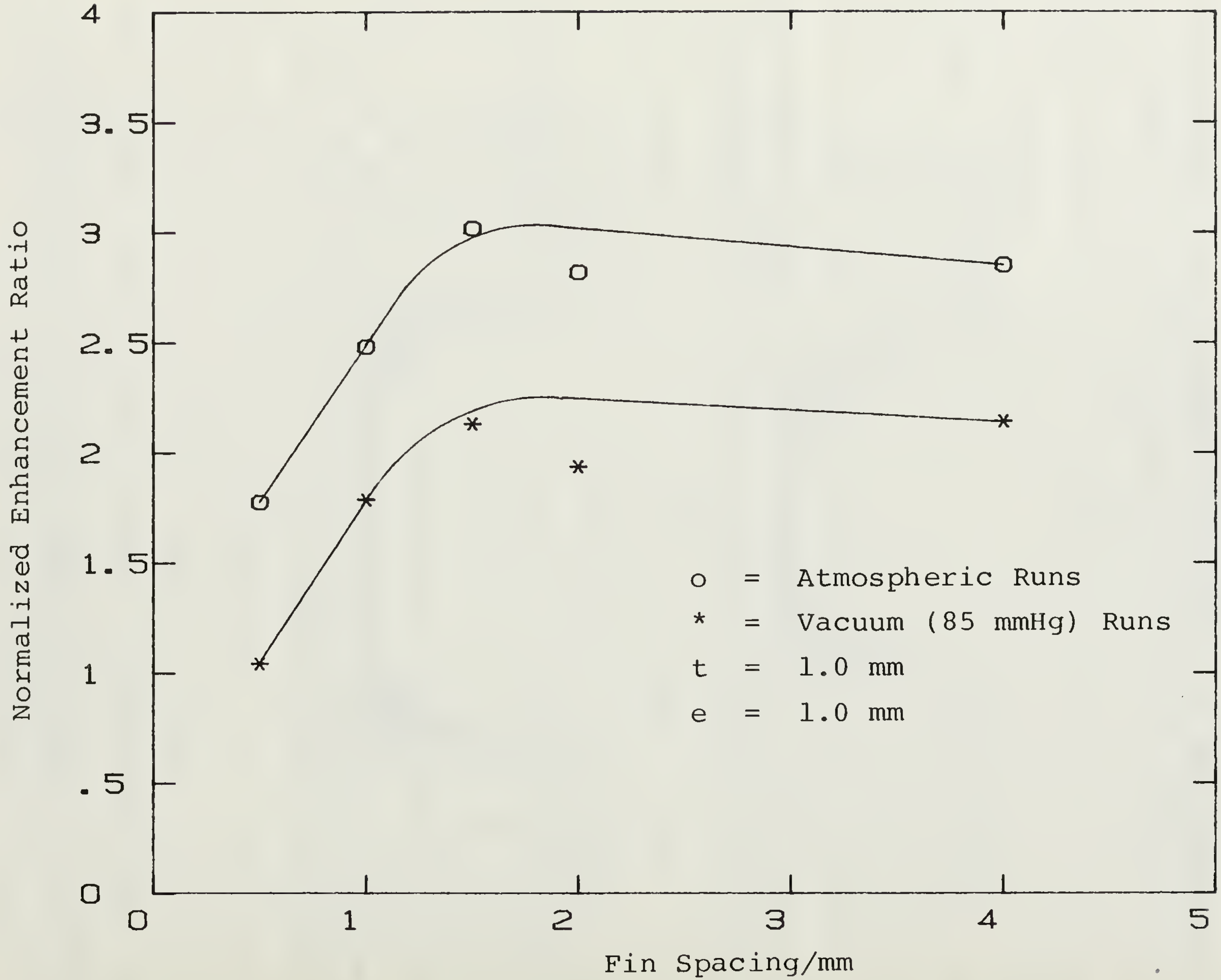

Figure 5.9. Normalized Enhancement Ratio Versus Fin Spacing for Tubes with Fins of t = 1.0 and e = 1.0 mm

more than just an area gain. This verifies the measurements of Yau et al. [Ref. 3], and an explanation for this behavior was presented in Chapter I. Also, Figure 5.9 shows that the normalized enhancement ratio increases as the spacing increases and that the rate of this effect gets smaller for fin spacings larger than 1.5 mm. This reduction is attributable to the fact that the pulling action (thinning effect) diminishes as the fins get further apart. Equation (5.9) gives that the pressure gradient between points C and B (see Figure 1.1) is inversely proportional to the increase of fin spacing (s).

$$\left.\frac{dP}{dx}\right)_{CB} \cong \frac{\Delta P_{CB}}{s/2} \tag{5.9}$$

Therefore, the thinning effect decreases as the fin spacing increases. It can be concluded that any assumption that neglects the surface-tension effect may not be realistic when modelling the steam condensation process on fins.

Careful observation of Figure 5.7 shows that the performance of the tubes of 0. 5 and 4.0-mm fin spacing interchanges between the vacuum and atmospheric runs, respectively. The heat that was removed during the vacuum runs was about three times smaller than the heat removed during the near-atmospheric runs; thus, the rate of condensate generation for the vacuum runs was three times smaller than for atmospheric runs. For all the vacuum runs, no matter which tube was used, the condensate flow pattern was invisible. During the near-atmospheric runs, the flow pattern was also invisible except for the tubes of 0.5 mm fin spacing. In these cases (0.5 mm fin spacing), the draining rate was very fast and ripples in the interfin space were clearly visible. If this is the case, then the convective action of the condensate layer should enhance the condensation process. After this observation, it became clear why the performance of the tubes with 0.5 mm spacing became better than the performance of the tubes with the 4.0 mm spacing, for the near-atmospheric runs.

As mentioned earlier, Honda and Nozu [Ref. 9] present a detailed comparison of various theoretical models to predict the condensing coefficient on finned tubes. All the models have the assumption that the inertia term in the momentum equation and the convective term in the energy equation can be neglected in comparison with the other terms. The author feels that the above assumption is realistic for all the fin spacings except those that correspond to completely flooded tubes. To further support this argument, the reader is referred to [Ref. 9] where comparison of the four models is presented with various experimental data, among which are the steam data given by Rose [Ref. 3]. Honda and Nozu show that the maximum disagreement between the data of Rose and predictions (all four models) is for the fin spacing of 0.5 mm (completely flooded tube).

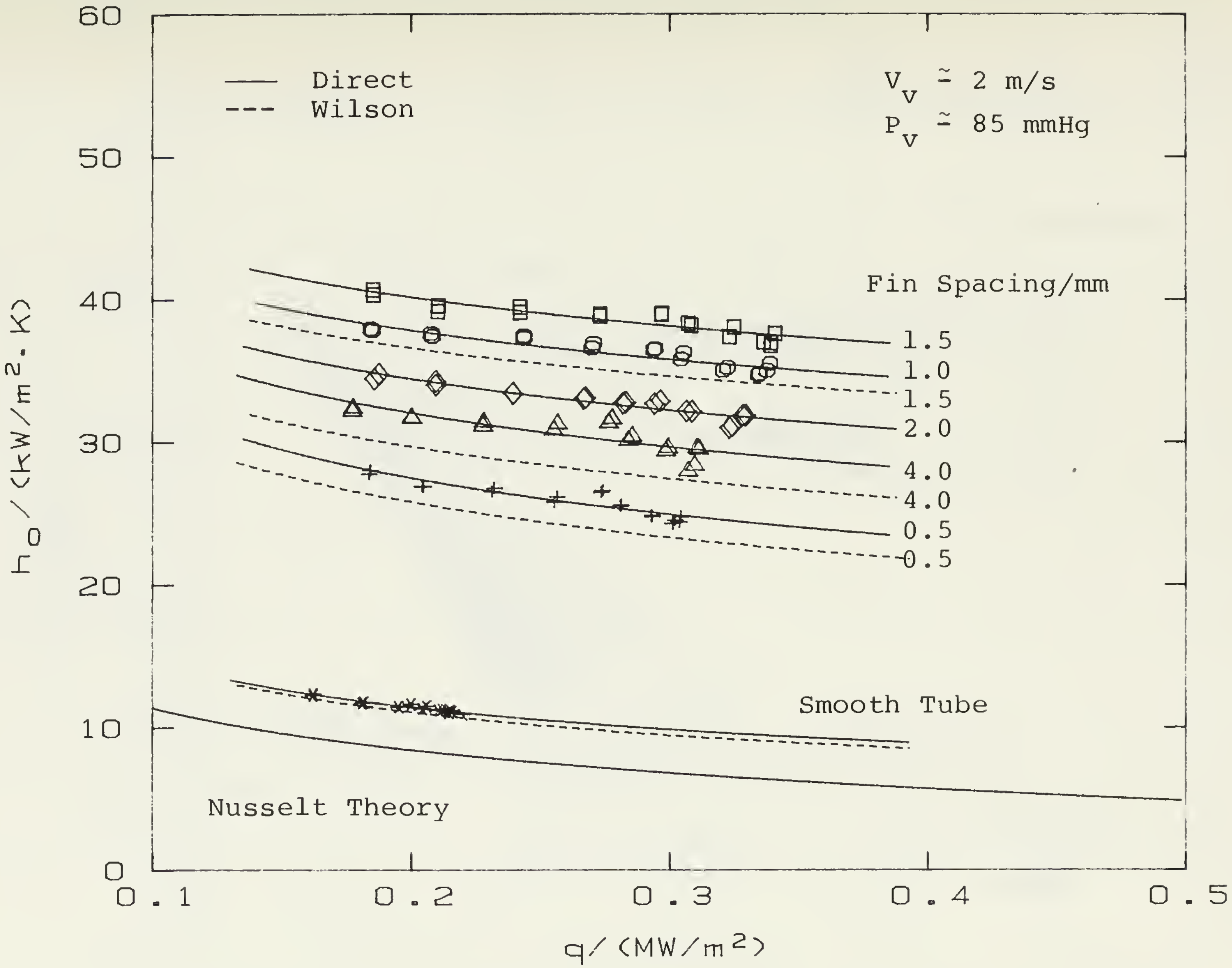

Figure 5.10. Variation of Condensing Coefficient with Heat Flux for the Set of Tubes with t = 1.0 and e = 1.0 mm (Vac. Runs)

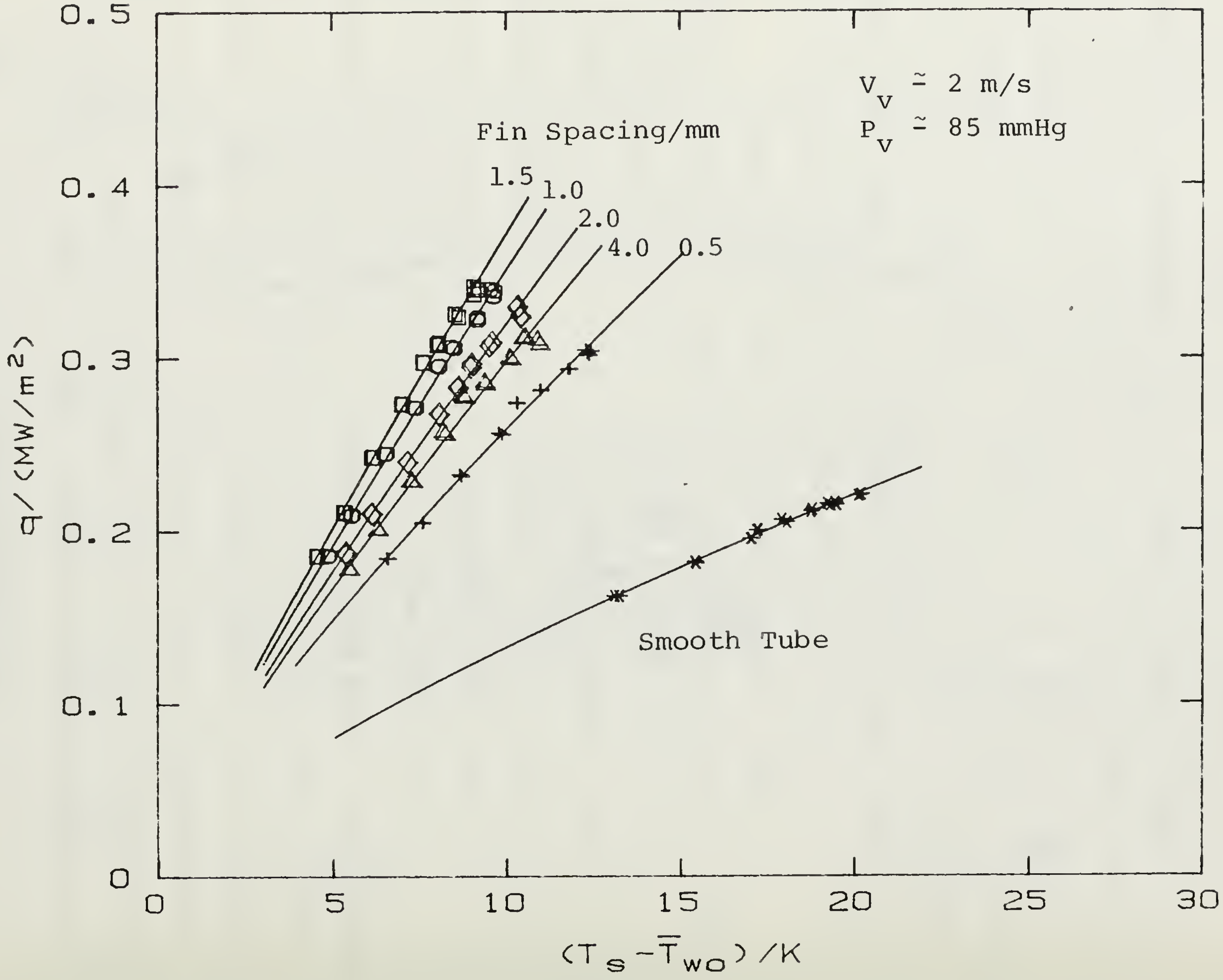

Figure 5.11. Variation of Heat Flux with Steam-Side Temperature Drop for Tubes with t = 1.0 and e = 1.0 mm (Vac. Runs)

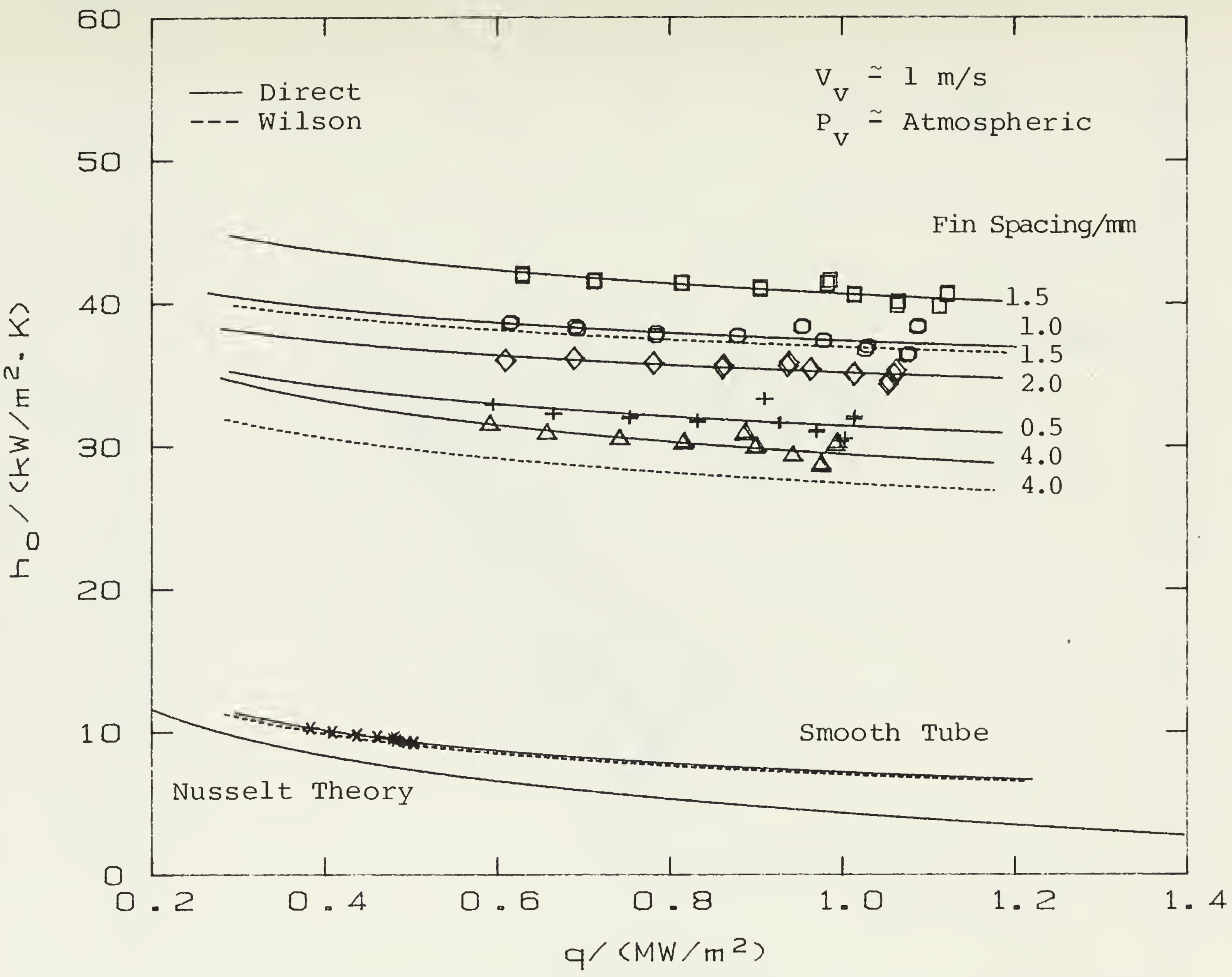

Figure 5.12. Variation of Condensing Coefficient with Heat Flux for the Set of Tubes with t = 1.0 and e = 1.0 mm (Atm. runs)

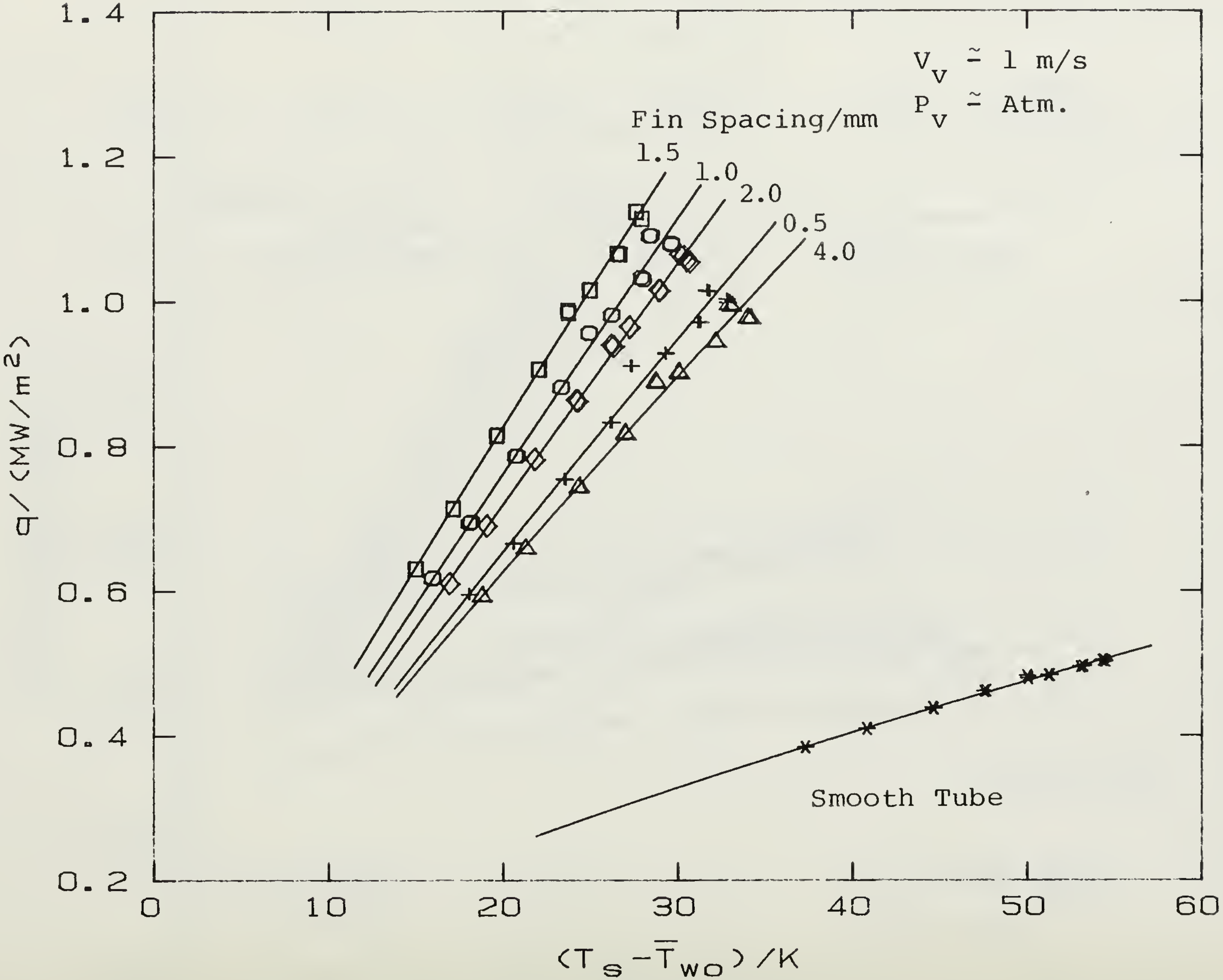

Figure 5.13. Variation of Heat Flux with Steam-Side Temperature Drop for the Set of Tubes with t = 1 and e = 1 mm (Atm. Runs)

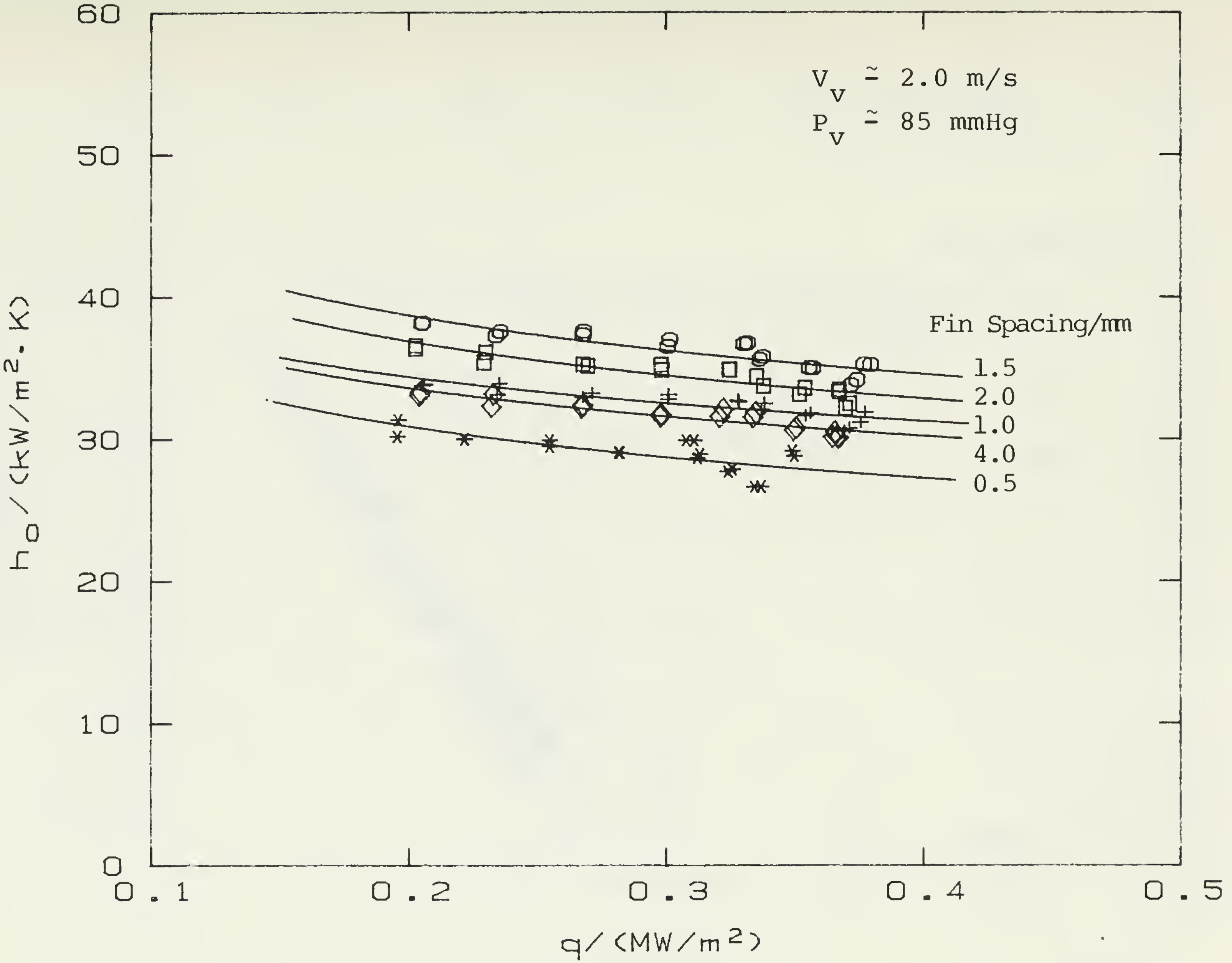

Figure 5.14. Variation of Condensing Coefficient with Heat Flux for the Set of Tubes with t = 0.75, e = 1.0 mm (Vac. Runs)

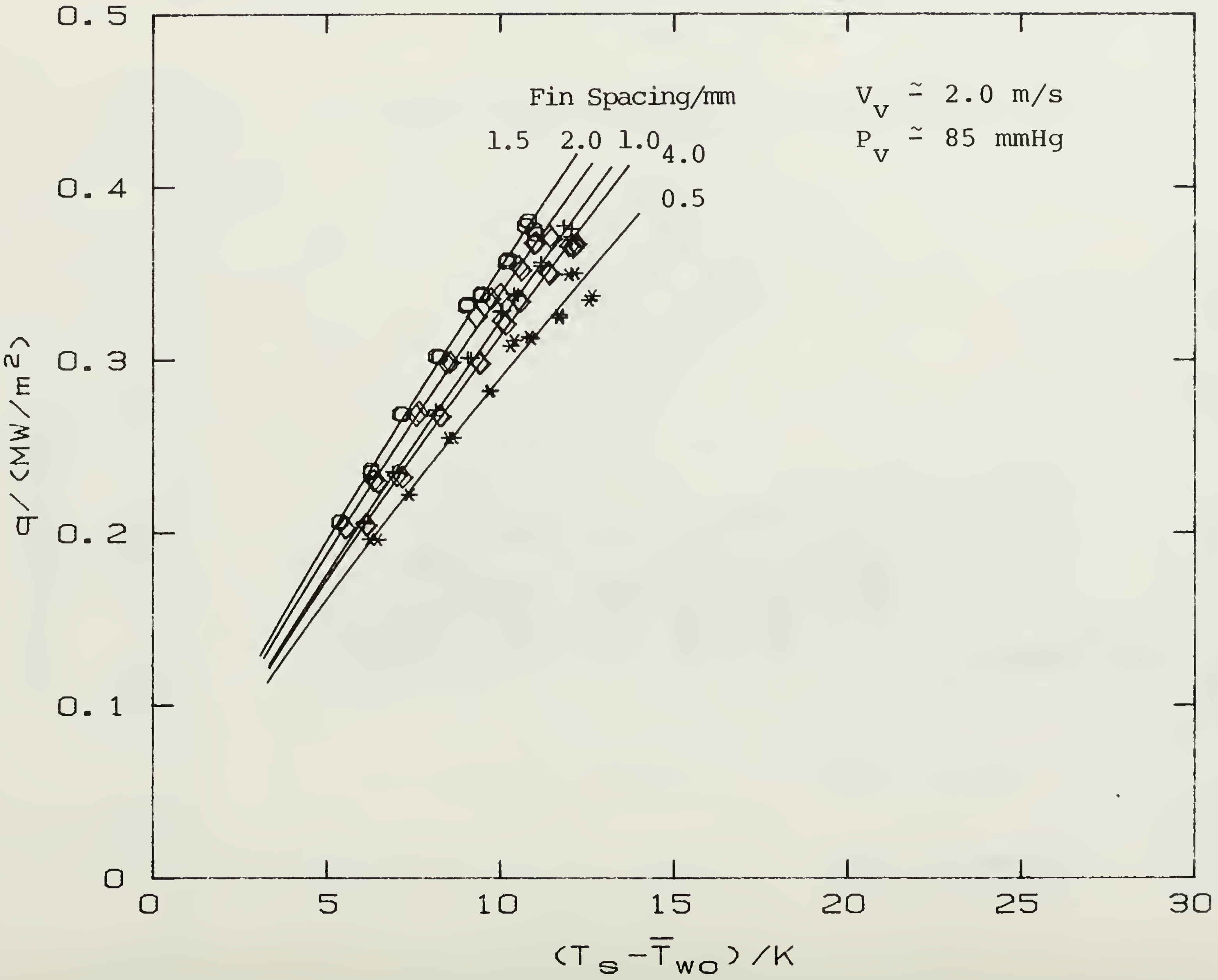

Figure 5.15. Variation of Heat Flux with Steam-Side Temperature Drop for the Set of Tubes with $t = 0.75$ and $e = 1.00$ mm (Vac. Runs)

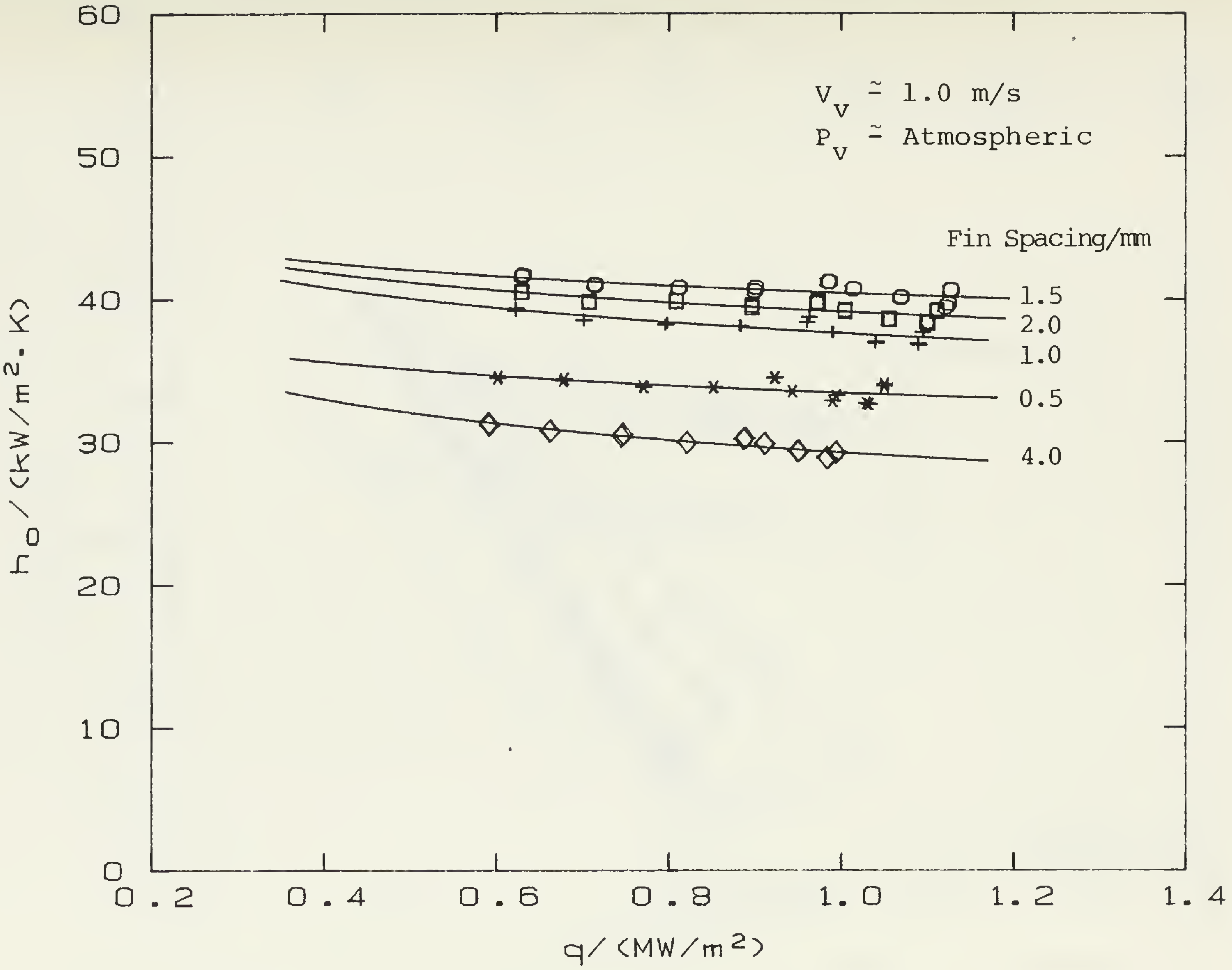

Figure 5.16. Variation of Condensing Coefficient with Heat Flux for the Set of Tubes with t = 0.75 and e = 1.0 mm (Atm. Runs)

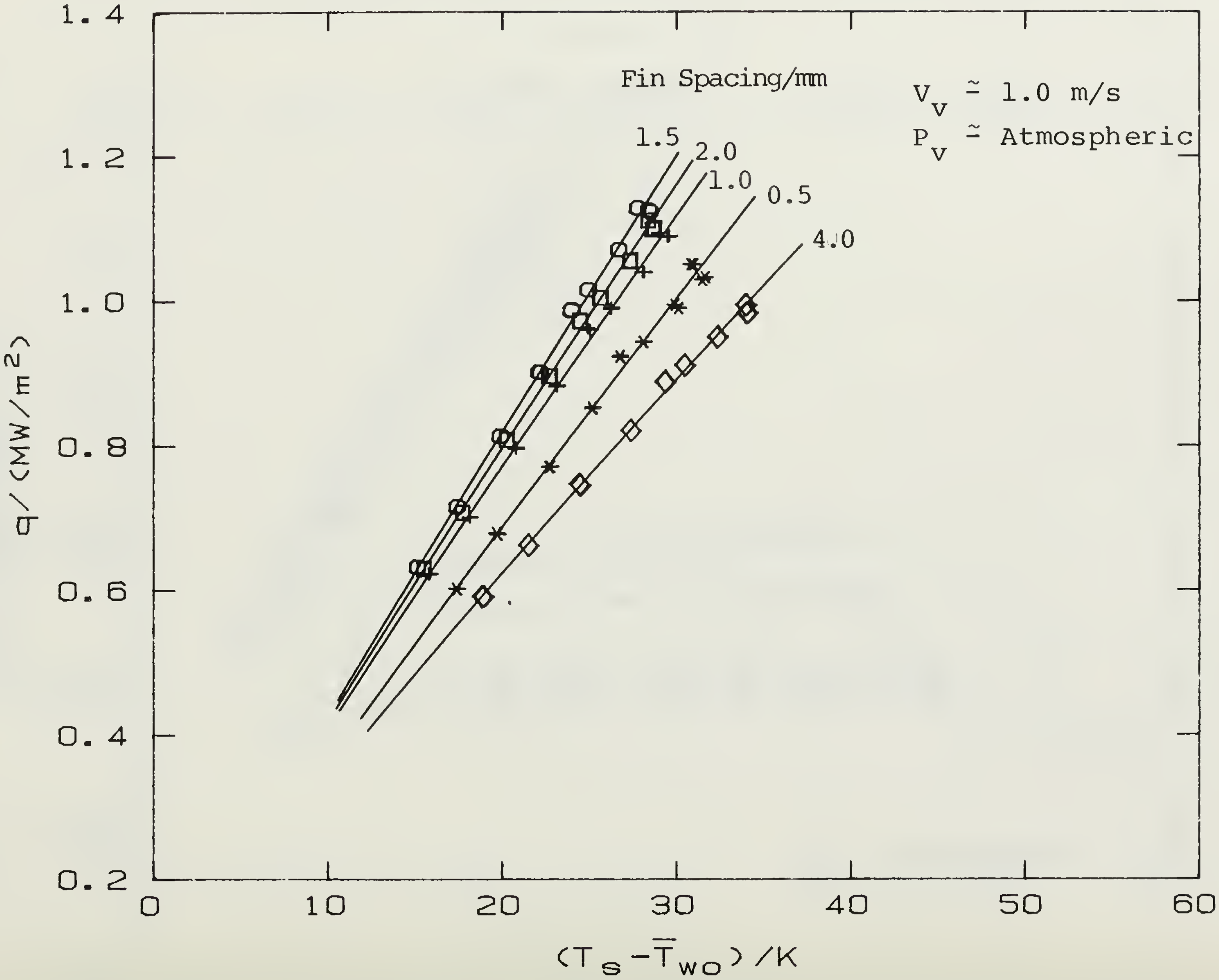

Figure 5.17. Variation of Heat Flux with Steam-Side Temperature Drop for the Set of Tubes with $t = 0.75$ and $e = 1.0$ mm (Atm. Runs)

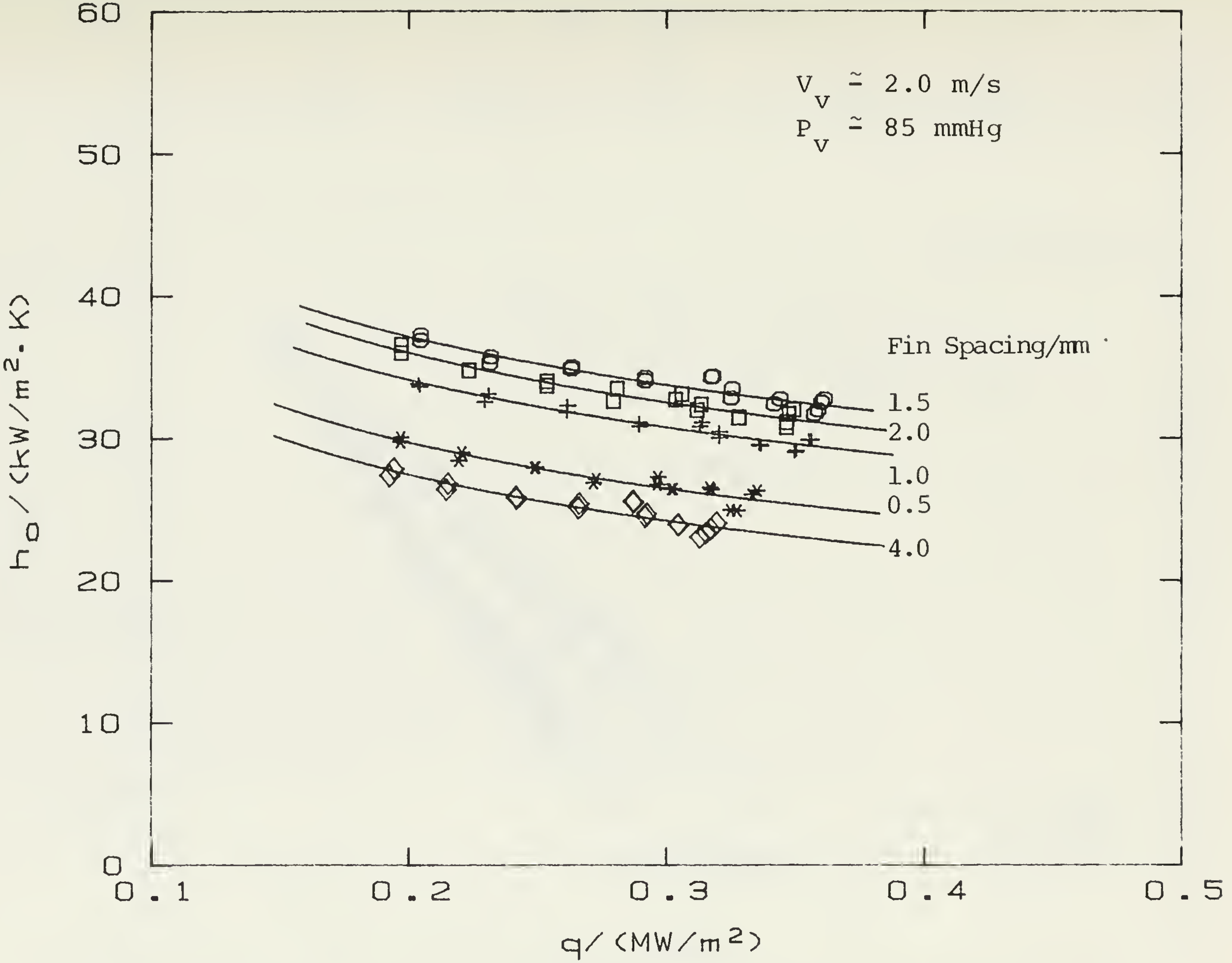

Figure 5.18. Variation of Condensing Coefficient with Heat Flux for the Set of Tubes with t = 0.5 and e = 1.0 mm (Vac. Runs)

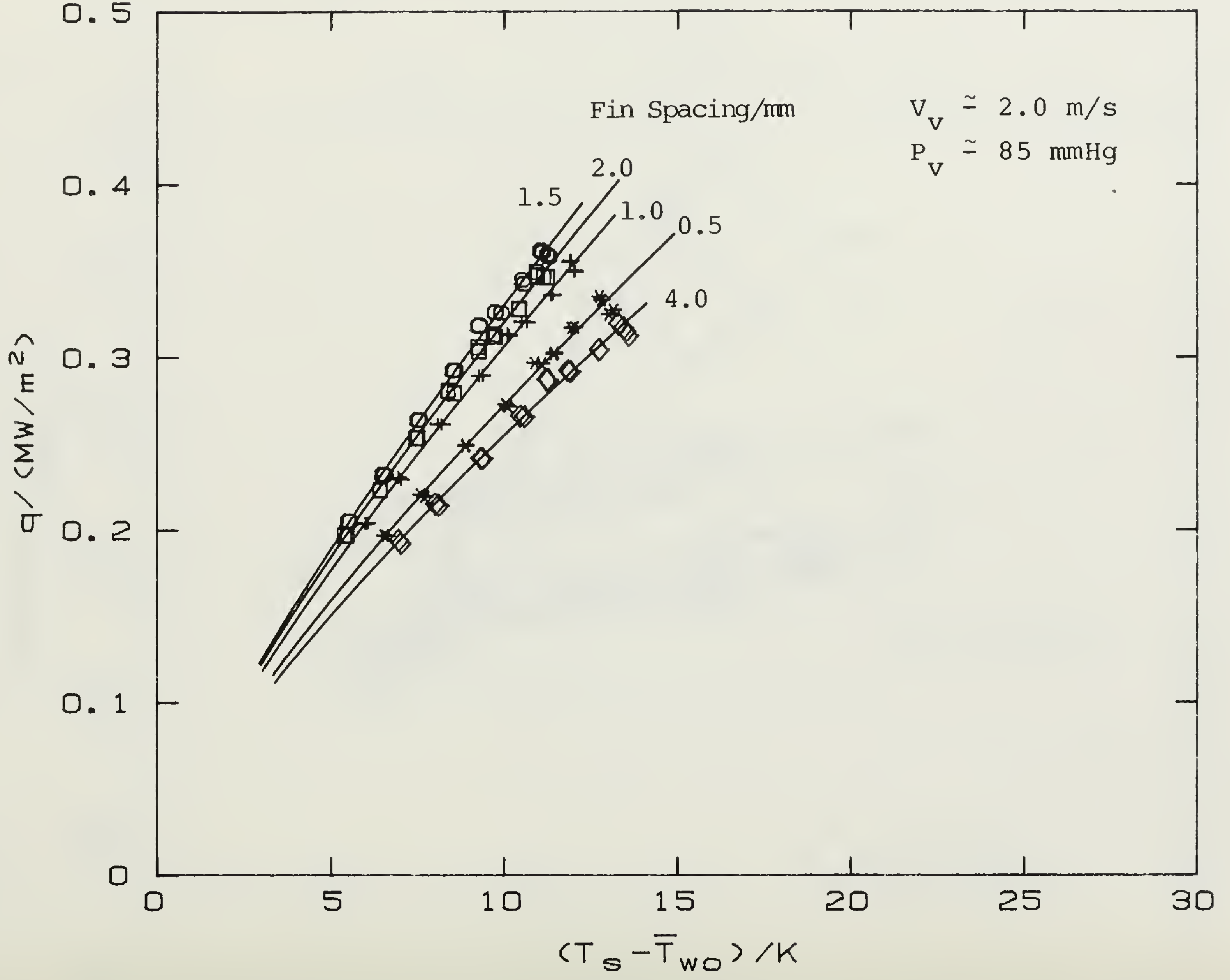

Figure 5.19. Variation of Heat Flux with Steam-side Temperature Drop for the Set of Tubes with t = 0.5 and e = 1.0 mm (Vac. Runs)

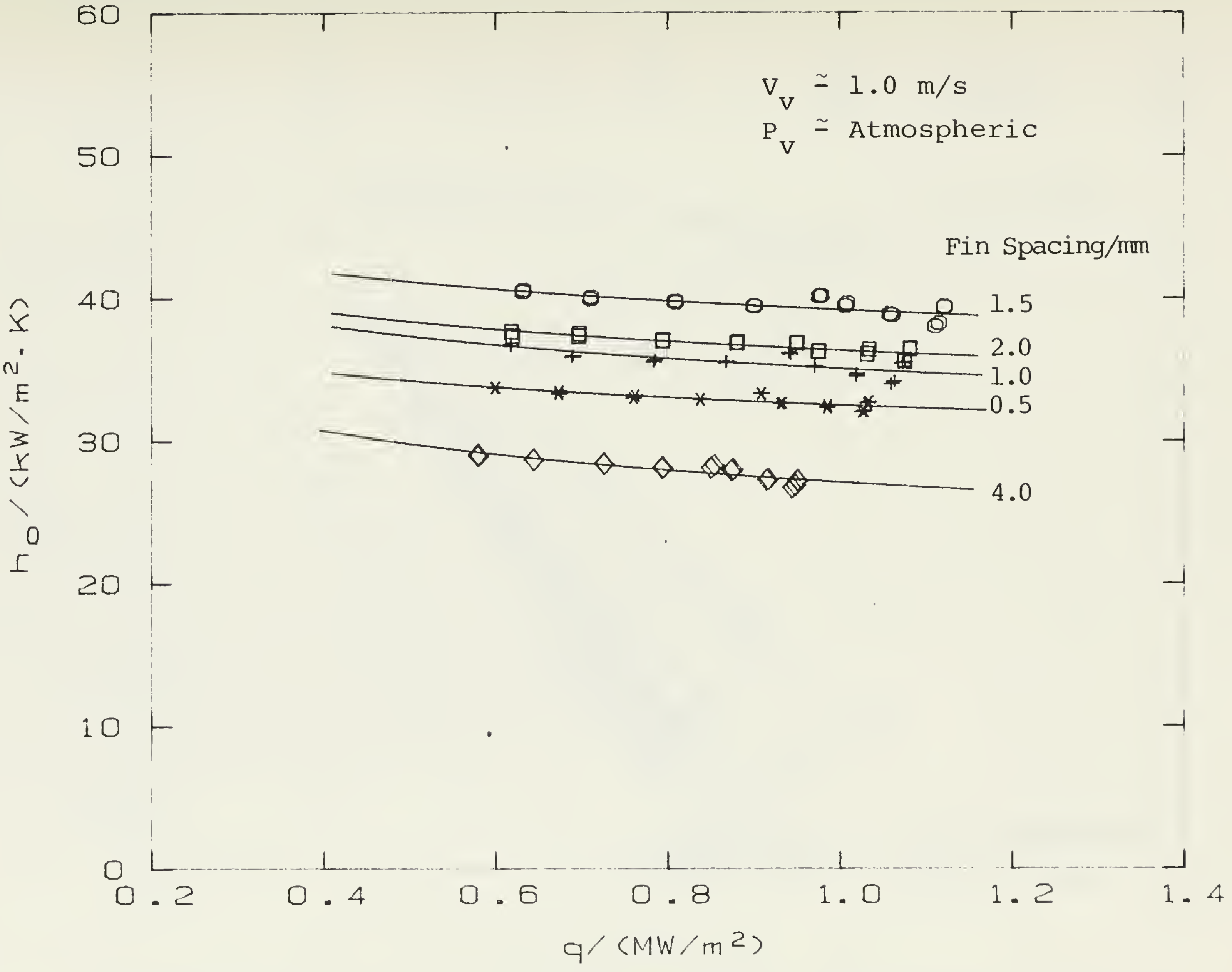

Figure 5.20. Variation of Condensing Coefficient with Heat Flux for the Set of Tubes with t = 0.5 and e = 1.0 mm (Atm. Runs)

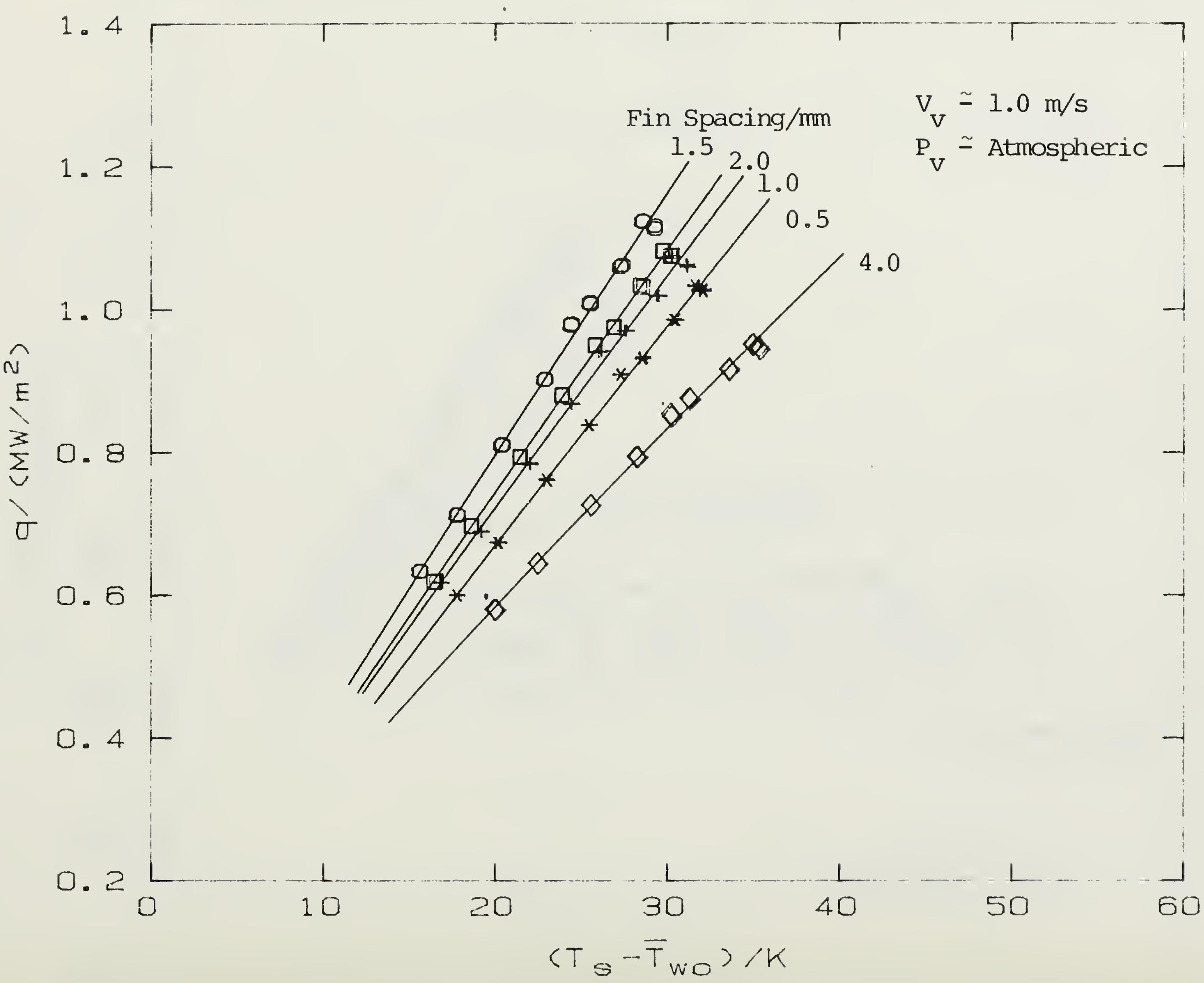

Figure 5.21. Variation of Heat Flux with Steam-Side Temperature Drop for the Set of Tubes with t = 0.25 and e = 1.0 mm (Atm. Runs)

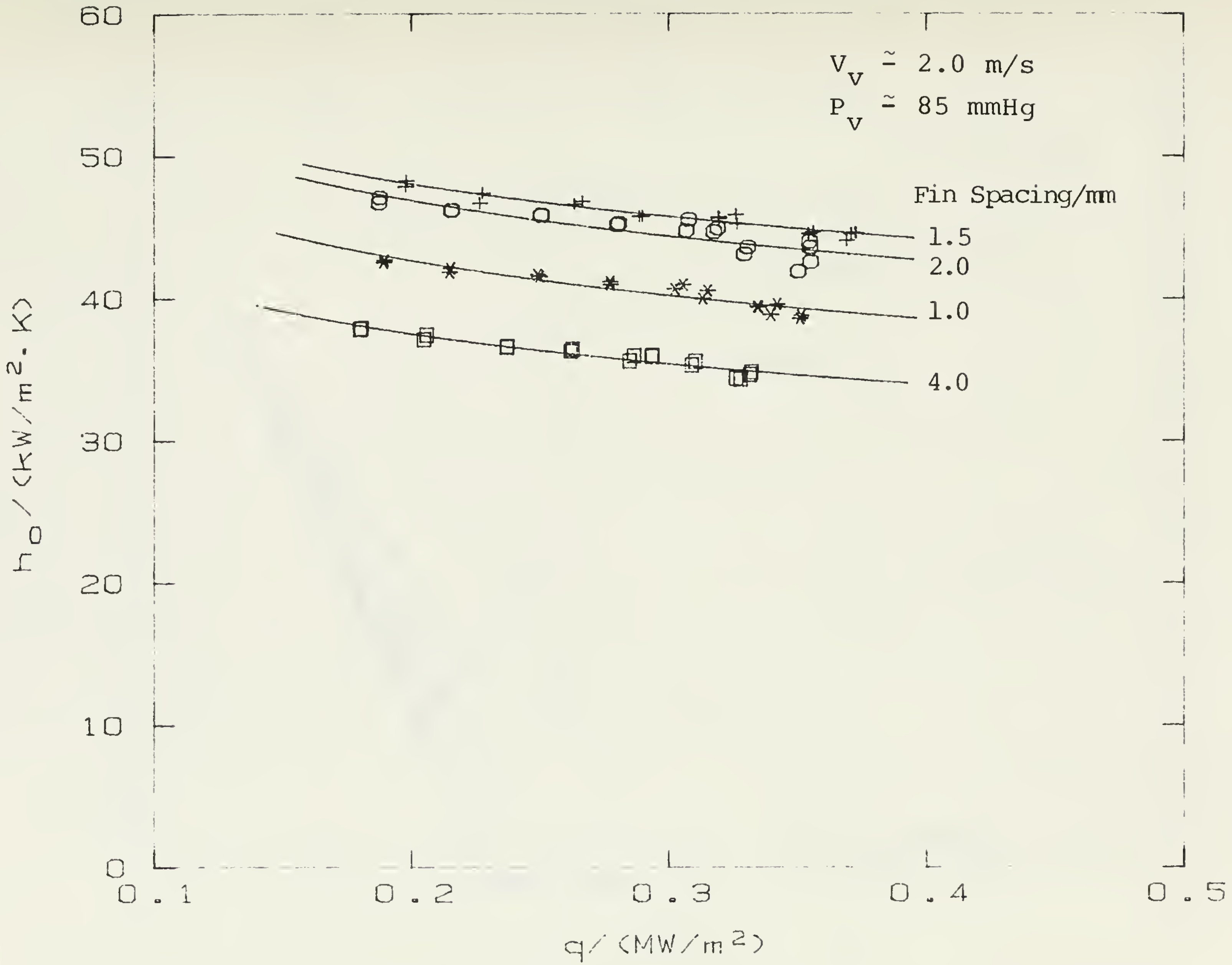

Figure 5.22. Variation of Condensing Coefficient with Heat Flux for the Set of Tubes with t = 1.0 and e = 2.0 mm (Vac. Runs)

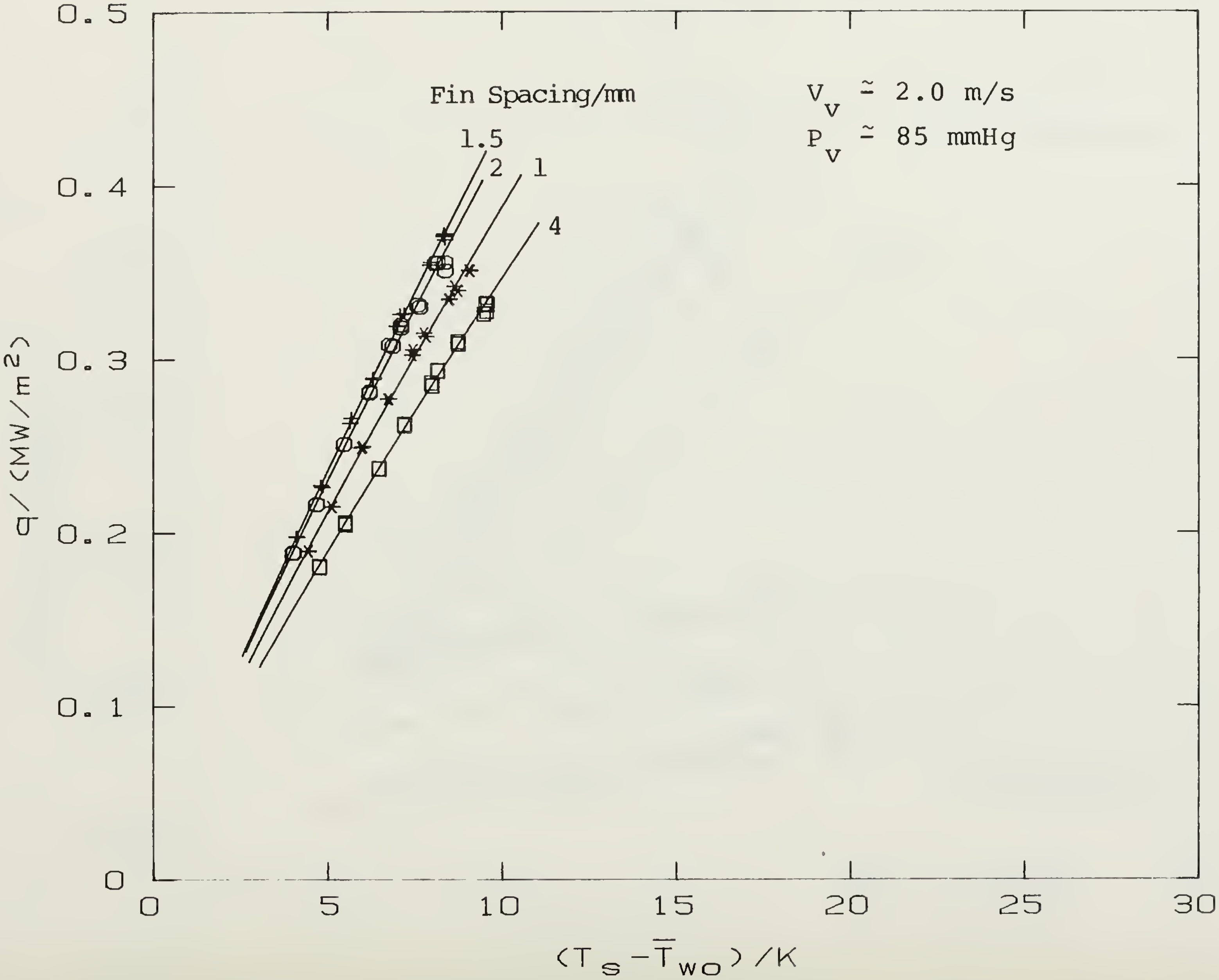

Figure 5.23. Variation of Heat Flux with Temperature Drop for the Set of Tubes with t = 1.0 and e = 2.0, mm (Vac. Runs)

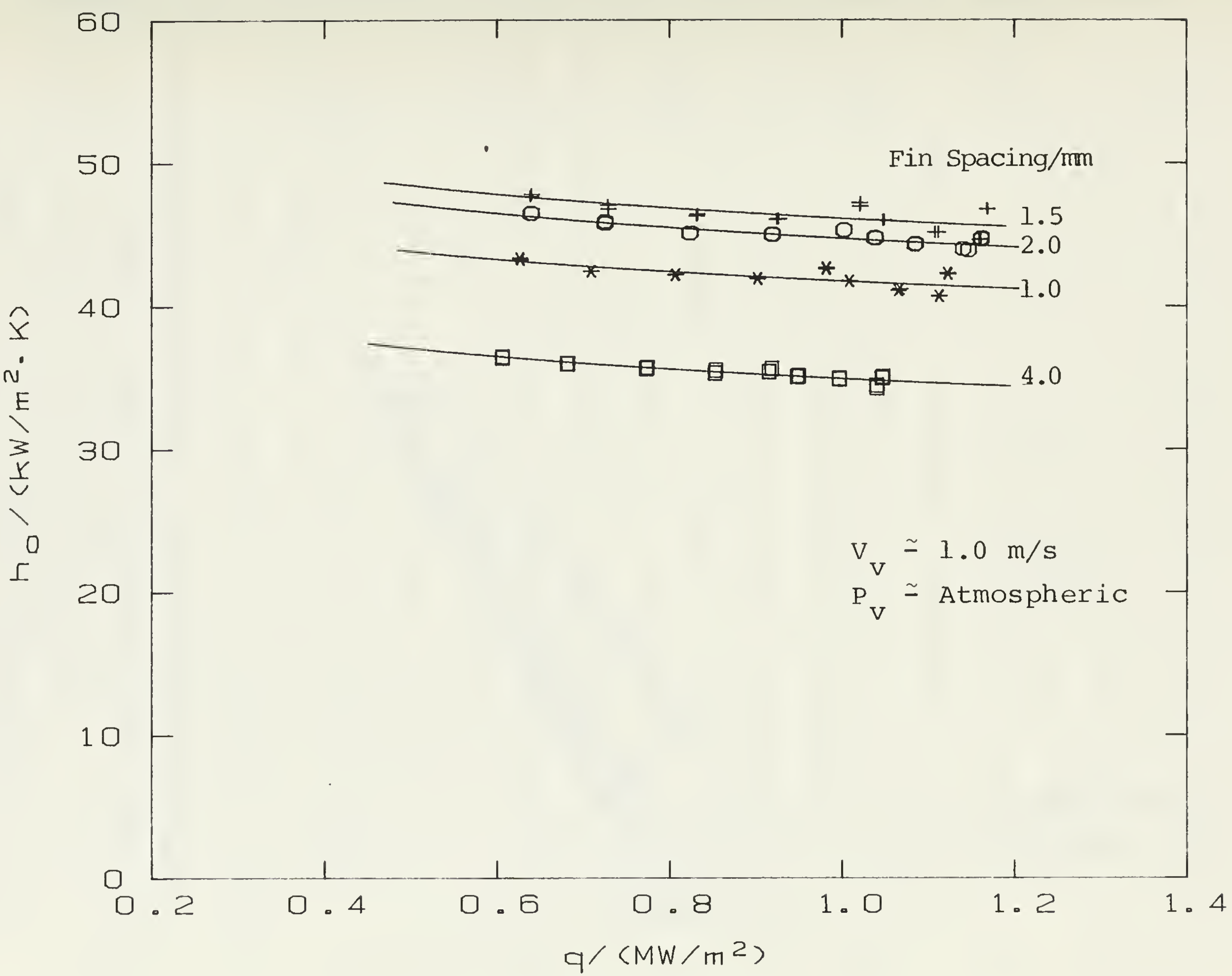

Figure 5.24. Variation of Condensing Coefficient with Heat Flux for the Set of Tubes with t = 1.0 and e = 2.0 mm (Atm. Runs)

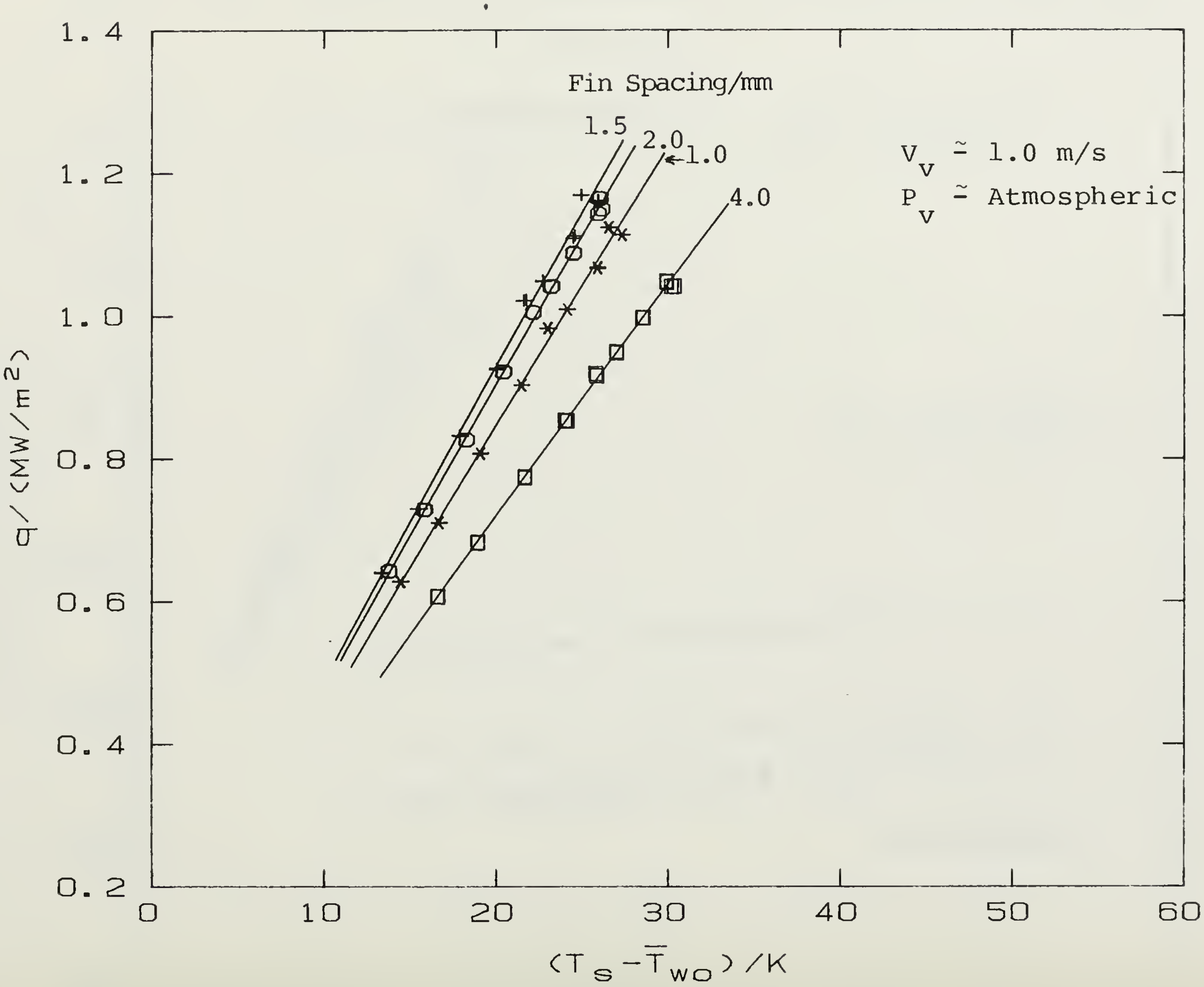

Figure 5.25. Variation of Heat Flux with Steam-Side Temperature Drop for the Set of Tubes with t = 1.0 mm and e = 2.0 mm (Atm. Runs)

3. Significance of Fin Thickness

Three sets of finned tubes were manufactured with fin thicknesses of 0.5, 0.75 and 1.0 mm, while the fin height was held constant at 1.0 mm. Each set consisted of five tubes with fin spacings of 0.5, 1.0, 1.5, 2.0 and 4.0 mm. The relative plots of the outside heat-transfer coefficient for each group of tubes, tested under vacuum and atmospheric conditions, were already shown in Figures 5.10 to 5.21. Notice that the shape of the curves to fit the data points is very nearly independent of the fin thickness. Figure 5.26 is a cross plot showing the enhancement ratio as a function of the fin spacing for both pressure conditions, with the fin thickness as a parameter. Notice that for almost all the fin spacings, the 0.5-mm fin thickness gave the smallest gain even though it provides the maximum condensing area. An effort to explain this phenomenon will be made at the end of this section. Between the 0.75 and 1.0-mm fin thicknesses, it is not very clear which of the two is superior. For the vacuum runs with fin spacing around the optimum value (i.e., 0.5 mm < s < 1.5 mm) it appears that the 1.0-mm thickness is a stronger candidate for the optimum fin thickness. On the other hand, for atmospheric runs with most fin spacings, the 0.75-mm fin thickness appears to be the best candidate.

In order to further study the dependence of fin thickness on the enhancement ratio, data shown in Figure

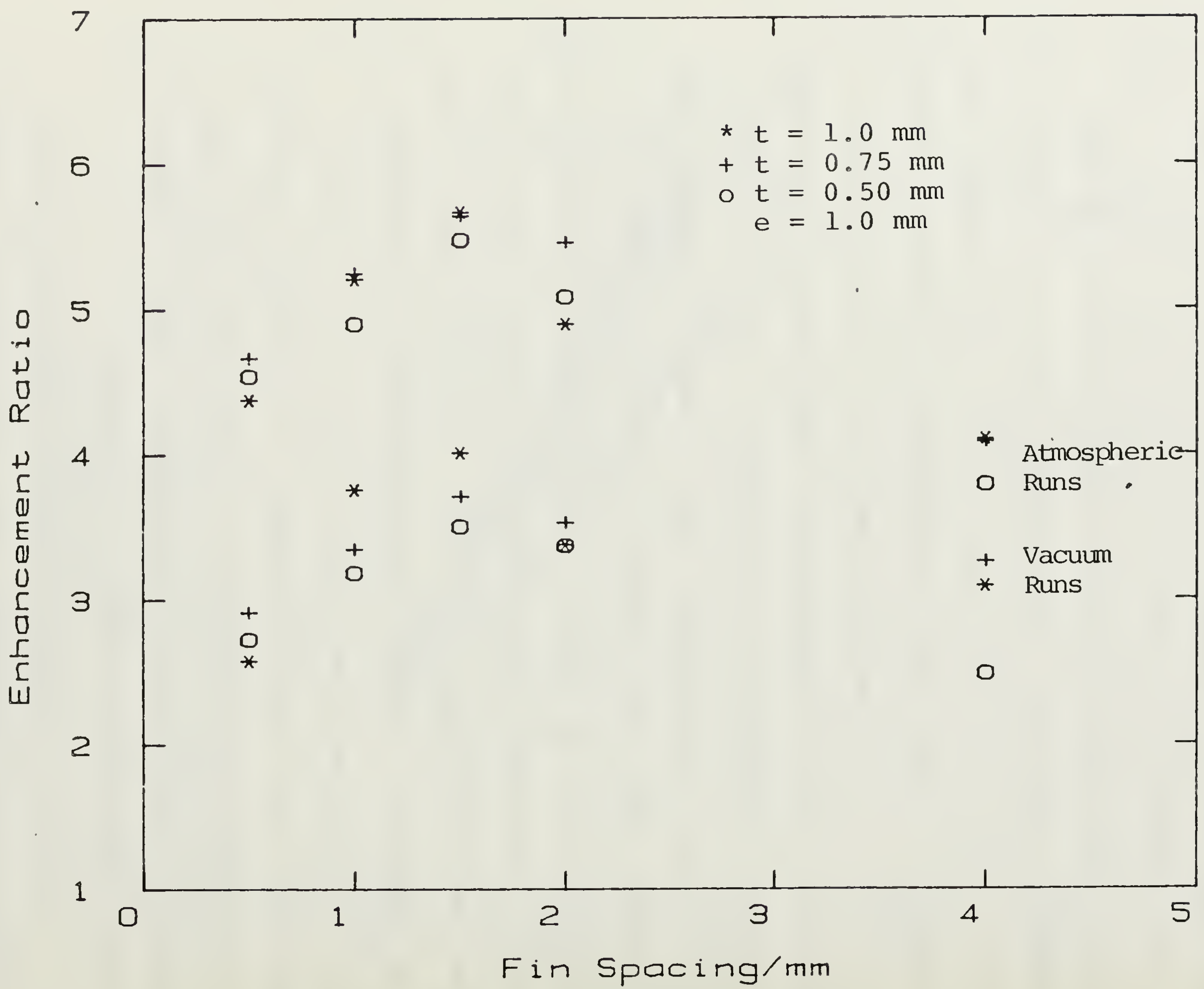

Figure 5.26. Cross Plots Showing Best Fin Spacing Among Sets of Tubes with t = 0.5, 0.75 and 1 mm

5.26 were cross plotted as shown in Figure 5.27. As mentioned earlier, initially there were only three tubes with fin thickness of 0.5, 0.75 and 1.0 mm. For vacuum conditions, the inadequacy of this fin thickness range can be seen since the optimum thickness has not been bracketed. Therefore, an additional tube with a fin thickness of 1.5 mm, a fin height of 1.0 mm and a fin spacing of 1.0 mm, was manufactured. The enhancement ratio found on this tube is also plotted in Figure 5.27. It can be seen that the tube with a 1.0-mm fin thickness is still the best candidate for the vacuum runs. This figure also shows possible error bands for the computed enhancement ratios. Since the possible error bands are in excess of the enhancement ratios at these two fin thicknesses, no attempts were made to explain why the optimum fin thickness is affected by the pressure condition. Therefore, it can be concluded that the optimum fin thickness is around 0.75 to 1.0 mm for both pressure conditions.

As the fin thickness increases with fin spacing held constant, the fin density (fins/mm) decreases. In the limit, the tube will become a smooth tube with an outer diameter qual to the fin diameter. Recall that in the Nusselt equation (5.3), the tube diameter is in the denominator; therefore, the condensing coefficient is inversely proportional to the $D_o^{1/4}$ for constant wall temperature, or, at a constant wall heat flux, the condensing coefficient is inversely proportional to $D_o^{1/3}$. Thus,

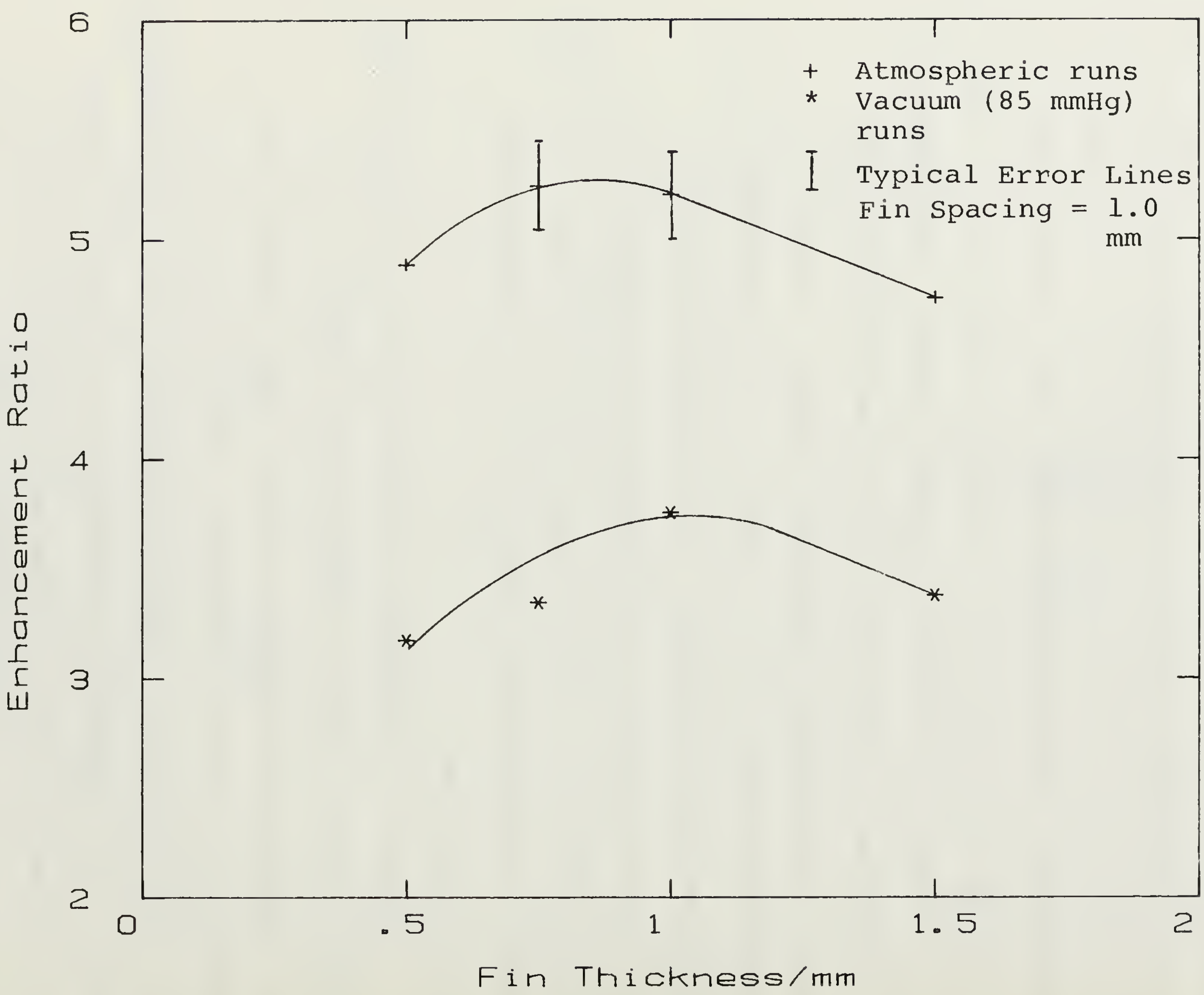

Figure 5.27. Influence of Fin Thickness on Enhancement Ratio for Tubes with ρ = 1.0 mm, for both Pressure Conditions

$$h'_{t\to\infty} = h_o\left(\frac{D_o}{D_f}\right)^{1/3} \tag{5.10}$$

where $h'_{t\to\infty}$ is based on the outer diameter of the tube, including the fin height. Now, if this condensing coefficient is based on root diameter (as it is done throughout this thesis), then

$$h_{t\to\infty}D_o = h'_{t\to\infty}D_f \tag{5.11}$$

The combination of equations (5.10) and (5.11) results in:

$$h_{t\to\infty} = h_o\left(\frac{D_f}{D_o}\right)^{2/3} \tag{5.12}$$

This means that there will be very little enhancement by increasing the fin thickness to the limit. For example, with D_f = 21.0 mm and D_o = 19.0 mm, the ratio $h_{t\to\infty}/h_o$ would equal 1.07.

When the fin thickness is reduced, there is a finite number of fins that can be added in a given tube length (i.e., it is not physically possible to take a smooth tube when fins of infinitesimal thickness are present). Since there is a significant increase in heat-transfer area as the fins become thinner, an enhancement for the condensing process may be expected on the basis of area increment. Unfortunately, this was not the case as discussed below. Equation (1.12) predicts the retention angle and it is shown that the condensate retention is independent of fin thickness. This was visually verified during this investigation. Comparing two tubes which have the same length and fin spacing, the one that has thinner fins would hold more condensate when the retention angle is the same. This means that part of the metal of a thick fin is replaced by condensate, or in other words, the thin-finned tube presents a smaller effective thermal conductivity than the thick-finned tube resulting in lower performance. Also, as the fin thickness decreases, the fin efficiency may play a role for tubes made of low-thermal-conductivity metal. However, for copper tubes with fins of 0.5 mm thickness and 1.0 mm height, the fin efficiency was estimated as 99 percent, when the outside heat-transfer coefficient was 40 $kW/m^2 \cdot K$.

Since both fin thickness extremes show that the heat-transfer process is not enhanced, it appears that the optimum thickness found (around 0.75 to 1.0 mm) is reasonable.

Careful observation of Figure 5.26 reveals that the tubes with 0.5-mm fin spacing do not follow the trend of the tubes with larger fin spacings. In this case, the maximum performance was given by the tube with the 0.75-mm thickness, then by the tube with 0.5-mm thickness and finally by the tube with 1.0-mm fin thickness. This sequence holds for both pressure conditions. The rate of condensate flow around the tube was observed to be dependent on the fin thickness. The fastest flow pattern was observed for the tube with 0.5 mm fin thickness, then for the tube with 0.75 mm and finally for the tube with 1.0 mm fin thickness. This surprising observation can be explained if the fin tip effect is introduced; i.e., since the fin tip is rectangular, there is a possibility that some of the condensate will fall into the interfin spacing and some will follow the circumferential path. If this condensate flow is realistic, it can be concluded that the thicker the fin, the more condensate will flow circumferentially along the fin tip.

To further support this conclusion, numerous runs were made at a different fin spacing (1.0 mm) where the miniscus in the interfin area at the top part of the tube is visible (recall that the tubes with 0.5-mm fin spacing are completely flooded). If the miniscus radius is different as the fin thickness changes, it can be concluded that the condensate flow pattern is influenced by the fin thickness. The tube with 0.5 mm fin thickness had a smaller miniscus radius than the tube with 1.0 and 1.5 mm fin thickness. This means that the previous conclusion may be correct; therefore, when the fin tip is wide and of course rectangular, there will be circumferential drainage along the fin tip. On the other hand, for tubes with narrow fin tips, most of the condensate will fall into the interfin spacing, resulting in a very fast flow pattern and the creation of ripples. If this is the case, the thin fins should show an increased performance due to the convective action of the condensate. However, the final performance is limited by the excessive condensate amount that is attached continuously on the tube. These may be the reasons why the tube with 0.5 mm fin thickness has better performance than the tube with 1.0 mm fin thickness when the fin spacing is 0.5 mm. Between the tubes with 0.5 and 0.75 mm fin thicknesses, there is no clear visible difference in the flow pattern; therefore, the last tube is superior because it presents less conduction resistance (it holds less condensate), and it certainly has a higher fin efficiency.

In general, it can be concluded that for fins of 1.0 mm height, the enhancement ratio was weakly dependent on fin thickness. The most significant reason is that the fin thickness has no influence on the retention problem as the fin spacing does.

In order to check the validity of some of the previous conclusions, data were taken for one more tube. This tube had a fin spacing, thickness and height of 1.25 mm, 1.25 mm and 1 mm, respectively, and it was made from the tube with 1.5 mm fin thickness whose fins were machined down by 0.25 mm. A tube with 1.25-mm fin spacing was expected to have a better heat-transfer performance than the tube of 1.0 mm fin spacing since the condensing heat-transfer coefficient increases up to a fin spacing of around 1.5 mm. However, the performance should be limited owing to the fact that the fin thickness is outside the optimum range

(0.75 to 1.0 mm). Figures 5.28 and 5.29 show the relative plots of the condensing coefficient with heat flux for both pressure conditions, for three tubes whose fin geometry is shown in these figures. It is shown that the performance of the new tube is almost the same as with the tube with 1.0 mm fin spacing and thickness. This means that what was gained by the spacing increment (from 1.0 to 1.25 mm) was lost by the fin thickness increase (from 1.0 to 1.25 mm); therefore the previous conclusions about the fin spacing and thickness effects seem to be reasonable.

4. Significance of Fin Height

As shown in Table I, two fin heights (1.0 and 2.0 mm) were examined during this thesis effort. The geometry of tubes tested is given in Table I. The heat-transfer performance of these tubes has already been shown with Figures 5.22 to 5.25, and for both sets of tubes, the optimum fin spacing was determined to be 1.5 mm. Figure 5.30 shows the enhancement ratio for the set of tubes with 2.0-mm fin height. It is shown that the maximum enhancement is about 5 and 6.5 for the vacuum and atmospheric runs, respectively. Figure 5.31 is a cross plot showing the enhancement ratio versus the fin spacing for both pressure conditions, with the fin height as a parameter. It is shown that the set of tubes with 2 mm fin height has better performance than the set of tubes with 1.0 mm fin height. The reasoning is two fold:

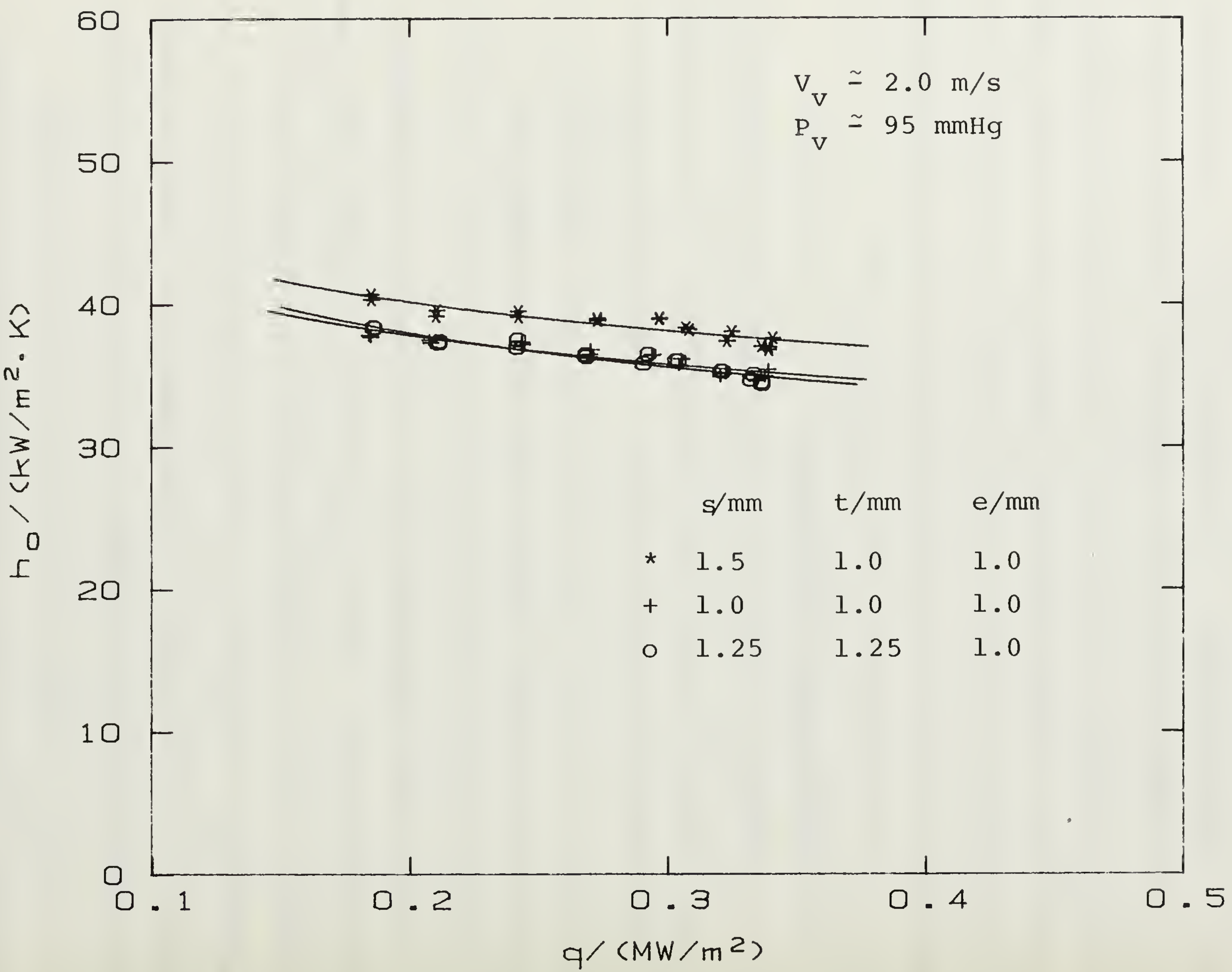

Figure 5.28. Variation of Condensing Coefficient with Heat Flux for Tubes with Fin Geometry Shown in the Figure (Vac. Runs)

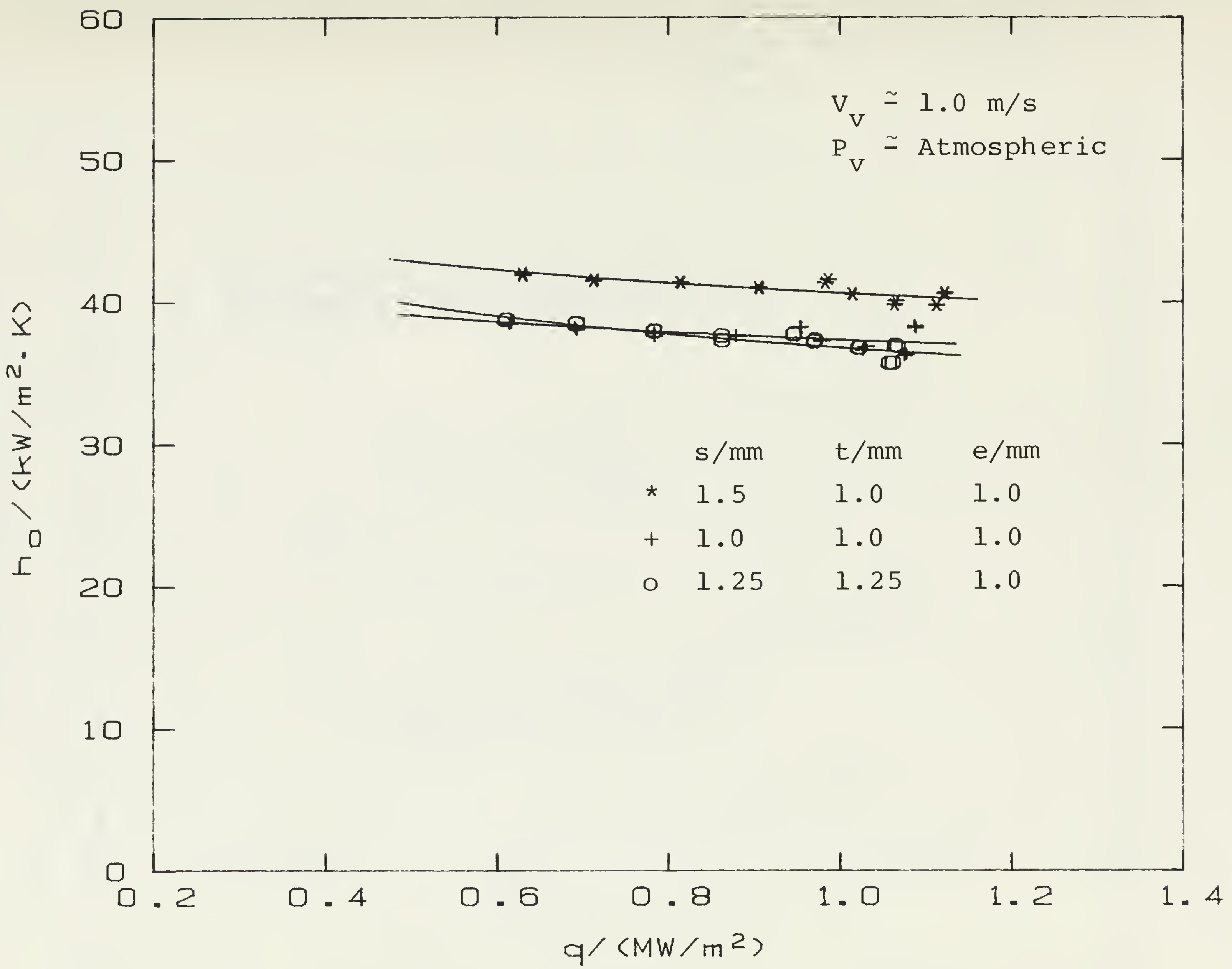

Figure 5.29. Variation of Condensing Coefficient with Heat Flux for Tubes with Fin Geometry Shown in the Figure (Atm. Runs)

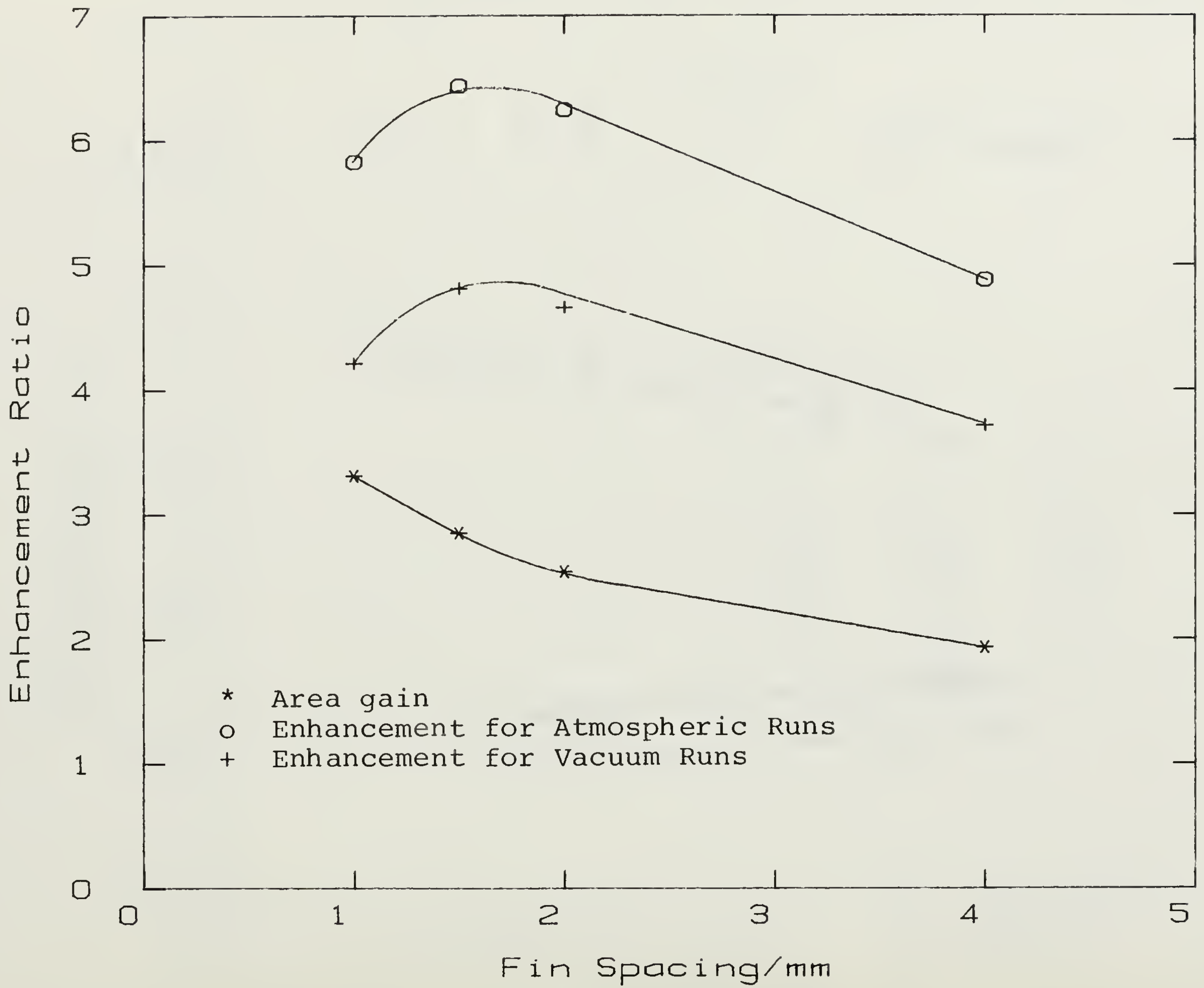

Figure 5.30. Cross Plot Showing Best Fin Spacing for Tubes with e = 2.0 mm and t = 1.0 mm, for both Pressure Conditions

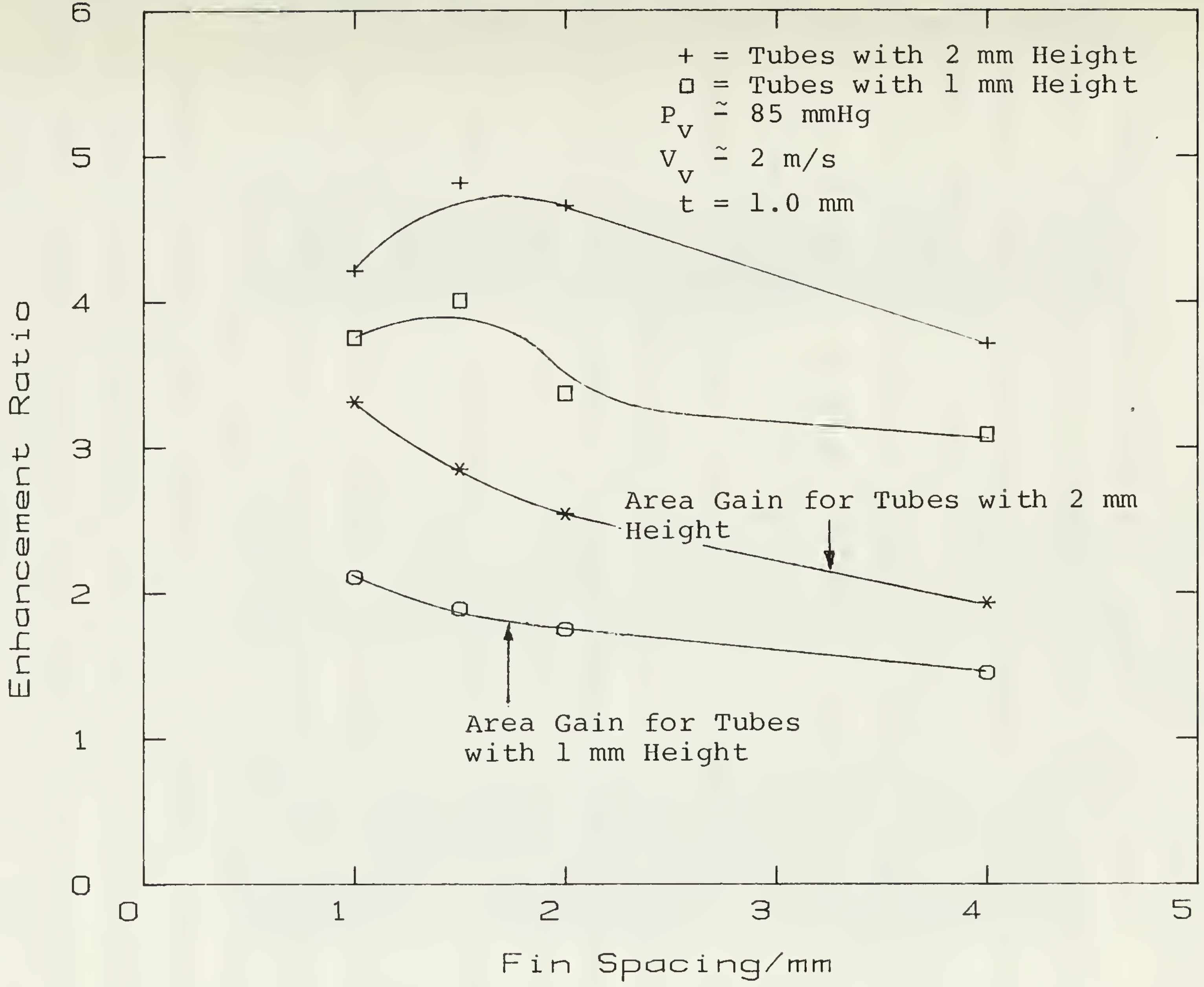

Figure 5.31. Comparison of Enhancement Ratio Obtained on Sets of Tubes with e = 1.0 and e = 2.0 mm (Vac. Runs)

1. Surface area increases with increasing fin height (see Figure 5.30).

2. The retention angle decreases and hence heat-transfer performance increases, with increasing fin height as predicted by equation (1.12). This was also visually verified during this thesis effort.

Examining carefully the above mentioned Figure 5.31, it can be seen that the performance sequence is not the same for both sets of tubes. The tube with 1.0-mm fin spacing is the second in performance among the set of tubes with 1.0-mm height. However, for the set of tubes with 2.0 mm height, the tube with 1.0-mm fin spacing is the third in performance while the tube of 2.0-mm fin spacing becomes second. This observation holds for both pressure conditions. This means that as the fin height increases, there is a tendency for the optimum spacing to move to a higher value. This tendency is mainly due to the increased amount of condensate which is retained between the fins at the top part of the tube, caused by the increased condensate generation. This fact was verified visually during the experiments, and Figure 5.32 shows a schematic of the condensate appearance on those two tubes which differ only by the fin height. It is shown that the interfin space at the top part of the tube with 1.0-mm fin height 'holds' less condensate than the tube with 2.0-mm fin height. This observation may reveal that the mechanism of thinning the film

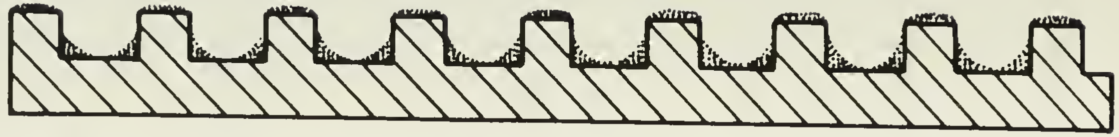

Finned Tube with s = 1.5, t = 1.0 and e = 1.0 mm

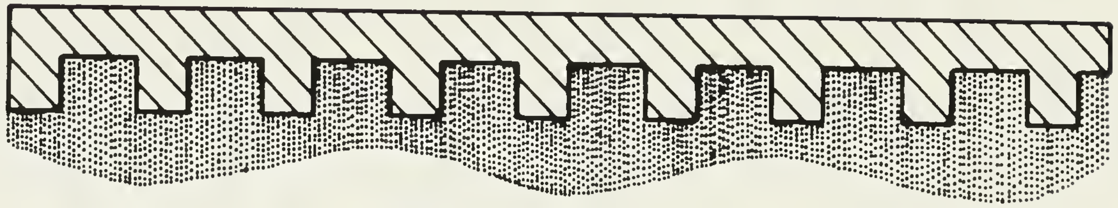

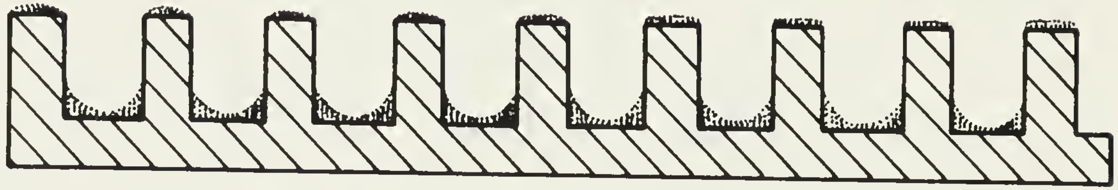

Finned Tube with s = 1.5, t = 1.0 and e = 2.0 mm

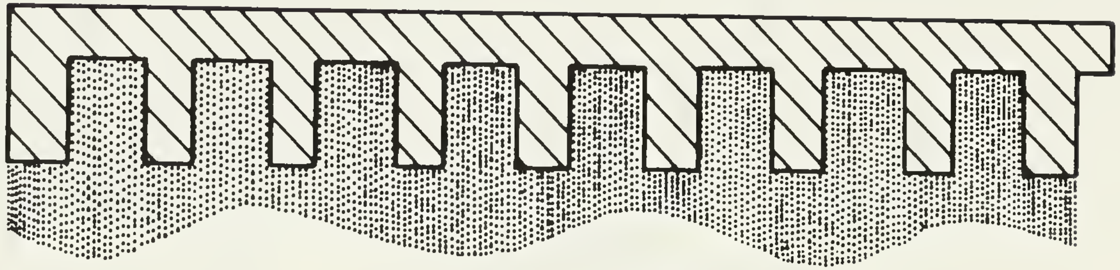

Figure 5.32. Condensate Profiles for Tubes with Fins of Different Height

diminishes when the fin height increases. The pressure gradient in the condensate film between points A and B (see Figure 1.1) can be approximated as:

$$\left.\frac{dP}{dy}\right)_{AB} \simeq \frac{\Delta P_{AB}}{e} \qquad (5.13)$$

Thus, the pressure gradient between points A and B decreases with increasing fin height (e); therefore, it should be expected that the tubes with 2.0-mm fin height would provide a less effective thinning effect. To prove this statement, one more cross plot was prepared by plotting the normalized enhancement ratio versus the fin spacing (i.e., separate the area addition effect). Figure 5.33 shows clearly that the set of tubes with 2.0-mm fin height is not improving the condensation enhancement mechanisms as effectively as the set of tubes with 1.0-mm fin height.

It is worth mentioning that as the fin height increases, the portion of the fin that extends above the top flooded part of the tube increases (see Figure 5.32 and compare the extending fin part for the tubes with 1.0 and 2.0 mm fin height); therefore, this part of the fin presents the highest heat-transfer performance since the condensate layer around the fin is extremely small. Of course, the performance of the tip is limited by the fin efficiency which decreases with increasing fin height; therefore, the set of tubes with 2.0-mm fin height has better performance mainly because of the excessive area addition.

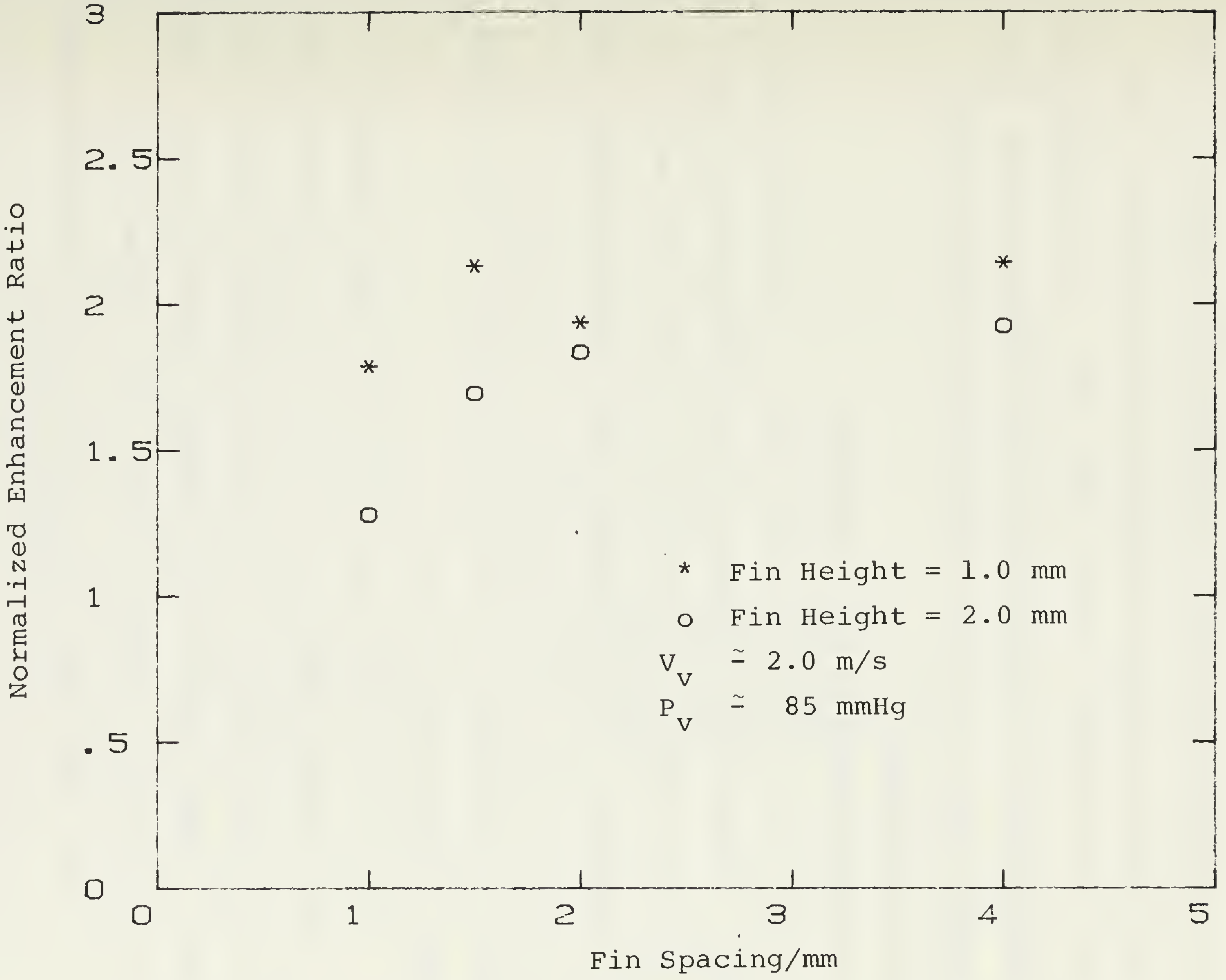

Figure 5.33. Normalized Enhancement Ratio of Sets of Tubes with Fins of 1.0 and 2.0 mm Height

Up to now, two ways to increase the external surface area of a tube were mentioned; i.e., either by reducing the fin thickness or by increasing the fin height. In the previous section it was shown that by changing the fin thickness there was not much enhancement, the reason being that the fin thickness does not improve the flooding problem and that the area addition happens in the regimes of the tube that are flooded. On the other hand, by increasing the fin height there is the benefit of area addition away from the flooded part of the tube resulting in a better heat-transfer performance.

5. Significance of Tube Diameter

Yau et al. [Ref. 3] took data for filmwise condensation on copper finned tubes under near-atmospheric pressure. The fin shape was rectangular and the fins were 0.5 mm in thickness, 1.0 mm in height, and the fin spacings were from 0.5 up to 20.5 mm (13 different fin spacings). The diameter of the tubes (at the root of fins) was 12.7 mm and the vapor velocity was 1.1 m/s.

Figure 5.34 shows the enhancement ratio versus fin spacing for the data taken by Yau et al. and the data taken during this thesis effort. The only difference between the two sets of tubes was the root diameter, which was 12.7 and 19 mm for Yau et al. and the present work, respectively. It can be seen that there is a similarity in the enhancement ratio curves and for both sets of tubes the best fin spacing

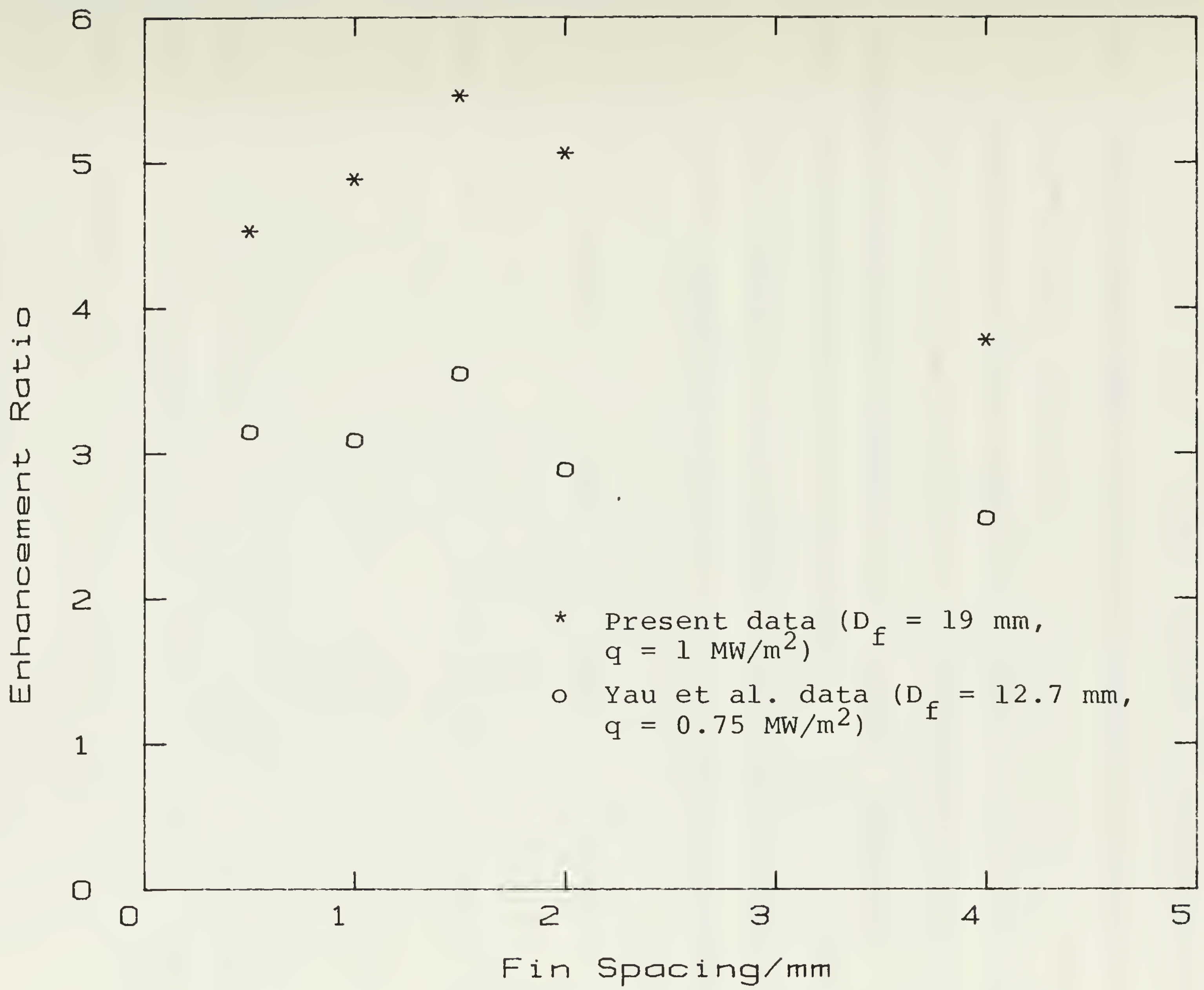

Figure 5.34. Cross Plots Showing Best Fin Spacing for Tubes of Different Diameter

found was 1.5 mm. However, there is a significant difference in the enhancement ratio, which can be explained by the following reasons:

1. The retention angle increases as the tube diameter decreases, as it is predicted by equation (1.12), resulting in a lower condensing coefficient.

2. The smooth-tube performance is predicted by the Nusselt equation, and it gives that a tube with smaller diameter will have higher condensing coefficient (recall that the tube diameter is in the denominator).

Therefore, when the enhancement ratio is computed, the tube with smaller diameter will have the numerator small and the denominator large, resulting in a smaller ratio than that which was obtained during this thesis effort.

VI. CONCLUSIONS AND RECOMMENDATIONS

A. CONCLUSIONS

1. For the best fin spacing of 1.5 mm, a fin thickness of 1.0 mm and a fin height of 2.0 mm, heat-transfer enhancements around 4 to 5 were realized for the vacuum runs and around 6 for the atmospheric runs, while the area increment was only about 3 times the smooth-tube area. The additional enhancement is due to the thinning effect; therefore, any theoretical model that neglects this effect may have severe deviations from the experimental data.

2. The 1.5 mm fin spacing appears to be the optimum among the fin spacings tested (0.5, 1.0, 1.5, 2.0 and 4.0 mm) for both vacuum and near-atmospheric pressure conditions.

3. The condensation enhancement does not strongly depend on the fin thickness. However, the tubes with fin thickness around 0.75 to 1.0 mm performed better than the tubes with 0.5 and 1.5 mm fin thicknesses.

4. As the fin height increased from 1.0 to 2.0 mm, the condensing coefficient increased only by about 20 percent, despite an area increase of about 50 percent. This lower-than-expected performance is believed to be owing to the poorer thinning effect of the condensate film with increasing fin height.

5. As the tube diameter increases, the retention angle decreases resulting in a better heat-transfer performance;

therefore, the tubes with a root diameter of 19.0 mm showed a superior enhancement over the tubes with a 12.7 mm root diameter.

6. The consistency of equation (1.12) that predicts the retention angle was visually verified throughout all the experiments. Certainly, it must be a very useful equation to predict the condensate retention angle when modelling steam condensation on finned tubes.

7. The leading coefficient of the Sieder-Tate-type equation used to determine the water-side resistance with the instrumented tube was 0.0635, while the modified Wilson plot technique gave the same coefficient as 0.071.

8. The test apparatus successfully operates under any pressure condition. An extremely tight apparatus is achieved resulting in minimization of the non-condensing gas effect.

9. A tube-cleaning and preparation procedure has been established to ensure filmwise condensation on copper tubes.

B. RECOMMENDATIONS

1. Calibrate the existing pressure transducer in order to replace the U-tube, mercury-in-glass manometer. This will make each run faster and more automatic (less data to be entered manually).

2. Install the relief valve on the test condenser.

3. Take data with different shaped fins (at the tip as well as at the root of the fin) to investigate the effect of fin geometry.

4. Take data with tubes that are fabricated with different thermal conductivity materials to investigate the effect of the material conductivity on the condensing heat-transfer coefficient.

5. Attach drainage strips on the existing tubes to investigate the effect of the drainage strips on steam condensation enhancement.

6. Take data to study the effect of vapor shear on finned tube enhancement. For the vacuum runs, it is recommended that vapor velocities of 1.0, 2.0, 3.0 and 4.0 m/s be used and for the atmospheric runs the vapor velocities of 0.7 and 1.0 m/s. Higher vapor velocities would be desirable if the apparatus could be modified.

7. Modify the existing apparatus to study the condensate inundation effect and take data to investigate if the enhancement and the optimum fin spacing are affected by inundation.

8. Take data on finned tubes that are coated with a dropwise promoter. Since the presence of the fins will result in a more effective bonding of the promoter, this combination may result in superior enhancement and promoter endurance. Also, the condensate may not be retained on dropwise-coated finned tubes with sufficient fin spacing.

9. Modify equation (1.14) of Owen et al. [Ref. 8] to include the surface-tension effect on the unflooded part of the tube. By including this effect, the Owen prediction for the steam data will become less conservative.

APPENDIX A

PREPARATION OF CONDENSER TUBES

Before every run, the tube was prepared by following the steps below. The operator must wear gloves to avoid contamination of the tube as well as to avoid skin irritation that may be caused by the cleaning solution.

1. Prepare a solution of equal parts of sodium hydroxide and methyl alcohol. Heat the solution until it becomes watery. Using a toothbrush, apply a coating of this mixture on the tube.
2. Place the coated tube in a steam bath for about one hour.
3. Rinse the tube with tap water to avoid contamination of the apparatus with the solution.
4. Clean the external surface of the tube with a brush using a weak solution of tap water and a detergent (Sparkleen). This will ensure that all the sodium hydroxide deposits are removed from the corners of the fins.
5. Using a brush, clean the inside surface of the tube. It is essential to remove any fouling.
6. Install the tube as soon as possible to avoid any system contamination from the environment.

APPENDIX B

SYSTEM START-UP AND SHUT-DOWN PROCEDURES

To start the system, the following procedure is recommended:

1. Ensure that the boiler water level in the boiler is at least six inches above the upper level of the heaters.

2. Close the venting valve and open the valve on the purge line (see Figure 2.1).

3. Ensure that the vacuum pump is filled with oil at the right level.

4. Turn on the vacuum pump.

5. If the run is for low pressure then turn on the boiler power when the system pressure approximates the desired pressure. Avoid boiling if the system pressure is greater by 50 mmHg than the desired pressure. Boiling at an elevated pressure causes the apparatus walls to reach a temperature higher than the desired saturation temperature. If this happens, a considerable time interval (as much as 30 minutes for a temperature difference of 10 K) will be needed to avoid superheated steam. Note that when the system walls are at an elevated temperature, the steam gains heat, thus causing superheating. The power input is controlled by a potentiometer until the voltmeter reads 90 units (note that each unit represents 2.2 Volts). This setting yields a 2.0

m/s vapor velocity at a system pressure of 85 mmHg. If the run is an atmospheric one, then, turn on the power right after the vacuum pump is energized. For a vapor velocity of 1.0 m/s, the voltmeter should be set at its maximum which is 170 units or (170.0 × 2.2) Volts.

6. Open the valve to fill the tap water sump.

7. Circulate tap water through the auxiliary condenser.

8. Check that the water sump is filled and then turn on the pumps that circulate water through the test bue.

9. When the steam reaches the tube (as can be seen from the viewport), adjust the water flowrate through the auxiliary condenser in order to achieve the desired pressure.

10. Energize the data acquisition system, the computer, the printer and insert in the driver of the computer the disk which contains the code "DRP4." Finally, load "DRP4" and follow the interactive program to gather and analyze data.

To secure the system:

1. Turn off the input power to the boiler.

2. Secure the water supply to the auxiliary condenser.

3. Open the venting valve to relieve the pressure in the apparatus.

4. Turn off the printer, the data acquisition system and the computer.

5. Secure the pumps that circulate tap water through the test tube.

APPENDIX C

RAW DATA OF UNINSTRUMENTED AND INSTRUMENTED TUBE

The following two tables contain the raw data taken for the uninstrumented and instrumented tubes under vacuum and near-atmospheric conditions.

TABLE V

Raw Data of Uninstrumented Smooth Tube

File Name : WSIV14
Pressure Condition: Vacuum (85 mmHg)
Vapor Velocity : 1.0 m/s

Vw m/s	Tin °C	Tout °C	Ts °C
4.47	18.58	19.37	49.45
3.93	18.63	19.48	49.59
3.38	18.70	19.65	49.46
3.10	18.71	19.72	49.76
2.71	18.81	19.92	49.41
1.99	18.99	20.34	49.84
1.48	19.19	20.87	49.49
1.15	19.46	21.46	49.53

File Name : WSIA16
Pressure Condition: Atmospheric
Vapor Velocity : 0.8 m/s

Vw m/s	Tin °C	Tout °C	Ts °C
4.49	18.84	20.65	99.81
3.93	18.91	20.94	99.96
3.38	18.99	21.31	100.11
3.10	19.00	21.48	99.93
2.71	19.11	21.85	100.31
1.99	19.32	22.84	100.26
1.48	19.56	23.92	99.98
1.15	19.91	25.20	99.97

TABLE VI

Raw Data of Instrumented Tube

Pressure Condition : Vacuum
File Name of the Run: SDV9

Vw m/s	Tin °C	Tout °C	Ts °C	Temperature of Thermocouples °C					
				1	2	3	4	5	6
4.24	17.71	18.46	48.26	26.35	28.39	29.20	29.33	25.96	23.65
3.61	17.76	18.63	48.21	27.28	29.29	30.19	30.27	26.84	24.55
2.80	17.85	18.92	48.47	28.72	30.87	31.89	31.92	28.39	26.01
2.25	17.93	19.21	48.52	29.96	32.19	33.19	33.16	29.78	27.29
1.98	17.96	19.36	48.59	30.74	33.05	33.98	33.88	30.51	27.93
1.55	18.03	19.71	48.54	32.06	34.26	35.28	35.27	31.99	29.55
1.17	18.17	20.23	48.56	33.63	35.79	36.78	36.88	33.70	31.23
2.53	17.79	18.96	48.42	29.28	31.48	32.41	32.36	29.98	26.57

Pressure Condition : Atmospheric
File Name of the Run: SD3

4.36	19.54	21.23	100.02	47.92	38.58	34.18	35.38	42.53	43.25
3.87	19.51	21.41	100.11	49.81	39.96	35.39	37.03	44.12	44.88
3.33	19.57	21.74	99.57	52.34	41.69	37.25	38.81	45.80	47.02
2.79	19.53	22.03	99.31	54.40	42.98	39.32	41.13	47.90	48.69
2.25	19.49	22.49	100.22	58.05	45.62	42.10	44.33	51.12	51.83
1.71	19.54	23.22	99.72	61.91	48.99	45.68	47.96	54.46	55.45
1.17	19.72	24.69	99.94	67.64	53.55	52.07	54.01	60.17	60.59
3.06	19.43	21.76	99.70	53.56	42.56	38.05	39.88	47.04	48.06

APPENDIX D

RAW DATA OF TUBES TESTED

The following pages contain tables with the raw data taken for all tubes tested under vacuum and near-atmospheric conditions.

TABLE VII

Raw Data of Tube with Fins of s = 0.5, t = 1.0 and e = 1.0 mm

File Name of Raw Data : F15IV87
Pressure condition : VACUUM
Vapor Velocity : 2.0 m/s

Data #	V_w (m/s)	Tin C	Tout C	Ts C
1	4.39	21.76	22.87	48.39
2	4.39	21.75	22.87	48.55
3	3.86	21.80	23.01	48.55
4	3.86	21.80	23.01	48.60
5	3.32	21.86	23.18	48.55
6	3.32	21.86	23.18	48.55
7	2.51	21.97	23.53	48.71
8	2.51	21.97	23.54	48.68
9	1.97	22.10	23.90	48.57
10	1.97	22.10	23.89	48.54
11	1.48	22.29	24.38	48.63
12	1.48	22.29	24.38	48.57
13	1.16	22.50	24.90	48.73
14	1.16	22.50	24.90	48.72
15	3.05	21.86	23.26	48.27
16	3.05	21.86	23.25	48.26
17	4.39	21.70	22.82	48.37
18	4.39	21.70	22.81	48.32

File Name of Raw Data : F15IA113
Pressure condition : ATMOSPHERIC
Vapor Velocity : 1.0 m/s

Data #	V_w (m/s)	Tin C	Tout C	Ts C
1	4.40	22.22	25.73	99.79
2	4.40	22.23	25.75	99.93
3	3.86	22.31	26.17	100.34
4	3.86	22.31	26.16	100.23
5	3.32	22.40	26.66	100.18
6	3.32	22.40	26.67	100.25
7	2.51	22.57	27.60	100.09
8	2.51	22.58	27.62	100.00
9	1.97	22.75	28.55	99.95
10	1.97	22.74	28.53	99.94
11	1.48	22.94	29.73	99.86
12	1.48	22.94	29.72	99.73
13	1.16	23.20	30.95	99.76
14	1.16	23.20	30.96	99.78
15	3.05	22.64	27.18	99.84
16	3.05	22.64	27.18	99.86
17	4.34	22.48	26.08	99.74
18	4.34	22.48	26.08	99.86

TABLE VIII

Raw Data of Tube with Fins of s = 1.0, t = 1.0 and e = 1.0 mm

File Name of Raw Data : F02IV170
Pressure condition : VACUUM
Vapor Velocity : 2.0 m/s

Data #	Vw (m/s)	Tin C	Tout C	Ts C
1	4.39	23.13	24.36	48.40
2	4.39	23.15	24.37	48.40
3	3.85	23.27	24.58	48.59
4	3.85	23.28	24.60	48.69
5	3.31	23.36	24.80	48.62
6	3.31	23.37	24.80	48.65
7	2.50	23.52	25.18	48.46
8	2.50	23.52	25.18	48.48
9	1.97	23.65	25.54	48.63
10	1.97	23.65	25.54	48.58
11	1.48	23.85	25.98	48.15
12	1.48	23.84	25.97	48.23
13	1.16	24.03	26.43	48.33
14	1.16	24.04	26.46	48.45
15	3.04	23.43	24.93	48.54
16	3.04	23.43	24.93	48.58
17	4.39	23.28	24.52	48.64
18	4.39	23.27	24.51	48.69

File Name of Raw Data : F02IA131
Pressure condition : ATMOSPHERIC
Vapor Velocity : 1.0 m/s

Data #	Vw (m/s)	Tin C	Tout C	Ts C
1	4.39	22.82	26.59	100.20
2	4.39	22.84	26.62	100.28
3	3.85	22.92	27.02	100.06
4	3.85	22.94	27.02	100.06
5	3.31	23.06	27.56	100.02
6	3.31	23.06	27.56	100.05
7	2.51	23.24	28.56	100.25
8	2.51	23.25	28.57	100.26
9	1.97	23.43	29.47	99.64
10	1.97	23.43	29.47	99.55
11	1.48	23.74	30.81	100.02
12	1.48	23.76	30.81	99.72
13	1.16	24.02	32.04	99.87
14	1.16	24.02	32.06	100.03
15	3.04	23.49	28.26	100.25
16	3.04	23.49	28.26	100.21
17	4.39	23.37	27.18	99.93
18	4.39	23.36	27.18	99.84

TABLE IX

Raw Data of Tube with Fins of s = 1.5, t = 1.0 and e = 1.0 mm

File Name of Raw Data : F25IV165
Pressure condition : VACUUM
Vapor Velocity : 2.0 m/s

Data #	Vw (m/s)	Tin C	Tout C	Ts C
1	4.39	23.53	24.78	48.53
2	4.39	23.54	24.79	48.49
3	3.85	23.66	24.99	48.50
4	3.85	23.65	24.98	48.52
5	3.31	23.75	25.20	48.76
6	3.31	23.75	25.20	48.63
7	2.50	23.90	25.57	48.63
8	2.50	23.90	25.57	48.60
9	1.96	24.05	25.93	48.44
10	1.96	24.05	25.93	48.51
11	1.48	24.24	26.39	48.54
12	1.48	24.24	26.39	48.52
13	1.16	24.43	26.85	48.46
14	1.16	24.43	26.85	48.51
15	3.04	23.82	25.34	48.61
16	3.04	23.82	25.33	48.60
17	4.39	23.67	24.92	48.57
18	4.39	23.66	24.90	48.39

File Name of Raw Data : F25IA118
Pressure condition : ATMOSPHERIC
Vapor Velocity : 1.0 m/s

Data #	Vw (m/s)	Tin C	Tout C	Ts C
1	4.39	22.60	26.50	99.92
2	4.39	22.59	26.49	99.90
3	3.86	22.63	26.86	99.86
4	3.86	22.61	26.84	99.94
5	3.32	22.66	27.32	100.20
6	3.32	22.64	27.30	100.30
7	2.51	22.72	28.19	100.05
8	2.51	22.71	28.18	100.15
9	1.97	22.82	29.07	99.94
10	1.97	22.82	29.08	100.09
11	1.48	23.02	30.29	100.09
12	1.48	23.00	30.26	99.96
13	1.16	23.23	31.43	99.79
14	1.16	23.21	31.41	99.69
15	3.05	22.56	27.48	100.03
16	3.05	22.55	27.46	99.91
17	4.40	22.40	26.33	99.82
18	4.40	22.39	26.32	99.84

TABLE X

Raw Data of Tube with Fins of s = 2.0, t = 1.0 and e = 1.0 mm

File Name of Raw Data : F03IV161
Pressure condition : VACUUM
Vapor Velocity : 2.0 m/s

Data #	Vw (m/s)	Tin C	Tout C	Ts C
1	4.39	22.88	24.07	48.46
2	4.39	22.89	24.08	48.44
3	3.85	22.95	24.22	48.15
4	3.85	22.95	24.21	47.97
5	3.31	23.00	24.38	48.27
6	3.31	23.00	24.39	48.40
7	2.51	23.12	24.75	48.63
8	2.51	23.12	24.76	48.66
9	1.97	23.25	25.11	48.59
10	1.97	23.25	25.10	48.58
11	1.48	23.43	25.58	48.59
12	1.48	23.43	25.58	48.54
13	1.16	23.63	26.06	48.67
14	1.16	23.64	26.09	48.87
15	3.04	23.01	24.44	48.05
16	3.04	23.00	24.44	48.12
17	4.39	22.62	24.03	48.59
18	4.39	22.82	24.03	48.50

File Name of Raw Data : F03IA117
Pressure condition : ATMOSPHERIC
Vapor Velocity : 1.0 m/s

Data #	Vw (m/s)	Tin C	Tout C	Ts C
1	4.40	22.27	25.96	99.97
2	4.40	22.27	25.97	99.82
3	3.86	22.33	26.36	100.02
4	3.86	22.34	26.37	99.95
5	3.32	22.44	26.87	99.93
6	3.32	22.46	26.88	99.93
7	2.51	22.62	27.83	99.83
8	2.51	22.62	27.84	99.77
9	1.97	22.79	28.80	100.07
10	1.97	22.80	28.81	100.04
11	1.48	23.06	30.09	100.18
12	1.48	23.07	30.10	100.23
13	1.16	23.28	31.23	99.98
14	1.16	23.29	31.23	99.96
15	3.05	22.67	27.35	100.15
16	3.05	22.68	27.35	100.25
17	4.39	22.51	26.24	99.94
18	4.39	22.52	26.24	100.09

TABLE XI

Raw Data of Tube with Fins of s = 4.0, t = 1.0 and e = 1.0 mm

File Name of Raw Data : F05IV153
Pressure condition : VACUUM
Vapor Velocity : 2.0 m/s

Data #	Vw (m/s)	Tin C	Tout C	Ts C
1	4.39	23.17	24.30	48.52
2	4.39	23.30	24.44	48.69
3	3.85	23.48	24.71	48.68
4	3.85	23.48	24.72	48.68
5	3.31	23.57	24.91	48.70
6	3.31	23.57	24.91	48.65
7	2.50	23.71	25.29	48.70
8	2.50	23.72	25.28	48.67
9	1.97	23.86	25.63	48.43
10	1.96	23.86	25.63	48.39
11	1.48	24.05	26.10	48.45
12	1.48	24.05	26.11	48.48
13	1.16	24.25	26.57	48.48
14	1.16	24.25	26.58	48.46
15	3.04	23.68	25.10	48.56
16	3.04	23.68	25.09	48.53
17	4.39	23.53	24.68	48.62
18	4.39	23.53	24.68	48.52

File Name of Raw Data : F05IA116
Pressure condition : ATMOSPHERIC
Vapor Velocity : 1.0 m/s

Data #	Vw (m/s)	Tin C	Tout C	Ts C
1	4.40	22.16	25.58	100.08
2	4.40	22.16	25.59	99.94
3	3.86	22.24	25.99	99.97
4	3.86	22.25	26.00	99.94
5	3.32	22.33	26.47	99.79
6	3.32	22.34	26.47	99.75
7	2.51	22.50	27.43	99.87
8	2.51	22.49	27.43	99.92
9	1.97	22.63	28.34	100.04
10	1.97	22.64	28.34	99.87
11	1.48	22.85	29.56	99.90
12	1.48	22.85	29.55	99.85
13	1.16	23.10	30.81	100.07
14	1.16	23.09	30.81	100.18
15	3.05	22.47	26.90	100.03
16	3.05	22.47	26.89	100.00
17	4.40	22.31	25.80	99.76
18	4.40	22.31	25.80	99.82

TABLE XII

Raw Data of Tube with Fins of s = 0.5, t = 0.75 and e = 1.0 mm

File Name of Raw Data : F125IV48
Pressure condition : VACUUM
Vapor Velocity : 2.0 m/s

Data #	Vw (m/s)	Tin C	Tout C	Ts C
1	4.41	19.84	21.05	48.47
2	4.41	19.83	21.03	48.25
3	3.87	19.87	21.18	48.20
4	3.87	19.87	21.19	48.28
5	3.33	19.93	21.38	48.29
6	3.33	19.92	21.37	48.28
7	2.52	20.05	21.75	48.46
8	2.52	20.04	21.74	48.52
9	1.98	20.18	22.14	48.56
10	1.98	20.17	22.13	48.43
11	1.49	20.36	22.63	48.36
12	1.49	20.36	22.63	48.35
13	1.16	20.57	23.15	48.40
14	1.16	20.57	23.15	48.20
15	3.06	19.91	21.45	48.36
16	3.06	19.91	21.46	48.63
17	4.41	19.72	20.98	48.46
18	4.41	19.71	20.97	48.25

File Name of Raw Data : F125IA101
Pressure condition : ATMOSPHERIC
Vapor Velocity : 1.0 m/s

Data #	Vw (m/s)	Tin C	Tout C	Ts C
1	4.39	22.48	26.10	99.87
2	4.40	22.47	26.10	100.17
3	3.86	22.49	26.43	100.17
4	3.86	22.46	26.42	100.14
5	3.32	22.50	26.84	99.88
6	3.32	22.51	26.84	99.83
7	2.51	22.61	27.76	100.11
8	2.51	22.60	27.76	100.20
9	1.97	22.74	28.66	100.16
10	1.97	22.74	28.66	100.29
11	1.48	22.91	29.83	99.89
12	1.48	22.91	29.81	99.82
13	1.16	23.13	30.96	99.61
14	1.16	23.13	30.98	99.65
15	3.05	22.49	27.10	99.80
16	3.05	22.49	27.11	99.88
17	4.40	22.33	26.02	100.02
18	4.40	22.34	26.02	100.15

TABLE XIII

Raw Data of Tube with Fins of s = 1.0, t = 0.75 and e = 1.0 mm

File Name of Raw Data : F175IV46
Pressure condition : VACUUM
Vapor Velocity : 2.0 m/s

Data #	Vw (m/s)	Tin C	Tout C	Ts C
1	4.42	18.88	20.21	48.49
2	4.42	18.90	20.23	48.57
3	3.88	19.01	20.44	48.47
4	3.88	19.02	20.44	48.37
5	3.33	19.10	20.66	48.50
6	3.33	19.10	20.65	48.52
7	2.52	19.23	21.04	48.48
8	2.52	19.23	21.04	48.40
9	1.98	19.33	21.39	48.28
10	1.98	19.31	21.40	48.56
11	1.49	19.50	21.90	48.46
12	1.49	19.50	21.90	48.38
13	1.17	19.69	22.41	48.38
14	1.17	19.69	22.39	48.24
15	3.06	19.01	20.65	48.44
16	3.06	19.01	20.65	48.50
17	4.42	18.82	20.17	48.71
18	4.42	18.80	20.15	48.56

File Name of Raw Data : F175IA104
Pressure condition : ATMOSPHERIC
Vapor Velocity : 1.0 m/s

Data #	Vw (m/s)	Tin C	Tout C	Ts C
1	4.40	22.06	25.88	100.25
2	4.40	22.08	25.89	100.10
3	3.86	22.18	26.31	100.04
4	3.86	22.19	26.32	99.99
5	3.32	22.28	26.83	100.17
6	3.32	22.29	26.83	100.03
7	2.51	22.49	27.83	99.86
8	2.51	22.50	27.83	99.73
9	1.97	22.66	28.78	99.90
10	1.97	22.68	28.81	100.01
11	1.48	22.90	30.05	100.11
12	1.48	22.90	30.05	100.07
13	1.16	23.13	31.23	99.91
14	1.16	23.13	31.24	99.89
15	3.05	22.52	27.33	99.98
16	3.05	22.53	27.32	100.01
17	4.40	22.36	26.20	100.09
18	4.40	22.36	26.20	100.10

TABLE XIV

Raw Data of Tube with Fins of s = 1.5, t = 0.75 and e = 1.0 mm

File Name of Raw Data : F225IV50
Pressure Condition : VACUUM
Vapor Velocity : 2.0 m/s

Data #	Vw (m/s)	Tin C	Tout C	Ts C
1	4.41	20.06	21.40	48.58
2	4.41	20.06	21.40	48.64
3	3.87	20.12	21.55	48.49
4	3.87	20.11	21.54	48.37
5	3.33	20.18	21.73	48.37
6	3.33	20.17	21.73	48.40
7	2.52	20.31	22.12	48.46
8	2.52	20.30	22.12	48.41
9	1.98	20.45	22.51	48.28
10	1.98	20.44	22.50	48.25
11	1.49	20.62	23.01	48.55
12	1.49	20.62	23.03	48.69
13	1.16	20.84	23.55	48.54
14	1.16	20.84	23.55	48.51
15	3.06	20.16	21.81	48.55
16	3.06	20.16	21.82	48.65
17	4.41	19.93	21.28	48.40
18	4.41	19.92	21.28	48.59

File Name of Raw Data : F225IA103
Pressure Condition : ATMOSPHERIC
Vapor Velocity : 1.0 m/s

Data #	Vw (m/s)	Tin C	Tout C	Ts C
1	4.40	21.96	25.89	100.19
2	4.40	21.97	25.91	100.22
3	3.86	22.05	26.29	99.80
4	3.86	22.06	26.30	99.80
5	3.32	22.15	26.80	99.84
6	3.32	22.15	26.81	99.85
7	2.51	22.32	27.76	99.67
8	2.51	22.33	27.77	99.63
9	1.97	22.49	28.73	99.90
10	1.97	22.49	28.73	99.93
11	1.48	22.72	30.00	100.26
12	1.48	22.73	30.00	100.17
13	1.16	23.00	31.20	99.75
14	1.16	22.98	31.20	99.86
15	3.05	22.35	27.27	100.19
16	3.05	22.35	27.26	100.08
17	4.40	22.20	26.14	100.03
18	4.40	22.20	26.15	99.93

TABLE XV

Raw Data of Tube with Fins of s = 2.0, t = 0.75 and e = 1.0 mm

File Name of Raw Data : F275IV51
Pressure Condition : VACUUM
Vapor Velocity : 2.0 m/s

Data #	Vw (m/s)	Tin C	Tout C	Ts C
1	4.41	19.73	21.06	48.66
2	4.41	19.73	21.06	48.68
3	3.87	19.81	21.23	48.38
4	3.87	19.82	21.24	48.37
5	3.33	19.91	21.46	48.35
6	3.33	19.96	21.52	48.82
7	2.52	20.19	21.99	48.52
8	2.52	20.19	22.00	48.40
9	1.98	20.38	22.44	48.63
10	1.98	20.40	22.48	48.87
11	1.49	20.63	22.98	48.34
12	1.49	20.64	22.99	48.29
13	1.16	20.91	23.58	48.48
14	1.16	20.92	23.59	48.47
15	3.06	20.26	21.89	48.63
16	3.06	20.26	21.89	48.60
17	4.41	20.09	21.41	48.42
18	4.41	20.10	21.41	48.34

File Name of Raw Data : F275IA98
Pressure Condition : ATMOSPHERIC
Vapor Velocity : 1.0 m/s

Data #	Vw (m/s)	Tin C	Tout C	Ts C
1	4.40	22.13	25.99	99.89
2	4.40	22.12	25.97	99.64
3	3.86	22.15	26.34	99.82
4	3.86	22.15	26.34	99.98
5	3.32	22.18	26.80	100.15
6	3.32	22.18	26.79	100.06
7	2.51	22.30	27.72	100.04
8	2.51	22.29	27.71	99.92
9	1.97	22.43	28.64	100.00
10	1.97	22.43	28.64	100.06
11	1.48	22.61	29.81	99.93
12	1.48	22.62	29.82	99.95
13	1.16	22.83	31.03	100.04
14	1.16	22.84	31.02	99.93
15	3.05	22.20	27.05	99.86
16	3.05	22.20	27.06	99.87
17	4.40	22.04	25.93	99.92
18	4.40	22.04	25.93	99.87

TABLE XVI

Raw Data of Tube with Fins of s = 4.0, t = 0.75 and e = 1.0 mm

File Name of Raw Data : F475IV30
Pressure Condition : VACUUM
Vapor Velocity : 2.0 m/s

Data #	Vw (m/s)	Tin C	Tout C	Ts C
1	4.46	19.25	20.55	48.40
2	4.46	19.26	20.56	48.49
3	3.87	19.33	20.74	48.59
4	3.87	19.34	20.74	48.59
5	3.33	19.41	20.95	48.62
6	3.33	19.41	20.96	48.61
7	2.52	19.55	21.35	48.72
8	2.52	19.56	21.35	48.75
9	1.98	19.71	21.76	48.65
10	1.98	19.71	21.76	48.65
11	1.49	19.91	22.29	48.60
12	1.49	19.91	22.30	48.53
13	1.17	20.14	22.84	48.50
14	1.17	20.14	22.83	48.50
15	3.06	19.46	21.08	48.46
16	3.06	19.47	21.07	48.50
17	4.46	19.27	20.58	48.63
18	4.46	19.27	20.58	48.70

File Name of Raw Data : F475IA97
Pressure Condition : ATMOSPHERIC
Vapor Velocity : 1.0 m/s

Data #	Vw (m/s)	Tin C	Tout C	Ts C
1	4.40	21.77	25.22	100.10
2	4.40	21.77	25.22	99.96
3	3.86	21.80	25.57	100.07
4	3.86	21.79	25.57	100.19
5	3.32	21.84	26.03	100.21
6	3.32	21.83	26.02	100.16
7	2.51	21.98	26.94	100.18
8	2.51	21.96	26.92	100.17
9	1.97	22.12	27.86	99.95
10	1.97	22.12	27.85	99.93
11	1.49	22.30	29.04	100.03
12	1.49	22.30	29.04	100.08
13	1.16	22.53	30.23	99.87
14	1.16	22.53	30.23	99.73
15	3.05	21.89	26.32	100.17
16	3.05	21.89	26.33	100.31
17	4.40	21.73	25.22	100.40
18	4.40	21.73	25.22	100.35

TABLE XVII

Raw Data of Tube with Fins of s = 0.5, t = 0.5 and e = 1.0 mm

File Name of Raw Data : F100IV55
Pressure Condition : VACUUM
Vapor Velocity : 2.0 m/s

Data #	Vw (m/s)	Tin C	Tout C	Ts C
1	4.41	19.92	21.11	48.48
2	4.41	19.91	21.11	48.73
3	3.87	19.94	21.24	48.37
4	3.87	19.94	21.24	48.26
5	3.33	19.98	21.39	48.41
6	3.33	19.98	21.40	48.48
7	2.52	20.10	21.75	48.35
8	2.52	20.10	21.76	48.36
9	1.98	20.21	22.13	48.45
10	1.98	20.21	22.13	48.39
11	1.49	20.40	22.64	48.42
12	1.49	20.40	22.65	48.41
13	1.16	20.60	23.16	48.45
14	1.16	20.60	23.16	48.40
15	3.06	19.93	21.43	48.41
16	3.06	19.92	21.42	48.59
17	4.41	19.71	20.93	48.51
18	4.41	19.70	20.92	48.47

File Name of Raw Data : F100IA112
Pressure Condition : ATMOSPHERIC
Vapor Velocity : 1.0 m/s

Data #	Vw (m/s)	Tin C	Tout C	Ts C
1	4.40	22.28	25.88	100.17
2	4.40	22.29	25.90	100.28
3	3.86	22.41	26.32	100.26
4	3.86	22.42	26.34	100.16
5	3.32	22.50	26.79	99.84
6	3.32	22.51	26.79	99.69
7	2.51	22.66	27.73	99.65
8	2.51	22.66	27.73	99.68
9	1.97	22.84	28.70	99.96
10	1.97	22.86	28.71	99.93
11	1.48	23.08	29.94	100.04
12	1.48	23.08	29.95	100.12
13	1.16	23.30	31.11	99.89
14	1.16	23.30	31.12	99.93
15	3.05	22.69	27.23	99.82
16	3.05	22.68	27.22	99.76
17	4.39	22.56	26.18	100.21
18	4.39	22.55	26.18	100.24

TABLE XVIII

Raw Data of Tube with Fins of s = 1.0, t = 0.5 and e = 1.0 mm

File Name of Raw Data : F150IV58
Pressure Condition : VACUUM
Vapor Velocity : 2.0 m/s

Data #	Vw (m/s)	Tin C	Tout C	Ts C
1	4.41	19.65	20.92	48.43
2	4.41	19.65	20.93	48.42
3	3.87	19.71	21.08	48.37
4	3.87	19.71	21.08	48.43
5	3.33	19.79	21.28	48.49
6	3.33	19.78	21.28	48.35
7	2.52	19.91	21.67	48.51
8	2.52	19.91	21.67	48.61
9	1.98	20.04	22.06	48.50
10	1.98	20.04	22.06	48.40
11	1.49	20.24	22.58	48.49
12	1.49	20.24	22.59	48.52
13	1.16	20.46	23.11	48.45
14	1.16	20.47	23.12	48.55
15	3.06	19.81	21.39	48.49
16	3.06	19.81	21.39	48.49
17	4.41	19.64	20.93	48.51
18	4.41	19.63	20.93	48.57

File Name of Raw Data : F150IA109
Pressure Condition : ATMOSPHERIC
Vapor Velocity : 1.0 m/s

Data #	Vw (m/s)	Tin C	Tout C	Ts C
1	4.40	21.63	25.35	100.27
2	4.40	21.64	25.37	100.35
3	3.85	21.71	25.76	100.16
4	3.86	21.71	25.76	100.06
5	3.32	21.81	26.27	100.14
6	3.32	21.82	26.28	100.21
7	2.51	21.97	27.21	99.92
8	2.51	21.97	27.21	99.90
9	1.97	22.12	28.14	99.97
10	1.97	22.13	28.16	100.05
11	1.49	22.36	29.38	99.86
12	1.49	22.36	29.39	99.88
13	1.16	22.60	30.65	100.11
14	1.16	22.59	30.64	100.18
15	3.05	21.95	26.65	99.85
16	3.05	21.96	26.65	99.65
17	4.40	21.79	25.55	99.99
18	4.40	21.79	25.56	100.11

TABLE XIX

Raw Data of Tube with Fins of s = 1.5, t = 0.5 and e = 1.0 mm

File Name of Raw Data : F200IV59
Pressure Condition : VACUUM
Vapor Velocity : 2.0 m/s

Data #	Vw (m/s)	Tin C	Tout C	Ts C
1	4.41	20.26	21.57	48.58
2	4.41	20.26	21.56	48.57
3	3.87	20.31	21.71	48.45
4	3.87	20.31	21.70	48.38
5	3.33	20.36	21.88	48.33
6	3.33	20.36	21.88	48.49
7	2.52	20.49	22.26	48.44
8	2.52	20.49	22.26	48.38
9	1.97	20.63	22.65	48.43
10	1.97	20.63	22.65	48.46
11	1.49	20.81	23.17	48.66
12	1.49	20.81	23.17	48.61
13	1.16	21.04	23.69	48.54
14	1.16	21.04	23.70	48.49
15	3.06	20.39	21.99	48.37
16	3.06	20.38	21.99	48.41
17	4.41	20.21	21.52	48.45
18	4.41	20.18	21.49	48.44

File Name of Raw Data : F200IA107
Pressure Condition : ATMOSPHERIC
Vapor Velocity : 1.0 m/s

Data #	Vw (m/s)	Tin C	Tout C	Ts C
1	4.40	21.57	25.46	100.31
2	4.40	21.57	25.47	100.45
3	3.86	21.63	25.83	99.84
4	3.86	21.63	25.83	99.60
5	3.32	21.72	26.34	99.80
6	3.32	21.72	26.34	99.86
7	2.51	21.85	27.28	100.07
8	2.51	21.85	27.29	100.14
9	1.97	21.99	28.20	99.84
10	1.97	22.00	28.21	99.96
11	1.49	22.19	29.43	100.01
12	1.49	22.20	29.43	100.01
13	1.16	22.43	30.65	100.07
14	1.16	22.44	30.66	100.06
15	3.05	21.79	26.66	99.70
16	3.05	21.79	26.67	99.83
17	4.40	21.63	25.56	100.06
18	4.40	21.63	25.56	100.07

TABLE XX

Raw Data of Tube with Fins of s = 2.0, t = 0.5 and e = 1.0 mm

File Name of Raw Data : F250IV68
Pressure Condition : VACUUM
Vapor Velocity : 2.0 m/s

Data #	Vw (m/s)	Tin C	Tout C	Ts C
1	4.40	20.99	22.26	48.66
2	4.40	21.01	22.28	48.55
3	3.86	21.10	22.44	48.29
4	3.86	21.11	22.45	48.31
5	3.32	21.19	22.66	48.34
6	3.32	21.20	22.66	48.33
7	2.51	21.39	23.09	48.38
8	2.51	21.38	23.09	48.31
9	1.97	21.52	23.48	48.42
10	1.97	21.53	23.49	48.48
11	1.49	21.74	24.61	48.57
12	1.49	21.74	24.01	48.57
13	1.16	21.95	24.52	48.46
14	1.16	21.96	24.52	48.39
15	3.05	21.31	22.85	48.38
16	3.05	21.31	22.86	48.48
17	4.40	21.14	22.42	48.58
18	4.40	21.14	22.41	48.54

File Name of Raw Data : F250IA108
Pressure Condition : ATMOSPHERIC
Vapor Velocity : 1.0 m/s

Data #	Vw (m/s)	Tin C	Tout C	Ts C
1	4.40	21.81	25.58	100.13
2	4.40	21.82	25.59	100.00
3	3.86	21.89	25.99	99.83
4	3.86	21.89	25.98	99.90
5	3.32	21.99	26.48	99.86
6	3.32	21.99	26.47	99.78
7	2.51	22.17	27.48	100.12
8	2.51	22.18	27.50	100.19
9	1.97	22.34	28.44	100.16
10	1.97	22.34	28.44	100.18
11	1.48	22.59	29.69	100.00
12	1.48	22.60	29.69	100.00
13	1.16	22.82	30.89	100.17
14	1.16	22.83	30.88	99.88
15	3.05	22.24	26.98	100.04
16	3.05	22.25	26.99	100.12
17	4.40	22.11	25.90	100.10
18	4.40	22.12	25.91	100.01

TABLE XXI

Raw Data of Tube with Fins of s = 4.0, t = 0.5 and e = 1.0 mm

File Name of Raw Data : F450IV57
Pressure Condition : VACUUM
Vapor Velocity : 2.0 m/s

Data #	Vw (m/s)	Tin C	Tout C	Ts C
1	4.41	19.98	21.13	48.53
2	4.41	19.98	21.14	48.58
3	3.87	20.07	21.32	48.52
4	3.87	20.07	21.32	48.55
5	3.33	20.16	21.53	48.50
6	3.33	20.16	21.53	48.46
7	2.52	20.30	21.93	48.52
8	2.52	20.31	21.93	48.62
9	1.98	20.45	22.31	48.48
10	1.98	20.44	22.31	48.55
11	1.49	20.65	22.83	48.59
12	1.49	20.65	22.84	48.54
13	1.16	20.87	23.37	48.64
14	1.16	20.88	23.40	48.76
15	3.06	20.24	21.69	48.46
16	3.06	20.23	21.69	48.51
17	4.41	20.01	21.18	48.58
18	4.41	19.86	21.02	48.49

File Name of Raw Data : F450IA110
Pressure Condition : ATMOSPHERIC
Vapor Velocity : 1.0 m/s

Data #	Vw (m/s)	Tin C	Tout C	Ts C
1	4.40	22.38	25.71	100.11
2	4.40	22.37	25.70	100.20
3	3.86	22.38	26.02	100.16
4	3.86	22.38	26.03	100.25
5	3.32	22.43	26.46	99.81
6	3.32	22.43	26.45	99.80
7	2.51	22.55	27.35	99.83
8	2.51	22.55	27.35	99.91
9	1.97	22.68	28.26	100.10
10	1.97	22.68	28.27	100.09
11	1.48	22.89	29.46	99.97
12	1.48	22.90	29.47	100.00
13	1.16	23.13	30.69	100.16
14	1.16	23.14	30.69	100.26
15	3.05	22.51	26.78	99.94
16	3.05	22.51	26.76	99.77
17	4.40	22.35	25.69	99.93
18	4.40	22.35	25.69	100.00

TABLE XXII

Raw Data of Tube with Fins of s = 1.0, t = 1.0 and e = 2.0 mm

File Name of Raw Data : F02E2V145
Pressure Condition : VACUUM
Vapor Velocity : 2.0 m/s

Data #	V_w (m/s)	T_{in} C	T_{out} C	T_s C
1	4.39	23.29	24.58	48.71
2	4.39	23.31	24.59	48.73
3	3.85	23.38	24.76	48.67
4	3.85	23.41	24.78	48.73
5	3.31	23.50	24.98	48.58
6	3.31	23.50	24.98	48.55
7	2.50	23.66	25.35	48.43
8	2.50	23.66	25.35	48.39
9	1.97	23.81	25.74	48.57
10	1.97	23.82	25.75	48.67
11	1.48	24.02	26.22	48.51
12	1.48	24.02	26.22	48.51
13	1.16	24.23	26.70	48.59
14	1.16	24.23	26.71	48.62
15	3.04	23.65	25.21	48.71
16	3.04	23.65	25.19	48.51
17	4.39	23.49	24.74	48.03
18	4.39	23.49	24.75	48.04

File Name of Raw Data : F02E2A137
Pressure Condition : ATMOSPHERIC
Vapor Velocity : 1.0 m/s

Data #	V_w (m/s)	T_{in} C	T_{out} C	T_s C
1	4.39	23.37	27.28	99.90
2	4.39	23.38	27.29	99.84
3	3.85	23.52	27.76	99.89
4	3.85	23.54	27.79	99.98
5	3.31	23.64	28.28	99.84
6	3.31	23.64	28.29	99.84
7	2.50	23.83	29.30	100.10
8	2.50	23.84	29.31	100.17
9	1.97	24.03	30.25	99.78
10	1.97	24.05	30.27	99.85
11	1.48	24.26	31.51	100.17
12	1.48	24.26	31.50	100.10
13	1.16	24.52	32.70	99.75
14	1.16	24.52	32.71	99.86
15	3.04	23.92	28.84	100.03
16	3.04	23.94	28.85	100.09
17	4.39	23.79	27.73	99.86
18	4.39	23.78	27.73	99.75

TABLE XXIII

Raw Data of Tube with Fins of s = 1.5, t = 1.0 and e = 2.0 mm

File Name of Raw Data : F25E2V146
Pressure Condition : VACUUM
Vapor Velocity : 2.0 m/s

Data #	Vw (m/s)	Tin C	Tout C	Ts C
1	4.39	22.72	24.07	48.35
2	4.39	22.74	24.08	48.33
3	3.85	22.81	24.26	48.56
4	3.85	22.83	24.28	48.66
5	3.31	22.90	24.43	48.06
6	3.31	22.90	24.43	47.92
7	2.51	23.02	24.79	48.13
8	2.51	23.02	24.79	48.20
9	1.97	23.15	25.19	48.72
10	1.97	23.16	25.22	48.97
11	1.48	23.33	25.66	48.69
12	1.48	23.33	25.65	48.65
13	1.16	23.52	26.11	48.53
14	1.16	23.53	26.11	48.53
15	3.04	22.93	24.55	48.40
16	3.04	22.93	24.55	48.38
17	4.39	22.77	24.12	48.47
18	4.39	22.76	24.12	48.50

File Name of Raw Data : F25E2A128
Pressure Condition : ATMOSPHERIC
Vapor Velocity : 1.0 m/s

Data #	Vw (m/s)	Tin C	Tout C	Ts C
1	4.39	22.89	26.96	99.98
2	4.39	22.90	26.96	99.87
3	3.85	23.00	27.40	100.01
4	3.85	23.02	27.43	100.26
5	3.31	23.12	27.94	99.95
6	3.31	23.12	27.94	100.03
7	2.51	23.27	28.88	99.73
8	2.51	23.27	28.87	99.59
9	1.97	23.44	29.83	99.84
10	1.97	23.45	29.86	99.89
11	1.48	23.66	31.11	100.15
12	1.48	23.66	31.10	100.03
13	1.16	23.96	32.32	99.57
14	1.16	23.96	32.29	99.43
15	3.04	23.40	28.50	100.25
16	3.04	23.39	28.50	100.41
17	4.39	23.29	27.38	99.58
18	4.39	23.29	27.38	99.53

TABLE XXIV

Raw Data of Tube with Fins of s = 2.0, t = 1.0 and e = 2.0 mm

File Name of Raw Data : F03E2V147
Pressure Condition : VACUUM
Vapor Velocity : 2.0 m/s

Data $\#$	Vw (m/s)	Tin C	Tout C	Ts C
1	4.39	23.75	25.05	48.57
2	4.39	23.81	25.10	48.43
3	3.85	23.98	25.34	48.12
4	3.85	24.02	25.37	48.14
5	3.31	24.20	25.69	48.67
6	3.31	24.20	25.70	48.75
7	2.50	24.33	26.05	48.66
8	2.50	24.33	26.05	48.62
9	1.96	24.46	26.41	48.72
10	1.96	24.46	26.41	48.74
11	1.48	24.64	26.85	48.65
12	1.48	24.64	26.85	48.65
13	1.16	24.85	27.30	48.52
14	1.16	24.85	27.30	48.51
15	3.04	24.25	25.81	48.71
16	3.04	24.25	25.82	48.67
17	4.38	24.10	25.40	48.68
18	4.38	24.09	25.39	48.58

File Name of Raw Data : F03E2A140
Pressure Condition : ATMOSPHERIC
Vapor Velocity : 1.0 m/s

Data $\#$	Vw (m/s)	Tin C	Tout C	Ts C
1	4.39	23.69	27.71	100.29
2	4.39	23.67	27.68	99.82
3	3.85	23.64	27.96	99.40
4	3.85	23.63	27.95	99.44
5	3.31	23.56	28.34	100.25
6	3.31	23.56	28.34	100.33
7	2.50	23.64	29.21	99.94
8	2.50	23.64	29.21	99.88
9	1.97	23.76	30.10	99.92
10	1.97	23.76	30.10	99.88
11	1.48	23.94	31.34	100.26
12	1.48	23.93	31.35	100.36
13	1.16	24.13	32.48	100.06
14	1.16	24.13	32.47	99.98
15	3.04	23.48	28.49	99.92
16	3.04	23.47	28.49	99.95
17	4.39	23.31	27.38	100.34
18	4.39	23.31	27.39	100.41

TABLE XXV

Raw Data of Tube with Fins of s = 4.0, t = 1.0 and e = 2.0 mm

File Name of Raw Data : F05E2V148
Pressure Condition : VACUUM
Vapor Velocity : 2.0 m/s

Data #	Vw (m/s)	Tin C	Tout C	Ts C
1	4.38	23.90	25.11	48.67
2	4.38	23.91	25.11	48.52
3	3.85	23.96	25.23	48.24
4	3.85	23.95	25.23	48.19
5	3.31	24.00	25.39	48.26
6	3.31	24.00	25.38	48.25
7	2.50	24.10	25.70	48.29
8	2.50	24.08	25.69	48.32
9	1.96	24.18	26.01	48.51
10	1.96	24.18	26.01	48.51
11	1.48	24.27	26.38	48.31
12	1.48	24.26	26.36	48.22
13	1.16	24.43	26.79	48.15
14	1.16	24.43	26.79	48.19
15	3.04	23.80	25.25	48.27
16	3.04	23.79	25.25	48.33
17	4.39	23.62	24.84	48.62
18	4.39	23.62	24.84	48.59

File Name of Raw Data : F05E2A139
Pressure Condition : ATMOSPHERIC
Vapor Velocity : 1.0 m/s

Data #	Vw (m/s)	Tin C	Tout C	Ts C
1	4.39	23.48	27.14	99.94
2	4.39	23.47	27.12	99.73
3	3.85	23.52	27.49	99.64
4	3.85	23.51	27.48	99.57
5	3.31	23.55	27.91	99.69
6	3.31	23.53	27.91	99.75
7	2.50	23.65	28.82	99.83
8	2.50	23.66	28.84	99.79
9	1.97	23.77	29.74	100.10
10	1.97	23.78	29.73	100.01
11	1.48	23.96	30.93	100.12
12	1.48	23.96	30.92	100.01
13	1.16	24.21	32.12	99.93
14	1.16	24.21	32.12	99.90
15	3.04	23.51	28.11	99.36
16	3.04	23.51	28.09	99.24
17	4.39	23.34	27.01	99.67
18	4.39	23.35	27.03	99.69

TABLE XXVI

Raw Data of Tube with Fins of s = 1.0, t = 1.5 and e = 1.0 mm

File Name of Raw Data : 25T15V154
Pressure Condition : VACUUM
Vapor Velocity : 2.0 m/s

Data #	Vw (m/s)	Tin C	Tout C	Ts C
1	4.39	23.77	24.94	48.47
2	4.39	23.78	24.94	48.36
3	3.85	23.87	25.10	48.29
4	3.85	23.87	25.11	48.28
5	3.31	23.93	25.28	48.32
6	3.31	23.94	25.29	48.48
7	2.50	24.06	25.64	48.60
8	2.50	24.06	25.64	48.55
9	1.96	24.19	25.97	48.23
10	1.96	24.19	25.97	48.22
11	1.48	24.37	26.43	48.45
12	1.48	24.37	26.44	48.53
13	1.16	24.55	26.91	48.69
14	1.16	24.56	26.91	48.71
15	3.04	23.97	25.41	48.87
16	3.04	23.97	25.40	48.73
17	4.38	23.82	24.99	48.71
18	4.38	23.83	25.00	48.76

File Name of Raw Data : 25T15A160
Pressure Condition : ATMOSPHERIC
Vapor Velocity : 1.0 m/s

Data #	Vw (m/s)	Tin C	Tout C	Ts C
1	4.39	23.12	26.72	99.85
2	4.39	23.14	26.76	100.21
3	3.85	23.23	27.17	99.89
4	3.85	23.23	27.16	99.62
5	3.31	23.34	27.68	99.85
6	3.31	23.34	27.69	99.95
7	2.51	23.49	28.62	99.81
8	2.51	23.49	28.62	99.81
9	1.97	23.64	29.55	99.81
10	1.97	23.64	29.56	99.76
11	1.48	23.85	30.82	100.27
12	1.48	23.86	30.83	100.40
13	1.16	24.07	31.93	99.79
14	1.16	24.07	31.90	99.45
15	3.04	23.47	28.09	100.01
16	3.04	23.47	28.07	99.97
17	4.39	23.31	26.99	100.09
18	4.39	23.31	26.98	99.89

TABLE XXVII

Raw Data of Rube with Fins of s = 1.25, t = 1.25 and e = 1.0 mm

File Name of Raw Data : FST125V173
Pressure Condition : VACUUM
Vapor Velocity : 2.0 m/s

Data #	Vw (m/s)	Tin C	Tout C	Ts C
1	4.39	23.18	24.41	48.62
2	4.39	23.19	24.43	48.70
3	3.85	23.28	24.60	48.59
4	3.85	23.28	24.60	48.53
5	3.31	23.39	24.82	48.60
6	3.31	23.40	24.83	48.53
7	2.50	23.57	25.21	48.47
8	2.50	23.58	25.22	48.40
9	1.97	23.73	25.60	48.46
10	1.97	23.73	25.60	48.54
11	1.48	23.93	26.09	48.67
12	1.48	23.93	26.10	48.68
13	1.16	24.14	26.58	48.65
14	1.16	24.15	26.58	48.59
15	3.04	23.56	25.04	48.54
16	3.04	23.56	25.05	48.54
17	4.39	23.41	24.62	48.47
18	4.39	23.40	24.63	48.47

File Name of Raw Data : FST125A172
Pressure Condition : ATMOSPHERIC
Vapor Velocity : 1.0 m/s

Data #	Vw (m/s)	Tin C	Tout C	Ts C
1	4.39	23.82	27.53	100.18
2	4.39	23.82	27.55	100.47
3	3.85	23.91	27.98	100.35
4	3.85	23.91	27.97	100.27
5	3.31	23.97	28.43	100.08
6	3.31	23.97	28.44	100.09
7	2.50	24.09	29.32	99.73
8	2.50	24.09	29.31	99.47
9	1.96	24.22	30.25	99.89
10	1.96	24.22	30.26	100.00
11	1.48	24.41	31.47	100.17
12	1.48	24.41	31.48	100.20
13	1.16	24.61	32.58	99.71
14	1.16	24.62	32.58	99.63
15	3.04	24.03	28.77	100.41
16	3.04	24.03	28.77	100.39
17	4.39	23.88	27.63	99.96
18	4.39	23.88	27.62	99.69

TABLE XXVIII

Raw Data of Smooth Tube

File Name of Raw Data : SV14
Pressure condition : VACUUM
Vapor Velocity : 2.0 m/s

Data #	Vw (m/s)	Tin C	Tout C	Ts C
1	4.22	17.64	18.50	48.98
2	4.22	17.63	18.49	48.87
3	3.88	17.65	18.55	48.56
4	3.88	17.65	18.54	48.54
5	3.34	17.67	18.67	48.68
6	3.34	17.67	18.67	48.80
7	2.80	17.72	18.86	48.98
8	2.80	17.72	18.85	49.03
9	2.25	17.78	19.11	49.24
10	2.25	17.78	19.11	49.29
11	1.71	17.84	19.45	49.17
12	1.71	17.84	19.45	49.15
13	1.17	18.04	20.13	49.15
14	1.17	18.03	20.13	49.26
15	2.53	17.70	18.92	48.75
16	2.53	17.70	18.92	48.70
17	3.61	17.61	18.56	48.80
18	3.61	17.61	18.56	48.82

File Name of Raw Data : SIA111
Pressure condition : ATMOSPHERIC
Vapor Velocity : 1.0 m/s

Data #	Vw (m/s)	Tin C	Tout C	Ts C
1	4.40	22.22	24.03	99.88
2	4.40	22.23	24.03	99.79
3	3.86	22.33	24.33	100.03
4	3.86	22.32	24.32	100.23
5	3.32	22.43	24.67	99.92
6	3.32	22.44	24.68	99.99
7	2.51	22.63	25.43	99.86
8	2.51	22.63	25.43	99.71
9	1.97	22.75	26.11	99.78
10	1.97	22.75	26.12	99.82
11	1.48	22.95	27.13	99.76
12	1.48	22.95	27.13	99.73
13	1.16	23.18	28.18	99.62
14	1.16	23.19	28.20	99.70
15.	3.05	22.56	24.98	100.09
16	3.05	22.56	24.97	99.96
17	4.39	22.40	24.21	100.08
18	4.39	22.40	24.21	100.00

APPENDIX E

ERROR ANALYSIS

The numerical data taken during an experiment are used together with theoretical formulations in order to obtain results about the objective of the experiment. Any measurement has an uncertainty which is a function of the device accuracy as well as the experience of the operator. Therefore, the final result may be severely distorted due to the error propagation during the computational steps. In cases where the final result has a large uncertainty, it may be unwise to draw any conclusions.

The probable uncertainty in a computation can be determined from the following equation, as taken from [Ref. 19]:

$$w_R = \left[\left(\frac{\partial R}{\partial x_1} w_1\right)^2 + \left(\frac{\partial R}{\partial x_2} w_2\right)^2 + \ldots + \left(\frac{\partial R}{\partial x_n} w_n\right)^2\right]^{1/2} \tag{E.1}$$

where:

R is the result

$x_1, x_2, \ldots, x_n$ are the measured (independent) variables

$w_1, w_2, \ldots, w_n$ are the uncertainties in the measured (independent) variables.

The above equation, together with the uncertainty of each measurement, was used to determine the possible error of the outside heat-transfer coefficient. As discussed in Chapter V, the outside resistance was found by subtracting the water-side and tube-wall resistances from the overall resistance. This means that the error in the condensing coefficient is mainly a function of the overall and the water-side resistances. In such cases, if the water-side resistance has a significant error it will be unavoidably reflected in the condensing heat-transfer coefficient. Further, if the value of the water-side resistance is much larger than the condensing resistance, then the error that will appear in the condensing coefficient will be highly amplified. The steam-side resistance is generally smaller, especially on finned tubes, then the water-side resistance (recall that the condensation process is a phase change phenomenon where the heat-transfer process is very effective). Therefore, to 'protect' the final result of the condensing coefficient from an excessive error, the water-side and condensing resistances should be as nearly balanced as possible. The water-side resistance can be reduced either by increasing the coolant velocity or by internal enhancement. Both ways promote turbulence and reduce the boundary layer thickness on the inside wall surface (recall that the coiled insert was used exactly for this purpose). However, since the water-side temperature rise decreases with increase in water velocity, the water velocity must not be too excessive. Since the water-side temperature rise is the most crucial measurement, a minimum value must be assigned to minimize experimental errors. For this reason, the internal enhancement is preferable than the increase in water velocity to obtain a lower thermal resistance on the waterside.

Based on the above discussion, it should be expected that as the cooling water flow rate decreases (i.e., less turbulence), the error in the outside heat-transfer coefficient should increase. Figures E.1 and E.2 show the error bands for three cooling water flow rates for the tube that showed the best heat-transfer performance (1.0 mm fin thickness, 1.5 mm fin spacing and 2.0 mm fin height) for both pressure conditions. It is shown that indeed the error gets larger as the cooling water flow rate (i.e., the heat flux) decreases. Also notice that the error bands shown with the atmospheric run are smaller than the corresponding value for the vacuum runs. This improvement can be explained by the increased water-side temperature rise. Note that the relative error decreases as the water-side temperature rise increases.

Based on the foregoing discussion, it is clear why the reference heat fluxes for computing the enhancement ratio of the cross plots in Chapter V were selected as high as possible (0.35 and 1.0 MW/m^2 for vacuum and atmospheric runs, respectively).

The uncertainty of the major variables that govern the condensation process (cooling water velocity, Reynolds

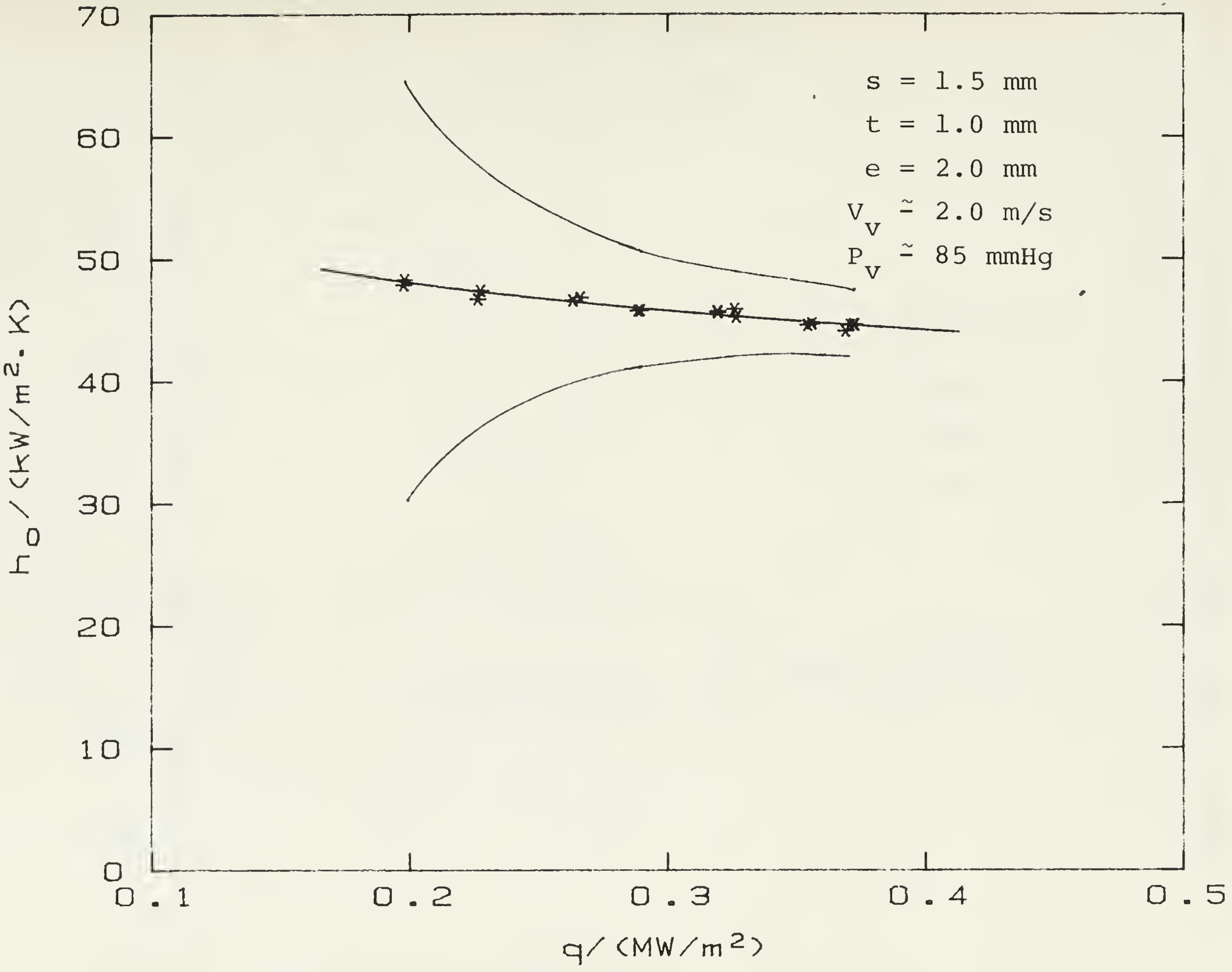

Figure E.1. Error Bands for a Tube Tested Under Vacuum Conditions

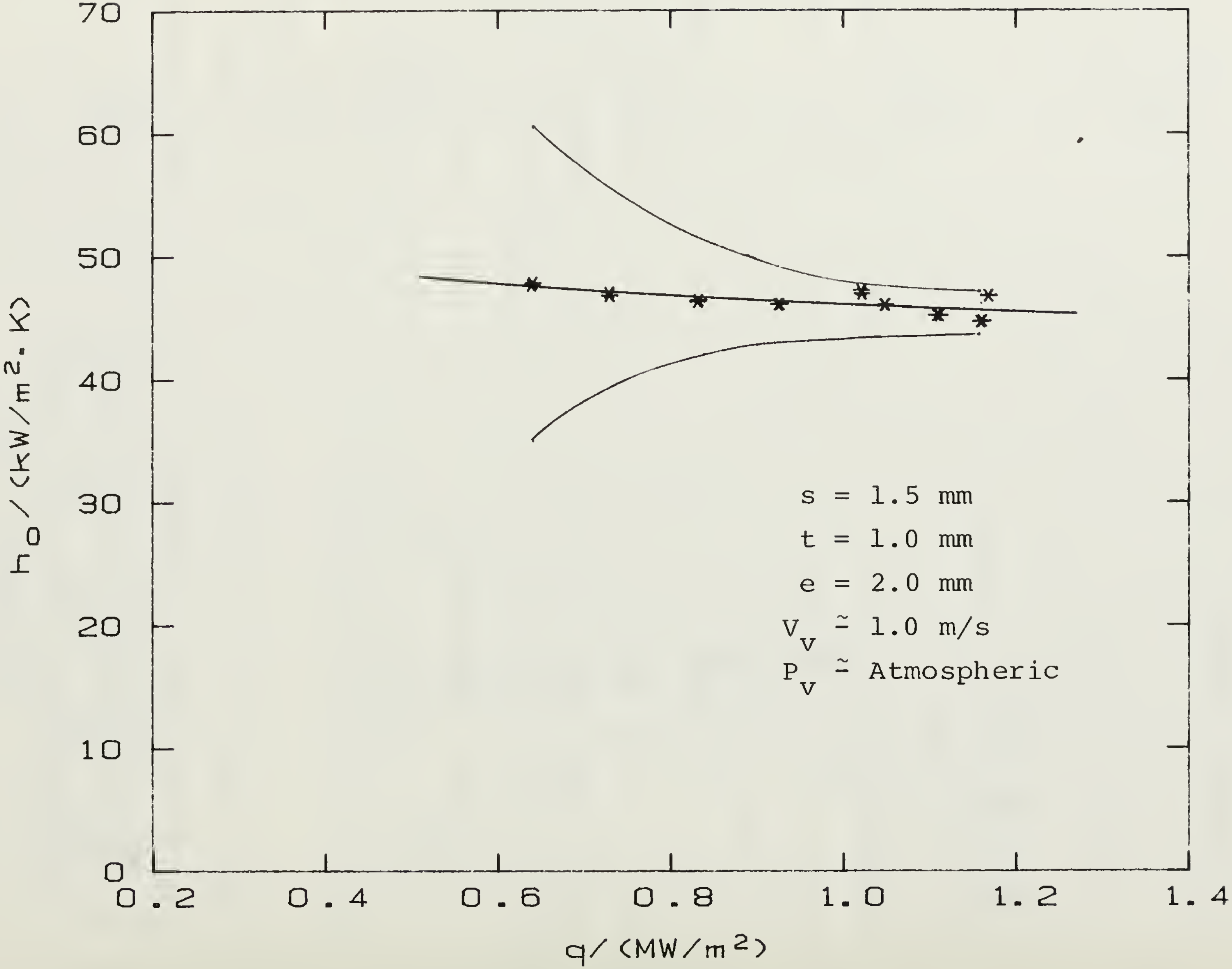

Figure E.2. Error Bands for a Tube Tested Under Atmospheric Conditions

number, heat flux, LMTD, water-side and outside heat-transfer coefficients) are given as percentages in the following computer outputs of the program "ERROR." At the end of this appendix, the listing of the program "ERROR" is provided for the Error Analysis.

```
DATA FOR THE ERROR ANALYSIS:

File Name:             F25E2V146
Pressure Condition:    VACUUM 11 kPa
Cooling Water Temperature In  =  22.72 (Deg C)
Cooling Water Temperature Out =  24.07 (Deg C)
Steam Temperature             =  48.35 (Deg C)
Water Flow Rate (%)           =  80.00
Water Velocity                =   4.39 (m/s)


ERROR ANALYSIS:

% Error in Mass Flow Rate     =  1.03
% Error in Reynolds Number    =  1.24
% Error in Heat Flux          =  0.79
% Error in LMTD               =  2.22
% Error in Uo                 =  2.36
% Error in Hi                 =  1.32
% Error in Ho                 =  8.36




DATA FOR THE ERROR ANALYSIS:

File Name:             F25E2V146
Pressure Condition:    VACUUM 11 kPa
Cooling Water Temperature In  =  23.02 (Deg C)
Cooling Water Temperature Out =  24.79 (Deg C)
Steam Temperature             =  48.20 (Deg C)
Water Flow Rate (%)           =  45.00
Water Velocity                =   2.51 (m/s)


ERROR ANALYSIS:

% Error in Mass Flow Rate     =  1.80
% Error in Reynolds Number    =  1.93
% Error in Heat Flux          =  0.78
% Error in LMTD               =  1.63
% Error in Uo                 =  1.31
% Error in Hi                 =  1.78
% Error in Ho                 = 10.53
```

```
DATA FOR THE ERROR ANALYSIS:

File Name:              F25E2V146
Pressure Condition:     VACUUM 11 kPa
Cooling Water Temperature In   =  23.53 (Deg C)
Cooling Water Temperature Out  =  26.11 (Deg C)
Steam Temperature              =  48.53 (Deg C)
Water Flow Rate (%)            =  20.00
Water Velocity                 =   1.16 (m/s)


ERROR ANALYSIS:

% Error in Mass Flow Rate      =  3.89
% Error in Reynolds Number     =  3.96
% Error in Heat Flux           =  1.30
% Error in LMTD                =  1.10
% Error in Uo                  =  1.70
% Error in Hi                  =  3.29
% Error in Ho                  = 36.25
```

```
DATA FOR THE ERROR ANALYSIS:

File Name:              F25E2A128
Pressure Condition:     ATMOSPHERIC 101 kPa
Cooling Water Temperature In   =  22.90 (Deg C)
Cooling Water Temperature Out  =  26.96 (Deg C)
Steam Temperature              =  99.87 (Deg C)
Water Flow Rate (%)            =  80.00
Water Velocity                 =   4.39 (m/s)


ERROR ANALYSIS:

% Error in Mass Flow Rate      =  1.03
% Error in Reynolds Number     =  1.25
% Error in Heat Flux           =  0.42
% Error in LMTD                =  0.71
% Error in Uo                  =  0.83
% Error in Hi                  =  1.33
% Error in Ho                  =  3.51
```

```
DATA FOR THE ERROR ANALYSIS:

File Name:              F25E2A128
Pressure Condition:   ATMOSPHERIC 101 kPa
Cooling Water Temperature In  =  23.27 (Deg C)
Cooling Water Temperature Out =  28.87 (Deg C)
Steam Temperature             =  99.59 (Deg C)
Water Flow Rate (%)           =  45.00
Water Velocity                =   2.51 (m/s)


ERROR ANALYSIS:

% Error in Mass Flow Rate     =  1.80
% Error in Reynolds Number    =  1.95
% Error in Heat Flux          =  0.61
% Error in LMTD               =  0.51
% Error in Uo                 =  0.80
% Error in Hi                 =  1.79
% Error in Ho                 =  6.34
```

```
DATA FOR THE ERROR ANALYSIS:

File Name:              F25E2A128
Pressure Condition:   ATMOSPHERIC 101 kPa
Cooling Water Temperature In  =  23.96 (Deg C)
Cooling Water Temperature Out =  32.30 (Deg C)
Steam Temperature             =  99.43 (Deg C)
Water Flow Rate (%)           =  20.00
Water Velocity                =   1.16 (m/s)


ERROR ANALYSIS:

% Error in Mass Flow Rate     =  3.90
% Error in Reynolds Number    =  3.97
% Error in Heat Flux          =  1.25
% Error in LMTD               =  0.34
% Error in Uo                 =  1.30
% Error in Hi                 =  3.30
% Error in Ho                 = 27.01
```

```
1000! FILE NAME : ERROR
1010! REVISED : JUNE 27, 1984
1020!
1030  PRINT USING "10X,""DATA FOR THE ERROR ANALYSIS:"""
1040  PRINT
1050  BEEP
1060  INPUT "ENTER FILE NAME",File$
1070  PRINT USING "10X,""File Name:            "",12A";File$
1080  BEEP
1090  INPUT "ENTER PRESSURE CONDITION (1=VACUUM,2=ATMOSPHERIC) ",Prc
1100  IF Prc=1 THEN
1110  BEEP
1120  PRINT USING "10X,""Pressure Condition:  VACUUM 11 kPa"""
1130  ELSE
1140  PRINT USING "10X,""Pressure Condition:  ATMOSPHERIC 101 kPa"""
1150  END IF
1160  BEEP
1170  INPUT "ENTER COOLING WATER TEMPERATURE IN",Tci
1180  PRINT USING "10X,""Cooling Water Temperature In  = "",3D.2D,"" (Deg C)""";
Tci
1190  BEEP
1200  INPUT "ENTER COOLING WATER TEMPERATURE DIFFERENCE",Dtw
1210  Tco=Tci+Dtw
1220  PRINT USING "10X,""Cooling Water Temperature Out = "",3D.2D,"" (Deg C)""";
Tco
1230  BEEP
1240  INPUT "ENTER STEAM TEMPERATURE",Ts
1250  PRINT USING "10X,""Steam Temperature             = "",3D.2D,"" (Deg C)""";
Ts
1260  BEEP
1270  INPUT "ENTER COOLING WATER FLOW RATE %",Fm
1280  PRINT USING "10X,""Water Flow Rate (%)           = "",3D.2D";Fm
1290  T=(Tci+Tco)/2  ! FILM TEMPERATURE
1300! UNCERTAINTY IN THE COOLING WATER
1310  Dfm=.10 ! ERROR IN FLOW METER READING
1320  Drho=1  ! ERROR IN WATER DENSITY
1330  Dmf=5.00049E-3+6.9861937E-3*Dfm ! ERROR IN MASS FLOW RATE
1340  Rho=FNRho(T) ! WATER DENSITY
1350  Mf=1.04805E-2+6.80932E-3*Fm  ! MASS FLOW RATE OF COOLING WATER
1360! CORRECT MF FOR THE TEMPERATURE EFFECT
1370  Mf=Mf*(1.0365-1.96644E-3*Tci+5.252E-6*Tci^2)/.995434
1380  Di=.0127  ! TUBE INSIDE DIAMETER
1390  Ai=(PI*Di^2)/4 ! TUBE INSIDE CROSS SECTION AREA
1400  Ddi=.000025
1410  Dai=(PI*Ddi^2)/4 ! ERROR OF INSIDE TUBE CROSS AREA
1420! COMPUTE THE WATER VELOCITY
1430  Vw=Mf/(Rho*Ai) ! WATER VELOCITY
1440  PRINT USING "10X,""Water Velocity                =   "",Z.DD,"" (m/s)""";V
w
1450! CORRECT OUTLET WATER TEMP. FOR THE MIXING CHAMBER EFFECT
1460  Tco=Tco-.004*Vw^2 ! COOLING WATER OUTLET TEMP.
1470  T=(Tci+Tco)*.5 ! FILM TEMPERATURE
1480! COMPUTE THE ERROR IN WATER VELOCITY
1490  Dvw=Vw*SQR((Dmf/Mf)^2+(Drho/Rho)^2+(Dai/Ai)^2)
1500! UNCERTAINTY IN THE REYNOLDS NUMBER
1510  Mw=FNMw(T) ! WATER VISCOSITY
1520  Dmw=6.E-6 ! ERROR OF WATER VISCOSITY
1530  Re=(Rho*Vw*Di)/Mw
1540  Dre=Re*SQR((Drho/Rho)^2+(Dvw/Vw)^2+(Ddi/Di)^2+(Dmw/Mw)^2)
```

```
1550! UNCERTAINTY IN THE HEAT TRANSFERED
1560  Cpw=FNCpw(T)
1570  Q=Mf*(Tco-Tci)*Cpw
1580  Dtco=.02
1590  Dtci=.02
1600  Dcpw=8
1610  Dq=Q*SQR((Dmf/Mf)^2+((Dtco/(Tco-Tci)))^2+((Dtci/(Tco-Tci)))^2+(Dcpw/Cpw)^2
)
1620! UNCERTAINTY IN THE HEAT FLUX
1630  Dl=.0005 ! ERROR IN TUBE LENGHT
1640  Do=.01905 ! SMOOTH TUBE OUTER DIAMETER
1650  Ddo=.000025
1660  L=.13335 ! FINNED TUBE LENGTH
1670  Qp=Q/(PI*Do*L) ! HEAT FLUX
1680  Dqp=(Qp/PI)*SQR((Dq/Q)^2+(Ddo/Do)^2+(Dl/L)^2)
1690  Dts=.02  ! ERROR IN TEMPERATURE MEASUREMENT
1700  Lmtd=(Tco-Tci)/LOG((Ts-Tci)/(Ts-Tco))
1710  Uo=Qp/Lmtd ! OVERALL HEAT TRANSFER COEF.
1720  A1=Dts*(Tci-Tco)/((Ts-Tci)*(Ts-Tco)*LOG((Ts-Tci)/(Ts-Tco)))
1730  A2=Dtci/((Ts-Tci)*LOG((Ts-Tci)/(Ts-Tco)))
1740  A3=Dtco/((Ts-Tco)*LOG((Ts-Tci)/(Ts-Tco)))
1750  Dlmtd=Lmtd*SQR(A1^2+A2^2+A3^2)
1760  Duo=Uo*SQR((Dqp/Qp)^2+(Dlmtd/Lmtd)^2)
1770  M=Mw
1780  T1=(T+273.15)/273.15
1790  Kw=FNKw(T1)
1800  Ci=.0635 ! SIEDER-TATE COEFFICIENT
1810  Ac=26.4  ! INTERSCEPT FROM SIEDER PROGRAM
1820  Kc=385 ! WALL THERMAL CONDUCTIVITY
1830  L1=.060325 ! LENGTH OF UNFINNED LEFT PART OF TUBE
1840  L2=.034925 ! LENGTH OF UNFINNED RIGHT PART OF TUBE
1850  Dr=.015875
1860  Pr=Cpw*Mw/Kw
1870  Muw=FNMuw(T)
1880! UNCERTAINTY OF INSIDE HEAT-TRANSFER COEFF.
1890  Cf=1.
1900  Hi=(Kw/Di)*(Ci*Re^.8*Pr^.333*Cf+Ac)
1910  Dti=Q/(PI*Di*(L+L1*Fe1+L2*Fe2)*Hi)
1920  Cfc=(Muw/FNMuw(T+Dti))^.14
1930  IF ABS((Cfc-Cf)/Cfc)>.01 THEN
1940  Cf=(Cf+Cfc)*.5
1950  GOTO 1900
1960  END IF
1970  P1=PI*(Di+Do)
1980  B1=(Do-Di)*PI*(Di+Do)*.5
1990  M1=(Hi*P1/(Kc*B1))^.5
2000  P2=PI*(Di+Dr)
2010  B2=(Dr-Di)*PI*(Di+Dr)*.5
2020  M2=(Hi*P2/(Kc*B2))^.5
2030  Fe1=FNTanh(M1*L1)/(M1*L1)
2040  Fe2=FNTanh(M2*L2)/(M2*L2)
2050  Dtc=Q/(PI*Di*(L+L1*Fe1+L2*Fe2)*Hi)
2060  IF ABS((Dtc-Dti)/Dtc)>.01 THEN 1900
2070  Dkw=.0010 ! ERROR IN WATER THERMAL CONDUCTIVITY
2080  Dci=.0005 ! ERROR IN SIEDER-TATE COEFFICIENT
2090  Dpr=.05 ! ERROR IN PRANDTL NUMBER
2100  Dcf=8.E-6
2110  A4=.14*Dcf/Cf
2120  Dhi=Hi*SQR((Dkw/Kw)^2+(Ddi/Di) 2+(.8*Dre/Re)^2+(.333*Dpr/Pr)^2+(Dci/Ci)^2+
A4)
2130! UNCERTAINTY OF OUTSIDE HEAT-TRANSFER COEFF.
```

```
2140   Dkc=1 ! ERROR IN TUBE THERMAL CONDUCTIVITY
2150   Rw=Do*LOG(Do/Di)/(2*Kc) ! WALL RESISTANCE
2160   Ho=1/((1/Uo)-(Do*L/(Di*(L+L1*Fe1+L2*Fe2)*Hi))-Rw)
2170   Drw=Rw*SQR((Ddo/Do)^2+(Dkc/Kc)^2+(Ddo/(Do*LOG(Do/Di)))^2+(Ddi/(Di*LOG(Do/D
i)))^2)
2180   A5=1/Uo-Rw-(Do/(Di*Hi))
2190   A6=Duo/(Uo^2*A5)
2200   A7=Drw/A5
2210   A8=((Do/(Di*Hi))*(Dhi/Hi))/A5
2220   PRINT
2230   Dho=Ho*SQR(A6^2+A7^2+A8^2)
2240! CALCULATE THE % ERROR IN Ho
2250   Prho=Dho*100/Ho
2260! CALCULATE THE % ERROR IN REYNOLDS NUMBER
2270   Prre=Dre*100/Re
2280! CALCULATE THE % ERROR IN MASS FLOW RATE
2290   Prmf=Dmf*100/Mf
2300! CALCULATE THE % ERROR IN HEAT TRANSFER
2310   Prqp=Dqp*100/Qp
2320! CALCULATE THE % ERROR IN LMTD
2330   Prlmtd=Dlmtd*100/Lmtd
2340! CALCULATE THE % ERROR IN OVERALL HEAT TRANSFER COEF.
2350   Pruo=Duo*100/Uo
2360! CALCULATE THE % ERROR IN INSIDE HEAT TRANSFER COEFF.
2370   Prhi=Dhi*100/Hi
2380   PRINT
2390   PRINT USING "10X',""ERROR ANALYSIS:"""
2400   PRINT
2410   PRINT USING "10X,""% Error in Mass Flow Rate      = "".2D.2D,";Prmf
2420   PRINT USING "10X,""% Error in Reynolds Number     = "".2D.2D.";Prre
2430   PRINT USING "10X.""% Error in Heat Flux           =  "".Z.2D,";Prqp
2440   PRINT USING "10X.""% Error in LMTD                =  "",Z.2D";Prlmtd
2450   PRINT USING "10X,""% Error in Uo                  =  "",Z.2D,";Pruo
2460   PRINT USING "10X,""% Error in Hi                  = "",2D.2D,";Prhi
2470   PRINT USING "10X,""% Error in Ho                  = "".2D.2D.";Prho
2480   END
2490   DEF FNMuw(T)
2500   A=247.8/(T+133.15)
2510   Muw=2.4E-5*10^A
2520   RETURN Muw
2530   FNEND
2540   DEF FNTanh(X)
2550   P=EXP(X)
2560   Q=EXP(-X)
2570   Tanh=(P-Q)/(P+Q)
2580   RETURN Tanh
2590   FNEND
2600   DEF FNKw(T1)
2610   Kw=-.92247+T1*(2.8395-T1*(1.8007-T1*(.52577-.07344*T1)))
2620   RETURN Kw
2630   FNEND
2640   DEF FNMw(T)
2650   A=247.8/(T+133.15)
2660   Mw=2.4E-5*10^A
2670   RETURN Mw
2680   FNEND
2690   DEF FNRho(T)
2700   Rho=999.52946+T*(.01269-T*(5.482513E-3-T*1.234147E-5))
2710   RETURN Rho
2720   FNEND
```

```
2730  DEF FNCpw(T)
2740  Cpw=(4.21120858-T*(2.26826E-3-T*(4.42361E-5+2.71428E-7*T)))*1000
2750  RETURN Cpw
2760  FNEND
```

LIST OF REFERENCES

1. Marto, P.J., "Heat Transfer and Two-Phase Flow During Shell-side Condensation," ASME-JSME Thermal Engineering Joint Conference Proceedings, Honolulu, Vol. 2, 1983, pp. 561-591.

2. Gregorig, R., "Hautkondensation an Feingewellten Oberflachen bei Berucksichtigung der Oberfachenspannungen," in Zeitschrift fur Angewandte Mathematik und Physik, Vol. V, 1954, pp. 36-49. Translation by Edwards, D.K.

3. Yau, K.K., and Rose, J.W., "Effects of Fin Spacing and Drainage Strip on the Condensation Heat-Transfer Performance of Horizontal Low Integral-fin Tubes," Project Report, Department of Mechanical Engineering, Queen Mary College, University of London, 1982.

4. Katz, D.L., Hope, R.E. and Dasko, S.C., "Liquid Retention on Finned Tubes," Dept. of Eng. Research, Univ. of Michigan, Ann Arbor, Michigan, Project M 592, 1946.

5. Rudy, T.M., and Webb, R.L., "Condensate Retention of Horizontal Integral-Fin Tubes," Advances in Enhanced Heat Transfer--1891, HTD--Vol. 18, presented at 20th National Heat Transfer Conference, Milwaukee, Wisconsin, August 1981.

6. Honda, H., Nozu, S., Mitsumori, K., "Augmentation of Condensation on Horizontal Finned Tubes by Attaching Porous Drainage Plates," Proc. ASME-JSME Thermal Engineering Joint Conference, Hawaii, 1983.

7. Beatty, K.O., and Katz, D.L., 1948, "Condensation of Vapors on Outside of Finned Tubes," Chemical Engineering Progress, 44, (1), January, 55-70.

8. Owen, R.G., Sardesai, R.G., Smith, R.A., and Lee, W. C., "Gravity Controlled Condensation on a Horizontal Low-Fin Tube," Condensers: Theory and Practice Inst. Chem. Engrs. Symp. Ser., No. 75, 1983, pp. 415-428.

9. Honda, H.,and Nozu, S., "A Prediction Method for Heat-Transfer During Film Condensation in Horizontal Low Integral-Fin Tubes," submitted for presentation at the ASME Winter Annual Meeting, New Orleans, Dec. 1984.

10. Staub, F.W., "Heat Transfer for Film Condensation on Vertical and Horizontal Fluted Tubes," General Electric Laboratory, Report No. 61GL175, October 11, 1961.

11. Krohn, R.L., An Experimental Apparatus to Study Enhanced Condensation Heat Transfer of Steam on Horizontal Tubes, MS Thesis, Naval Postgraduate School, Monterey, California, June 1982.

12. Graber, K.A., Condensation Heat Transfer of Steam on a Single Horizontal Tube, MS Thesis, Naval Postgraduate School, Monterey, California, June 1983.

13. Poole, M.W., Filmwise Condensation of Steam on Externally-finned Horizontal Tubes, MS Thesis, Naval Postgraduate School, Monterey, California, December 1983.

14. Barrington, A.E., High Vaccum Engineering, Prentice-Hall, p. 190, 1963.

15. Lee, W.C., Filmwise Condensation on a Horizontal Tube in the Presence of Forced Convection and Non-Condensing Gas, Ph.D. Thesis, Queen Mary College, London, 1981.

16. Incorpera, F.P., and DeWitt, D.P., Fundamentals of Heat-Transfer, Wiley, 1981, pp. 406-407.

17. Nobbs, D.W., The Effect of Downward Vapour Velocity and Inundation on the Condensation Rates of Horizontal Tubes and Tube Banks, Ph.D. Dissertation, University of Bristol, Bristol, England, April 1975.

18. Fujii, T., Honda, H., "Condensation of Steam on a Horizontal Tube," Condensation Heat Transfer, ASME New York, 1979, pp. 35-43.

19. Kline, S.J., and McClintock, F.A., "Describing Uncertainties in Single-sample Experiments," Mech. Eng., Volume 74, pp. 3-8, January 1953.

INITIAL DISTRIBUTION LIST

		No. Copies
1.	Defense Technical Information Center Cameron Station Alexandria, Virginia 22314	2
2.	Library, Code 0142 Naval Postgraduate School Monterey, California 93943	2
3.	Department Chairman, Code 69 Department of Mechanical Engineering Naval Postgraduate School Monterey, California 93943	1
4.	Professor P.J. Marto, Code 69Mx Department of Mechanical Engineering Naval Postgraduate School Monterey, California 93943	5
5.	Dr. John W. Rose Department of Mechanical Engineering Queen Mary College University of London London El 4NS England	1
6.	Dr. A.S. Wanniarachchii, Code 69Wa Department of Mechanical Engineering Naval Postgraduate School Monterey, California 93943	1
7.	Dr. Win Aung Program Director for Heat Transfer Division of Engineering National Science Foundation Washington, D.C. 20550	2
8.	Hellenic Navy General Staff Department of Education c/o Embassy of Greece Office of Naval Attache 2228 Massachusetts Avenue, N.W. Washington, D.C. 20008	3
9.	Lt. Ioannis Georgiadis, H.N. 67, Peloponisou St, Agia Paraskevi Attiki, Athens Greece	3

10. Lt. Evangelos Mitrou, H. N. 1
SMC #2777,
Naval Postgraduate School
Monterey, California 93943

11. Professor T. Sarpkaya, Code 69Sl 1
Department of Mechanical Engineering
Naval Postgraduate School
Monterey, California 93943

13 37 5

thesG2655
Filmwise condensation of steam on low in
3 2768 002 02589 2
DUDLEY KNOX LIBRARY